



ΕΘΝΙΚΟ ΜΕΤΣΟΒΙΟ ΠΟΛΥΤΕΧΝΕΙΟ
ΣΧΟΛΗ ΗΛΕΚΤΡΟΛΟΓΩΝ ΜΗΧΑΝΙΚΩΝ
ΚΑΙ ΜΗΧΑΝΙΚΩΝ ΥΠΟΛΟΓΙΣΤΩΝ
ΤΟΜΕΑΣ ΣΥΣΤΗΜΑΤΩΝ ΜΕΤΑΔΟΣΗΣ ΠΛΗΡΟΦΟΡΙΑΣ
ΚΑΙ ΤΕΧΝΟΛΟΓΙΑΣ ΥΛΙΚΩΝ

**Σχεδίαση και Κατασκευή Πρωτότυπης Κεραίας σε Χάρτινο
Υπόστρωμα με Χρήση Τεχνολογίας Εκτύπωσης Ψεκασμού
Αγώγιμου Μελανιού για Εφαρμογές Ραδιοσυχνικής
Αναγνώρισης (RFID)**

ΔΙΠΛΩΜΑΤΙΚΗ ΕΡΓΑΣΙΑ

Ζήσης Ε. Κώνστας

Επιβλέποντες : Νικόλαος Ουζούνογλου
Καθηγητής Ε.Μ.Π.

Μάνος Τεντζέρης
Associate Professor Georgia Tech

Αθήνα, Οκτώβριος 2008



NATIONAL TECHNICAL UNIVERSITY OF ATHENS
SCHOOL OF ELECTRICAL
AND COMPUTER ENGINEERING
DIVISION OF INFORMATION TRANSMISSION SYSTEMS
AND MATERIAL TECHNOLOGY

Design and Fabrication of a Novel Conductive Inkjet Printed Antenna on Paper Substrate for RFID Applications

DIPLOMA THESIS

Zissis E. Konstas

Advisors : Nikolaos Uzunoglu
Professor NTUA

Manos Tentzeris
Associate Professor Georgia Tech

Athens, October 2008



ΕΘΝΙΚΟ ΜΕΤΣΟΒΙΟ ΠΟΛΥΤΕΧΝΕΙΟ
ΣΧΟΛΗ ΗΛΕΚΤΡΟΛΟΓΩΝ ΜΗΧΑΝΙΚΩΝ
ΚΑΙ ΜΗΧΑΝΙΚΩΝ ΥΠΟΛΟΓΙΣΤΩΝ
ΤΟΜΕΑΣ ΣΥΣΤΗΜΑΤΩΝ ΜΕΤΑΔΟΣΗΣ ΠΛΗΡΟΦΟΡΙΑΣ
ΚΑΙ ΤΕΧΝΟΛΟΓΙΑΣ ΥΛΙΚΩΝ

**Σχεδίαση και Κατασκευή Πρωτότυπης Κεραίας σε Χάρτινο
Υπόστρωμα με Χρήση Τεχνολογίας Εκτύπωσης Ψεκασμού
Αγώγιμου Μελανιού για Εφαρμογές Ραδιοσυχνικής
Αναγνώρισης (RFID)**

ΔΙΠΛΩΜΑΤΙΚΗ ΕΡΓΑΣΙΑ

Ζήσης Ε. Κώνστας

Επιβλέποντες : Νικόλαος Ουζούνογλου
Καθηγητής Ε.Μ.Π.

Μάνος Τεντζέρης
Associate Professor Georgia Tech

Εγκρίθηκε από την τριμελή εξεταστική επιτροπή την 17^η Οκτωβρίου 2008

.....
Νικόλαος Ουζούνογλου
Καθηγητής Ε.Μ.Π.

.....
Δήμητρα Κακλαμάνη
Αν. Καθηγήτρια Ε.Μ.Π.

.....
Ιάκωβος Βενιέρης
Καθηγητής Ε.Μ.Π.

Αθήνα, Οκτώβριος 2008

.....
Ζήσης Ε. Κώνστας

Διπλωματούχος Ηλεκτρολόγος Μηχανικός και Μηχανικός Υπολογιστών Ε.Μ.Π.

Copyright © Ζήσης Κώνστας, 2008

Με επιφύλαξη παντός δικαιώματος. All rights reserved.

Απαγορεύεται η αντιγραφή, αποθήκευση και διανομή της παρούσας εργασίας, εξ ολοκλήρου ή τμήματος αυτής, για εμπορικό σκοπό. Επιτρέπεται η ανατύπωση, αποθήκευση και διανομή για σκοπό μη κερδοσκοπικό, εκπαιδευτικής ή ερευνητικής φύσης, υπό την προϋπόθεση να αναφέρεται η πηγή προέλευσης και να διατηρείται το παρόν μήνυμα. Ερωτήματα που αφορούν τη χρήση της εργασίας για κερδοσκοπικό σκοπό πρέπει να απευθύνονται προς τον συγγραφέα.

Οι απόψεις και τα συμπεράσματα που περιέχονται σε αυτό το έγγραφο εκφράζουν τον συγγραφέα και δεν πρέπει να ερμηνευθεί ότι αντιπροσωπεύουν τις επίσημες θέσεις του Εθνικού Μετσόβιου Πολυτεχνείου.

ΠΕΡΙΛΗΨΗ

Η παρούσα διπλωματική εργασία παρουσιάζει την σχεδίαση και κατασκευή μιας πρωτότυπης τυπωμένης κεραίας σε χάρτινο υπόστρωμα με χρήση τεχνολογίας εκτύπωσης ψεκασμού αγωγίμου μελανιού για εφαρμογές ραδιοσυχνικής αναγνώρισης. Η ραδιοσυχνική αναγνώριση (RFID) αποτελεί μια ταχέως μεταβαλλόμενη ασύρματη τεχνολογία που εκμεταλλεύεται ηλεκτρομαγνητικά κύματα για την αυτόματη αναγνώριση και τον εντοπισμό αντικειμένων. Ένα σύστημα ραδιοσυχνικής αναγνώρισης αποτελείται από έναν πομποδέκτη ή ετικέτα (tag), ο οποίος τοποθετείται σε ένα αντικείμενο και χρησιμοποιεί μια κεραία για να επικοινωνήσει με έναν αναγνώστη (reader).

Η προτεινόμενη κεραία σχεδιάστηκε με την βοήθεια του λογισμικού ηλεκτρομαγνητικής προσομοίωσης HFSS για έναν ενεργό πομποδέκτη ο οποίος λειτουργεί στην UHF ζώνη συχνοτήτων. Για την σχεδίαση της κεραίας επιλέχθηκε ένα μονόπολο με οπές, τροφοδοτούμενο από γραμμή μεταφοράς ομοεπίπεδου κυματοδηγού, λόγω των ελκυστικών χαρακτηριστικών του. Το σχέδιο βελτιστοποιήθηκε ώστε να επιτευχθούν συγκεκριμένοι στόχοι όπως συζυγής προσαρμογή της κεραίας στο φορτίο της.

Ένα πρωτότυπο της προτεινόμενης κεραίας κατασκευάστηκε χρησιμοποιώντας τεχνολογία εκτύπωσης ψεκασμού σε εύκαμπτο, χαμηλού κόστους χάρτινο υπόστρωμα. Η εκτύπωση ψεκασμού είναι μια πρωτοποριακή τεχνολογία για την άμεση εκτύπωση ηλεκτρονικών κυκλωμάτων σε χαρτί χρησιμοποιώντας αγωγίμο ασημένιο μελάνι. Στην εργασία αυτή, αφενός επισημαίνονται τα προτερήματα της χρήσης χαρτιού σαν υπόστρωμα και αφετέρου παρουσιάζεται μια επισκόπηση του μικροκυματικού χαρακτηρισμού του χαρτιού, ώστε να προσδιοριστούν οι ηλεκτρικές του ιδιότητες. Επιπρόσθετα περιγράφεται η κατασκευαστική διαδικασία εκτύπωσης ψεκασμού αγωγίμου μελανιού, τονίζοντας τα πλεονεκτήματα της τεχνολογίας αυτής και αναλύοντας τα χαρακτηριστικά λειτουργίας του εκτυπωτή ψεκασμού.

Τέλος πραγματοποιήθηκαν μετρήσεις εξασθένησης από επιστροφή και μετρήσεις κέρδους, ώστε να διερευνηθεί η επίδοση της κεραίας και να εξεταστεί αν η κεραία ικανοποιεί τις απαιτήσεις σχεδίασης. Συμπερασματικά, τα πειραματικά αποτελέσματα εμφάνισαν πολύ καλή συμφωνία με την προσομοίωση, επαληθεύοντας την επιτευξιμότητα της τεχνολογίας εκτύπωσης ψεκασμού ως μια εξαιρετική κατασκευαστική τεχνική για την υλοποίηση κεραίων RFID σε υπόστρωμα βασισμένο σε χαρτί.

Λέξεις Κλειδιά

Ραδιοσυχνική αναγνώριση (RFID), ενεργός πομποδέκτης, ηλεκτρομαγνητική αντανάκλαση, τυπωμένη κεραία, μονόπολο, συζυγής προσαρμογή, εκτύπωση ψεκασμού μελανιού, χάρτινο υπόστρωμα, ασημένιο μελάνι

ABSTRACT

This thesis presents the design and fabrication of a novel inkjet printed antenna on paper substrate for RFID applications. Radio Frequency Identification (RFID) is a rapidly developing wireless technology that utilizes electromagnetic waves for the automatic identification and tracking of objects. An RFID system composes of a transponder or tag, which is attached to an object and uses an antenna to communicate with a reader.

The proposed antenna is designed using the electromagnetic simulation software HFSS for an active RFID tag operating in the UHF frequency band. A slotted CPW-fed monopole configuration is selected, due its many attractive characteristics. The design is optimized to achieve specific design goals, such as conjugate impedance matching of the antenna to its load.

A prototype has been fabricated using inkjet-printing technology on a flexible, low-cost paper substrate. Inkjet printing is an innovative technology for directly printing electronics on paper using conductive silver ink, without the requirement of a photolithographic mask. The benefits of using paper as a substrate are highlighted and an overview of RF characterization to determine the electrical properties of paper is presented. In addition, the inkjet printing fabrication process is described, emphasizing the advantages of this technology and detailing the operation characteristics of the inkjet printer.

Return loss and gain measurements were carried out to investigate the antenna performance and examine if the antenna satisfies the design requirements. The experimental results showed good agreement with the simulation, verifying the feasibility of inkjet printing technology as an excellent prototyping technique for implementing RFID antennas on paper-based substrates.

Keywords

RFID, active transponder, backscatter, UHF, printed antenna, monopole, conjugate impedance matching, inkjet printing, paper substrate, silver ink

ACKNOWLEDGEMENTS

First and foremost, I would like to express my deepest gratitude to my Professor, Nikolaos Uzunoglu, for giving me the opportunity to compile my diploma thesis at Georgia Institute of Technology in Atlanta, US. I would like to thank him for his continuous support, encouragement and concern, throughout the years of my undergraduate studies. I would also like to thank my advisor Manos Tentzeris, for accommodating me in his laboratory in GEDC at Georgia Tech. The completion of my thesis would not have been possible without his valuable guidance, knowledge and constant encouragement.

I am deeply thankful to my mentor Amin Rida, as well as to Rushi Vyas, Scot Travis and the other group members at Georgia Tech for their assistance and willingness to solve any questions and concerns I had. I would also like to acknowledge the hospitality and help that all the Greeks I met in Atlanta provided me.

I am especially grateful to Andreas Katsiamis, not only for his priceless knowledge and expertise that proved to be critical for the accomplishment of my thesis, but also for the constant encouragement and motivation he provided me during and after my stay in Atlanta. In addition, I have to recognize the vital advice and mentoring of my university classmate George Dogiamis. If it hadn't been for him, I may have never made the decision to carry out my diploma thesis in the United States.

Last but not least, I would like to thank my godfather Ioannis Minis for his constant help and my family for their unconditional love, support, and encouragement.

ΠΕΡΙΛΗΨΗ ΚΕΦΑΛΑΙΩΝ

1 Εισαγωγή

Το Κεφάλαιο 1 παρουσιάζει μια γενική περιγραφή των θεμάτων που πραγματεύεται η εργασία αυτή. Πρώτα τονίζεται η ραγδαία ανάπτυξη των συστημάτων ραδιοσυχνικής αναγνώρισης καθώς και τα πλεονεκτήματά της τεχνολογίας αυτής σε σχέση με άλλες τεχνικές αναγνώρισης. Αναφέρεται επίσης η βασική δομή ενός πομποδέκτη RFID και τονίζεται η σημασία που έχει η κεραία του για την επίδοσή του συστήματος. Στη συνέχεια απαριθμούνται τα προβλήματα που συναντούνται στην σχεδίαση κεραιών για πομποδέκτες RFID. Συγκεκριμένα είναι: 1) μέγεθος 2) κόστος 3) απόδοση 4) λειτουργία στην παγκόσμια μπάντα συχνοτήτων RFID 5) συμβατότητα με ηλεκτρονικά. Τέλος αφού περιγραφεί η προτεινόμενη κεραία αυτής της εργασίας, αναφέρεται επιγραμματικά η δομή της εργασίας και τα περιεχόμενα του κάθε κεφαλαίου.

2 Θεωρητικό Υπόβαθρο και Σχετική Έρευνα

Στο κεφάλαιο αυτό παρουσιάζεται μια επισκόπηση των συστημάτων ραδιοσυχνικής αναγνώρισης (RFID). Ραδιοσυχνική αναγνώριση είναι η αυτόματη αναγνώριση ενός αντικειμένου χρησιμοποιώντας ηλεκτρομαγνητικά κύματα. Ένα σύστημα RFID αποτελείται από δύο τμήματα: 1) Έναν πομποδέκτη ή ετικέτα ο οποίος τοποθετείται επάνω στο αντικείμενο 2) Έναν αναγνώστη ο οποίος επικοινωνεί με τον πομποδέκτη και “διαβάζει” τα δεδομένα ταυτοποίησης που βρίσκονται αποθηκευμένα σε αυτόν. Ο πομποδέκτης αποτελείται από ένα ολοκληρωμένο κύκλωμα (IC) το οποίο αποθηκεύει τις πληροφορίες και από μια κεραία, μέσω της οποίας επιτυγχάνεται η επικοινωνία με τον αναγνώστη. Τα συστήματα ραδιοσυχνικής αναγνώρισης βρίσκουν πολύ μεγάλη εφαρμογή στην βιομηχανία, στην γραμμή παραγωγής, στην ασφάλεια, και αλλού, αλλά και σε νέες περιοχές όπως στα ασύρματα δίκτυα αισθητήρων.

Οι πομποδέκτες RFID κατηγοριοποιούνται σε 3 τύπους ανάλογα με τον τρόπο τροφοδοσίας τους: Οι παθητικοί πομποδέκτες δεν ενσωματώνουν κάποια πηγή ενέργειας, όπως μπαταρία, και τόσο η ενεργοποίηση του ολοκληρωμένου κυκλώματος τους όσο και η επικοινωνία με τον αναγνώστη πραγματοποιείται από την ενέργεια που ανακτούν από το πεδίο του αναγνώστη. Οι ενεργητικοί πομποδέκτες από την άλλη μεριά ενσωματώνουν μια μπαταρία η οποία χρησιμοποιείται για την εκτέλεση και των δυο παραπάνω λειτουργιών. Τέλος οι ημι-παθητικοί πομποδέκτες χρησιμοποιούν την μπαταρία μόνο για την τροφοδότηση του ολοκληρωμένου κυκλώματος. Οι πομποδέκτες διαφοροποιούνται επίσης και ως προς τον τρόπο λειτουργίας τους σε δύο κατηγορίες: 1) οι χαμηλής συχνότητας πομποδέκτες που λειτουργούν στο κοντινό πεδίο του αναγνώστη και επικοινωνούν με αυτόν με επαγωγική σύζευξη. 2) οι υψηλής συχνότητας πομποδέκτες οι οποίοι λειτουργούν στο

μακρινό πεδίο του αναγνώστη και επικοινωνούν με αυτόν με την μέθοδο της ηλεκτρομαγνητικής αντανάκλασης.

Το πιο σημαντικό τμήμα ενός πομποδέκτη είναι η κεραία του και γι' αυτό η σχεδίασή της αποτελεί καθοριστικό παράγοντα στην επίδοση ενός συστήματος RFID. Κατά την διαδικασία σχεδίασης της κεραίας ενός πομποδέκτη είναι απαραίτητο να προσδιοριστούν όλες οι αναγκαίες παράμετροι και απαιτήσεις της εφαρμογής, ώστε να υπολογιστούν τα απαραίτητα χαρακτηριστικά της κεραίας που ικανοποιούν της προδιαγραφές. Οι περισσότερες κεραίες που χρησιμοποιούνται σε πομποδέκτες RFID είναι οι τυπωμένες κεραίες μονού στρώματος. Συνήθως είναι η χρήση τυπωμένων διπόλων μαιανδρικής μορφής και τυπωμένων ορθογωνίων μονοπόλων με ή χωρίς οπές. Στην εργασία αυτή παρουσιάζεται ένα τυπωμένο μονόπολο μονού στρώματος. Η σχεδίαση της προτεινόμενης κεραίας πραγματοποιήθηκε με την βοήθεια του ηλεκτρομαγνητικού λογισμικού Ansoft HFSS v10.0.

Η τεχνολογία RFID έχει υποστεί ραγδαίες εξελίξεις τα τελευταία χρόνια. Εμφάνιση έχουν κάνει μικροσκοπικοί πομποδέκτες που ενσωματώνουν την κεραία στο ολοκληρωμένο τους κύκλωμα και έχουν μέγεθος ενός τσιπ. Ακόμα έχουν αναπτυχθεί ενεργοί πομποδέκτες με αισθητήρες, τυπωμένοι σε χάρτινο υπόστρωμα με χρήση τεχνολογίας εκτύπωσης ψεκασμού αγωγίμου μελανιού. Τέλος πρέπει να αναφερθεί, ότι ερευνούνται επίσης πομποδέκτες που ενσωματώνουν κυκλώματα ανάκτησης ενέργειας (ηλιακή, πιεζοηλεκτρική, ηλεκτρομαγνητική) ώστε να εξαιρεθεί η ανάγκη χρήσης μπαταρίας στις ενεργές ετικέτες.

3 Σχεδίαση Κεραίας

Στο κεφάλαιο αυτό αναλύεται η διαδικασία σχεδίασης της προτεινόμενης κεραίας και προσομοιώνεται η επίδοσή της. Η συζυγής προσαρμογή της κεραίας στο φορτίο του πομποδέκτη αποτελεί την πιο σημαντική απαίτηση της κεραίας και για αυτό αρχικά δίνεται ένα θεωρητικό υπόβαθρο στην προσαρμογή αντίστασης στα συστήματα RFID. Για να εξασφαλιστεί η μέγιστη μεταφορά ισχύος από την κεραία του πομποδέκτη στο φορτίο του, πρέπει η κεραία να είναι προσαρμοσμένη στο φορτίο και να έχει μιγαδική τιμή αντίστασης εισόδου. Αυτό αποτελεί ουσιώδη διαφορά μεταξύ σχεδίασης κοινών κεραιών και κεραιών RFID, καθώς η κεραία του πομποδέκτη δεν λειτουργεί ούτε στην περιοχή συντονισμού της αλλά ούτε είναι προσαρμοσμένη σε γραμμή μεταφοράς 50Ω.

Στην συνέχεια του κεφαλαίου προσδιορίζονται οι απαιτήσεις της κεραίας. Συγκεκριμένα οι προδιαγραφές που πρέπει να ικανοποιεί η κεραία είναι: 1) λειτουργία στην UHF περιοχή συχνοτήτων με κεντρική συχνότητα 904.5MHz 2) εύρος ζώνης 866-928MHz 3) ομοιοκατευθυντικό διάγραμμα ακτινοβολίας στο αζιμούθιο επίπεδο 4) αντίσταση εισόδου με τιμή $37.31-j65.96\Omega$ 5) θετική κατευθυντικότητα σε dB 6) κέρδος κοντά στα 0dB 7) απόδοση μεγαλύτερη από 80% 8) γραμμική πόλωση.

Έπειτα περιγράφεται η γεωμετρία της κεραίας και εξηγούνται τα χαρακτηριστικά της. Ο κεραία είναι ένα τυπωμένο μονόπολο μονού στρώματος που αποτελείται από 3 τμήματα: 1) Το στοιχείο ακτινοβολίας που συνίσταται σε μια επίπεδη ορθογώνια επιφάνεια με δύο οπές. 2) Το τυπωμένο επίπεδο γης που βρίσκεται κάτω από το στοιχείο ακτινοβολίας 3) Την γραμμή τροφοδοσίας της κεραίας που αποτελούν τα δύο επίπεδα γης και ένας απομονωμένος αγωγός ανάμεσά τους (γραμμή μεταφοράς ομοεπίπεδου αγωγού). Στο τέλος αυτής της παραγράφου παραθέτονται τα πλεονεκτήματα της χρήσης του μονοπόλου ως κεραία αντί ενός δίπολου και δίνονται περισσότερες λεπτομέρειες πάνω στα τμήματα της κεραίας.

Μετά εξηγείται η διαδικασία σχεδίασης και βελτιστοποίησης της κεραίας, ώστε να ικανοποιεί τις απαιτούμενες προδιαγραφές. Πρώτα σχεδιάζεται ένα απλό τυπωμένο ορθογώνιο μονόπολο το οποίο να λειτουργεί κοντά στην συχνότητα λειτουργίας του πομποδέκτη και να παρουσιάζει ομοιοκατευθυντικό διάγραμμα ακτινοβολίας. Αναλύεται ο τρόπος υπολογισμού των διαστάσεων του και παρουσιάζονται τα αποτελέσματα της προσομοίωσης τα οποία ικανοποιούν τις απαιτήσεις. Έπειτα παρουσιάζεται ο τρόπος βελτιστοποίησης της κεραίας, μέσω προσομοίωσης της αντίστασης εισόδου της ώστε να επιτευχθεί προσαρμογή στο φορτίο.

Στο τέλος του κεφαλαίου παρουσιάζονται τα αποτελέσματα προσομοίωσης της επίδοσης της κεραίας. Συγκεκριμένα παραθέτεται η προσομοίωση της εξασθένησης από επιστροφή σε συνάρτηση με την συχνότητα, των δισδιάστατων και τρισδιάστατων διαγραμμάτων ακτινοβολίας, της κατευθυντικότητας, του κέρδους και της απόδοσης της κεραίας. Δίνεται επίσης γραφικά και η κατανομή του επιφανειακού ρεύματος στο ίχνος της κεραίας από όπου εξάγονται ορισμένα συμπεράσματα.

4 Κατασκευή Κεραίας

Η προτεινόμενη κεραία κατασκευάστηκε σε χάρτινο υπόστρωμα με χρήση τεχνολογίας εκτύπωσης ψεκασμού αγωγίμου μελανιού. Σε αυτό το κεφάλαιο παρουσιάζονται τα χαρακτηριστικά και η διαδικασία υλοποίησης της. Πρώτα περιγράφονται τα πλεονεκτήματα της χρήσης του χαρτιού ως υπόστρωμα για υλοποίηση μικροκυματικών κυκλωμάτων. Για να είναι εφικτή η μοντελοποίηση και η χρήση του χαρτιού ως υπόστρωμα στην σχεδίαση κεραιών είναι απαραίτητος ο διηλεκτρικός χαρακτηρισμός του. Έτσι, περιγράφεται μια μέθοδος για τον προσδιορισμό της διηλεκτρικής σταθεράς (ϵ_r) καθώς και της σταθεράς απωλειών ($\tan\delta$) του χάρτινου υποστρώματος. Η μέθοδος αυτή βασίζεται στην κατασκευή ενός δακτυλίου συντονισμού σε χάρτινο υπόστρωμα. Η εξαγωγή των διηλεκτρικών σταθερών επιτυγχάνεται από τον προσδιορισμό των συχνοτήτων συντονισμού του δακτυλίου.

Στις επόμενες παραγράφους παρουσιάζεται η τεχνολογία εκτύπωσης ψεκασμού αγωγίμου μελανιού. Στην τεχνολογία αυτή χρησιμοποιείται ένας εξειδικευμένος εκτυπωτής ο οποίος τυπώνει απευθείας το σχέδιο του κυκλώματος επάνω στο χάρτινο υπόστρωμα χρησιμοποιώντας αγωγίμο μελάνι που αποτελείται από νανοσφαιρίδια ασημιού.

Πρώτα παραθέτονται τα πλεονεκτήματα της τεχνικής αυτής σε σχέση με τις συμβατικές μεθόδους κατασκευής τυπωμένων κυκλωμάτων. Έπειτα αναλύονται τα τεχνικά χαρακτηριστικά και ο τρόπος λειτουργίας του εκτυπωτή ψεκασμού. Ο εκτυπωτής αυτός αποτελείται από ποικίλα τμήματα και ενσωματωμένα συστήματα. Συγκεκριμένα διαθέτει: 1) μεταλλική πλάκα δημιουργίας κενού αέρος για την σταθεροποίηση του υποστρώματος 2) κεφαλή εκτύπωσης που συγκρατεί το μελανοδοχείο 3) κάμερα υψηλής ανάλυσης για την επισκόπηση της περιοχής εκτύπωσης 4) κάμερα υψηλής ταχύτητας για την παρακολούθηση της εκτόξευσης των σταγονιδίων του ασημένιου μελανιού 5) πλατφόρμα καθαρισμού των κεφαλών εκτύπωσης. Πρέπει να σημειωθεί ότι ο εκτυπωτής μπορεί να χρησιμοποιήσει δύο διαφορετικούς τύπους κεφαλών εκτύπωσης. Η μια κεφαλή προσφέρει εκτύπωση υψηλής ακρίβειας ενώ η άλλη εξασφαλίζει εκτύπωση υψηλής αγωγιμότητας αλλά μικρότερης ακρίβειας.

Η διαδικασία εκτύπωσης του σχεδίου της κεραίας στο χαρτί πραγματοποιείται σε εννέα βήματα τα οποία περιγράφονται στην συνέχεια του κεφαλαίου αυτού. Ο έλεγχος του εκτυπωτή πραγματοποιείται εξ ολοκλήρου μέσω υπολογιστή και είναι σχετικά απλός. Η κεραία εκτυπώθηκε χρησιμοποιώντας και τους δύο τύπους κεφάλων εκτύπωσης και τυπώνοντας συνολικά δώδεκα στρώματα αγωγίμου μελανιού.

Στο επόμενο στάδιο της κατασκευής της κεραίας, το εκτυπωμένο πρωτότυπο θερμαίνεται σε βιομηχανικό φούρνο ακριβείας στους 100° C για 10 ώρες. Η θέρμανση της υλοποιημένης κεραίας είναι απαραίτητη ώστε να αυξηθεί η αγωγιμότητα του τυπωμένου ασημένιου μελανιού. Τέλος ένας συνδετήρας SMA συνδέεται στο άκρο της τυπωμένης γραμμής τροφοδοσίας της κεραίας. Επειδή η χρήση κολλητηριού και καλά κρίνεται απαγορευτική λόγω της χαμηλής αντοχής του χαρτιού στις υψηλές θερμοκρασίες, χρησιμοποιείται μια ειδικής μορφής ασημένια αλοιφή που εξασφαλίζει μηχανική και ηλεκτρική σύνδεση του ακροδέκτη με την κεραία.

Τέλος η κεραία υλοποιείται και με την μέθοδο κατασκευής επικόλλησης χάλκινης ταινίας. Η διαδικασία αυτής της κατασκευαστικής τεχνικής είναι σχετικά απλή και πραγματοποιείται σε τρία βήματα: 1) το χάρτινο υπόστρωμα επικαλύπτεται με χάλκινη ταινία. 2) το επιθυμητό σχήμα της κεραίας χαράσσεται πάνω στην χάλκινη ταινία 3) τα κομμάτια του χαλκού που αποτελούν το συμπληρωματικό τμήμα της κεραίας αφαιρούνται με αποτέλεσμα να απομείνει του επιθυμητό ίχνος της κεραίας από χάλκινη ταινία.

5 Πειραματικά Αποτελέσματα

Η επίδοση της προτεινόμενης κεραίας μετρήθηκε πειραματικά και τα αποτελέσματα των μετρήσεων παρουσιάζονται σε αυτό το κεφάλαιο. Συγκεκριμένα μετρήθηκε η εξασθένηση από επιστροφή σε συνάρτηση με την συχνότητα και το κέρδος της κεραίας.

Στην αρχή του κεφαλαίου αναλύεται η διαδικασία της μέτρησης της εξασθένησης από επιστροφή της κεραίας. Πρώτα τονίζεται ότι η μέτρηση της εξασθένησης από επιστροφή πρέπει να γίνει έμμεσα μέσω της μέτρησης της αντίστασης εισόδου της κεραίας. Η μέτρηση της αντίστασης εισόδου επιτυγχάνεται με την βοήθεια ενός Vector Network Analyzer. Έπειτα αναφέρονται τα όργανα των μετρήσεων και περιγράφεται η πειραματική διάταξη. Αφού παρουσιαστεί η διαδικασία αντιστάθμισης του Vector Network Analyzer, παραθέτονται οι πειραματικές μετρήσεις της αντίστασης εισόδου της κεραίας. Στο τέλος της παραγράφου αυτής παρουσιάζονται τα αποτελέσματα της εξασθένησης από επιστροφή της κεραίας σε συνάρτηση με την συχνότητα, τόσο των πειραματικών μετρήσεων όσο και της προσομοίωσης για σύγκριση των αποτελεσμάτων.

Στο τέλος του κεφαλαίου περιγράφεται η διαδικασία μετρήσεων του κέρδους της κεραίας. Οι μετρήσεις κέρδους επιτυγχάνονται με την δημιουργία μια ασύρματης ζεύξης όπου πομπός είναι η πρωτότυπη κεραία και δέκτης μια άλλη κεραία γνωστών χαρακτηριστικών. Ένας Vector Signal Generator τροφοδοτεί τον πομπό με ένα σήμα συχνότητας ίση με την συχνότητα λειτουργίας της κεραίας και ένας Real Time Spectrum Analyzer συνδέεται στον δέκτη για την μέτρηση του λαμβανομένου σήματος.

Αφού περιγραφούν τα όργανα και η διάταξη του πειράματος επαληθεύεται ότι ο δέκτης βρίσκεται στο μακρινό πεδίο της προς μέτρησης κεραίας ώστε τα αποτελέσματα των μετρήσεων να είναι σωστά. Έπειτα παρουσιάζεται ο τρόπος

ρύθμισης των οργάνων, προσδιορίζονται οι απώλειες της ασύρματης ζεύξης και πραγματοποιείται η μέτρηση της ισχύος λήψης στον δέκτη μέσω του Spectrum Analyzer. Μετά εφαρμόζεται το μοντέλο ελευθέρου χώρου για την ασύρματη ζεύξη, αφού επαληθευθεί ότι κανένα εμπόδιο δεν βρίσκεται μέσα στην 1^η ζώνη Fresnel της ζεύξης. Έτσι χρησιμοποιώντας την εξίσωση του Friis υπολογίζεται η πειραματική τιμή του κέρδους της κεραίας η οποία συμφωνεί με την προσομοίωση.

Στο τέλος του κεφαλαίου παρουσιάζεται μια σύνοψη όλων των αποτελεσμάτων, τόσο των πειραματικών μετρήσεων όσο και της προσομοίωσης Συγκρίνοντας τα δεδομένα αυτά επιβεβαιώνεται ότι η κεραία ικανοποιεί όλες τις απαιτήσεις και προδιαγραφές που ορίστηκαν στο κεφάλαιο 3. Συνεπώς η χρήση της τεχνολογίας εκτύπωσης ψεκασμού αγωγίμου μελανιού επαληθεύεται ως μια αξιόπιστη και αποδοτική κατασκευαστική τεχνική για την υλοποίηση κεραίων σε χάρτινο υπόστρωμα.

6 Συμπεράσματα και Μελλοντική Εργασία

Στο κεφάλαιο αυτό παρουσιάζονται τα συμπεράσματα από την διεξαγωγή αυτής της εργασίας. Πρώτα γίνεται μια ανακεφαλαίωση των θεμάτων που αναλύθηκαν και έπειτα αναφέρονται τα χαρακτηριστικά της γεωμετρίας της κεραίας που αποδείχθηκαν αποτελεσματικά τόσο στον σχεδιασμό της όσο και στην υλοποίηση της. Η κατασκευή μονοπόλου μονού στρώματος, η χρήση επιπέδου γης αλλά και η εισαγωγή οπών για την βελτιστοποίηση και προσαρμογή της κεραίας στο φορτίο αποτέλεσαν σημαντικά πλεονεκτήματα της ως προς άλλες γεωμετρίες.

Στην συνέχεια του κεφαλαίου αναφέρονται άλλες πιθανές μετρήσεις για τον περαιτέρω χαρακτηρισμό της τυπωμένης κεραίας όπως: πειραματική μέτρηση του διαγράμματος ακτινοβολίας της κεραίας: διερεύνηση της επίδοσής της όταν βρίσκεται κοντά σε διάφορα υλικά. Στο τέλος του κεφαλαίου αναφέρονται ιδέες για περαιτέρω βελτιστοποίηση της κεραίας όπως: μείωση του μεγέθους της κεραίας, κατασκευή γραμμής τροφοδοσίας με μεγαλύτερο διάκενο, διερεύνηση διαφορετικού συνδυασμού οπών, διερεύνηση διαφορετικών ειδών κεραίας, βελτίωση της μεθόδου προσαρμογής.

TABLE OF CONTENTS

CHAPTER 1

Introduction.....	25
--------------------------	-----------

CHAPTER 2

Background and Related Work.....	27
---	-----------

2.1	RFID Technology	27
2.1.1	RFID system overview	27
2.1.2	Applications	27
2.1.3	Transponder types	29
2.2	RFID Transponder Characteristics	31
2.2.1	Operating principles	31
2.2.1.1	Inductive Coupling.....	31
2.2.1.2	Electromagnetic backscatter	32
2.2.2	Operating frequency ranges	34
2.3	RFID Tag Antenna Design	35
2.3.1	Dipole and monopole antenna theory	35
2.3.1.1	$\lambda/2$ dipole.....	35
2.3.1.2	$\lambda/4$ monopole.....	36
2.3.2	Antenna design process.....	37
2.3.3	Examples of RFID antennas	38
2.4	State of the Art in RFID.....	40
2.4.1	Miniaturized transponders	41
2.4.2	Flexible, paper based transponders	41
2.4.3	Tags with power scavenging circuits.....	42
2.4.4	Other developments in RFID	43

CHAPTER 3

Antenna Design	45
-----------------------------	-----------

3.1	Introduction.....	45
3.2	Impedance Matching.....	45
3.3	Antenna Requirements.....	48
3.4	Antenna Configuration.....	49
3.4.1	Antenna geometry details	49
3.4.2	Ground plane and monopole antenna advantages.....	51
3.4.3	Feeding line.....	52
3.4.4	Radiation element	52
3.5	Design Process	52
3.5.1	Planar rectangular monopole antenna.....	53
3.5.2	Impedance matching	56
3.6	Simulation Results	62
3.6.1	Input impedance.....	62
3.6.2	Return loss	63

3.6.3	Radiation pattern	63
3.6.4	Directivity, Efficiency and Gain simulation	65
3.6.5	Current distribution	67
CHAPTER 4		
Prototype Fabrication.....		69
4.1	Introduction.....	69
4.2	Paper Substrate Advantages.....	69
4.3	Dielectric Characterization of the Paper Substrate	70
4.3.1	Dielectric constant	72
4.3.2	Dielectric loss tangent.....	73
4.4	Conductive Inkjet Printing Technology.....	74
4.4.1	Inkjet printing technology advantages	75
4.4.2	Inkjet printer details	75
4.4.3	Silver ink and inkjet system.....	79
4.4.4	Antenna printing process	80
4.4.5	Curing and assembly.....	82
4.5	Copper Tape Fabrication.....	85
CHAPTER 5		
Experimental Results and Discussion		87
5.1	Introduction.....	87
5.2	Antenna Return Loss Measurement.....	87
5.2.1	Experimental setup.....	87
5.2.1.1	Vector network analyzer calibration	88
5.2.1.2	Input impedance measurement	88
5.2.2	Input impedance measurement results	89
5.2.3	Return loss calculation	91
5.3	Antenna Gain Measurement	92
5.3.1	Experimental setup.....	92
5.3.2	Measurement process and results.....	95
5.3.3	Antenna gain calculation.....	96
5.4	Summary and Discussion.....	98
CHAPTER 6		
Conclusions and Future Work		99
6.1	Conclusions.....	99
6.2	Directions for Future Work.....	100
6.2.1	Antenna further experimental measurements	100
6.2.2	Antenna further optimization.....	100
APPENDIX.....		103
REFERENCES.....		105

TABLE OF FIGURES

CHAPTER 2

Figure 2.1 Reader and transponder in an RFID system	27
Figure 2.2 Various RFID applications	28
Figure 2.3 Wireless Sensor Network Node.....	29
Figure 2.4 Wearable Electronics	29
Figure 2.5 Operation principle of an inductively coupled transponder	31
Figure 2.6 Example of an inductively coupled passive RFID transponder used in London underground transportation system. Left: Oyster card casing. Right: RFID transponder inside Oyster card.....	32
Figure 2.7 Operating principle of a backscatter transponder	32
Figure 2.8 Analysis of the backscatter operating principle of a passive RFID tag.....	33
Figure 2.9 Intellitag card and passive UHF RFID transponder that operates via backscatter.....	33
Figure 2.10 Available RFID operation frequencies in the RF band.	34
Figure 2.11 Frequency allocations of UHF RFID tags	34
Figure 2.12 A theoretical $\lambda/2$ dipole antenna	35
Figure 2.13 Radiation patterns of a $\lambda/2$ dipole.....	35
Figure 2.14 Theoretical $\lambda/4$ monopole antenna.....	36
Figure 2.15 Radiation patterns of an ideal $\lambda/4$ monopole antenna.....	36
Figure 2.16 Radiation patterns of a $\lambda/4$ monopole antenna with finite ground plane.....	37
Figure 2.17 RFID tag antenna design process	37
Figure 2.18 Cross-section of a single layer, printed RFID antenna.....	38
Figure 2.19 Geometry of a meandered RFID dipole antenna.....	39
Figure 2.20 Examples of planar monopole RFID antennas. Left: Rectangular monopole configuration. Middle: Rectangular slotted monopole configuration. Right: Meander line monopole configuration.....	40
Figure 2.21 Different types and configurations of RFID antennas.....	40
Figure 2.22 Coil-on-chip miniaturized RFID transponders.....	41
Figure 2.23 RFID-enabled wireless sensor platform on paper substrate using inkjet printing technology	42

CHAPTER 3

Figure 3.1 Block diagram of an active UHF RFID tag.....	46
Figure 3.2 Antenna-Load equivalent circuit	46
Figure 3.3 Antenna impedance and load impedance as functions of frequency for a typical RFID tag.....	48
Figure 3.4 Configuration of the proposed printed monopole antenna	50
Figure 3.5 Parts of the proposed monopole antenna.....	51
Figure 3.6 Planar rectangular UHF monopole antenna configuration.....	53
Figure 3.7 Return loss versus frequency of the planar UHF rectangular monopole antenna	55
Figure 3.8 Normalized radiation patterns of the planar UHF rectangular monopole antenna	55

Figure 3.9 Simulated input impedance for different lengths l_2 of the slot with $l_1=15\text{mm}$	57
Figure 3.10 Simulated input impedance for different lengths l_2 of the slot with $l_1=25\text{mm}$	58
Figure 3.11 Simulated input impedance for different lengths l_2 of the slot with $l_1=35\text{mm}$	59
Figure 3.12 Simulated input impedance for different lengths l_2 of the slot with $l_1=45\text{mm}$	60
Figure 3.13 Simulated input impedance at the operating frequency 904.5MHz versus slot length l_2 with $l_1=40\text{mm}$	61
Figure 3.14 Simulated input impedance vs frequency of the proposed UHF monopole antenna.....	62
Figure 3.15 Frequency response of the return loss of the proposed antenna.....	63
Figure 3.16 Two dimensional normalized radiation patterns of the proposed monopole antenna.....	64
Figure 3.17 Three dimensional normalized radiation pattern of the proposed antenna.....	65
Figure 3.18 Directivity versus frequency of the proposed monopole antenna.....	66
Figure 3.19 Simulated current distribution of the proposed antenna at the operation frequency of 904.5MHz.....	67

CHAPTER 4

Figure 4.1 Reel-to-reel mass paper production.....	70
Figure 4.2 Magnified droplet of water sitting on a paper substrate.....	70
Figure 4.3 Inkjet printed antenna on flexible paper substrate.....	70
Figure 4.4 Wearable RFID tag on wrist for medical monitoring.....	70
Figure 4.5 Microstrip ring resonator configuration diagram.....	71
Figure 4.6 Photo of fabricated microstrip ring resonators and TRL lines bonded to SMA connectors.....	72
Figure 4.7 Measured and simulated S_{21} results of ring resonator configuration A.....	72
Figure 4.8 Extracted relative dielectric constant ϵ_r of paper versus frequency.....	73
Figure 4.9 Paper loss tangent $\tan\delta$ versus frequency measured with the microstrip ring resonator method and the TL method.....	74
Figure 4.10 Dimatix Materials Inkjet Printer DMP-2800 Series.....	75
Figure 4.11 Different parts of the inkjet printer.....	76
Figure 4.12 Inkjet-printer cartridge.....	77
Figure 4.13 Image of a printed silver ink conductive trace captured by the fiducial camera.....	77
Figure 4.14 Image captured with the drop watcher camera that depicts the cartridge nozzles while jetting silver ink drops.....	78
Figure 4.15 Nano-sized silver ink.....	79
Figure 4.16 Inkjet mechanism of silver ink droplets sprayed from the cartridge nozzles.....	79
Figure 4.17 Prototype of the conductive inkjet-printed antenna.....	81
Figure 4.18 Multiple silver ink layers printed using the 10pL inkjet cartridge.....	81
Figure 4.19 Close-up image of the CPW transmission line printed with the 1pL inkjet cartridge, showing the gap between the signal strip and the ground planes.....	81
Figure 4.20 Test Equity FS series industrial oven for performing curing of the prototype antenna.....	82
Figure 4.21 Images of a layer of printed silver ink before (top) and after (bottom).....	83

Figure 4.22 Prototype of the fabricated inkjet printed antenna on paper substrate with attached SMA connector	84
Figure 4.23 Close-up image of the SMA connector attached with silver epoxy to the printed silver antenna trace	84
Figure 4.24 Prototype of the copper tape fabricated antenna with attached SMA connector.....	85

CHAPTER 5

Figure 5.1 Vector network analyzer calibration setup	88
Figure 5.2 Antenna input impedance measurement setup	89
Figure 5.3 Simulated and measured input impedance versus frequency of the inkjet-printed and copper tape fabricated antenna	90
Figure 5.4 Measured and simulated frequency response of the return loss of the inkjet printed and copper tape fabricated antenna	91
Figure 5.5 Gain measurement experimental setup.....	93
Figure 5.6 Prototype antenna (transmitter) and vector signal generator setup	93
Figure 5.7 AN-400 RFID reader antenna (receiver) and real time spectrum analyzer setup	94
Figure 5.8 Received power at the AN-400 RFID reader antenna (receiver) terminals	96
Figure 5.9 First Fresnel zone cross section at the middle point of the wireless link setup between the prototype antenna (transmitter) and the reader antenna (receiver).	97

LIST OF TABLES

Table 3.1 Antenna Requirements.....	49
Table 3.2 Simulated monopole antenna parameters at the centre frequency of 904.5MHz	66
Table 5.1 Simulated and measured input impedance of the proposed antenna at the operation frequency of 904.5MHz.....	89
Table 5.2 Antenna return loss comparison between experimental and simulated results	92
Table 5.3 Comparison of simulated and experimental results with the design requirements.....	98

CHAPTER 1

Introduction

RFID (Radio Frequency Identification) is an emerging compact wireless technology for the identification of objects, that utilizes electromagnetic waves for transmitting and receiving information stored in a tag or transponder to/from a reader. RFID has many advantages compared to conventional ways of identification (e.g. barcodes), such as higher read range and no requirement for line of sight. This technology has become indispensable in a wide range of applications, such as electronic toll collection, access control, asset identification and retail item management.

The demand for low cost and efficient RFID tags with high read range and sensing capabilities has witnessed a vast increase in the last couple of years, due to the proliferation of the applications mentioned above and the development of other state of the art areas, such as ubiquitous wireless sensor networks. For these reasons active (with battery) RFID tags operating in the UHF frequency band see the widest use, due to their higher read range, larger memory capacity and higher data transfer rate compared to lower frequency passive (batteryless) tags. An active transponder is composed of three parts. An antenna, an Integrated Circuit (IC) that stores the identification data and other electronic components and circuits, such as power sources and sensors. The antenna is the actual element that transmits and receives the electromagnetic signals and as a result antenna design is the most critical part in the transponder's performance.

RFID antenna design faces many challenges: 1) size and flexibility; antennas have to be compact and flexible so that practical tags can be implemented 2) cost; RFID antennas have to be extremely inexpensive in order to be realized in mass production amounts 3) efficiency; maximum efficiency is demanded from RFID antennas to increase the range and the reliability of the transponders 4) Global UHF RFID band operability; each country has its own frequency allocation for RFID and therefore a tag has to operate globally 5) Integration with electronics; in order to maximize the power transfer from the antenna to the IC the RFID antenna has to be matched to its load without at the same time causing interference with the rest electronics of the tag.

This thesis presents a novel conductive inkjet-printed monopole antenna on flexible, low cost paper substrate for RFID applications. The design and fabrication of the proposed antenna demonstrates the feasibility of tackling the above challenges, enabling the integration of the antenna with an active RFID transponder. The structure of this thesis is organized as follows:

In Chapter 2 an overview of RFID systems is presented. First, the characteristics, operating principles and applications of RFID tags are discussed. Then a step by step RFID antenna design process is outlined and different antenna configurations are given as examples. In the end of this chapter the state of the art in RFID technology is highlighted.

Chapter 3 details the design of the proposed RFID antenna. First the importance of impedance matching of the antenna to the tag's load is emphasized. The antenna

requirements are determined and summarized. Then the antenna configuration is explained, while highlighting the advantages of the use of the ground plane in the proposed monopole geometry. Moreover, the performance of the proposed antenna is simulated while it is optimized to achieve the desired design goals

In Chapter 4 the fabrication of the presented antenna is studied. Paper is proposed as a low cost, flexible and environmentally friendly substrate material for RFID antenna implementation. Conductive inkjet-printing technology is utilized to print the antenna on to the paper substrate and therefore the characteristics and the fabrication process of this technique are analyzed.

The proposed antenna is experimentally tested and the obtained results are discussed in Chapter 5. Return loss and gain measurements were carried out to verify the antenna performance. The setup of each measurement is explained and the experimental results are compared to the simulation showing good agreement.

Finally in Chapter 6 the compiled work is summarized and conclusions are presented. Further experimental measurements of the proposed antenna and possible optimization approaches are proposed as future work.

CHAPTER 2

Background and Related Work

2.1 RFID Technology

2.1.1 RFID system overview

Radio Frequency Identification (RFID) is the automatic identification of tagged objects using RF signals [1]. The basic structure of an RFID system always consists of two components, as shown in Figure 2.1.

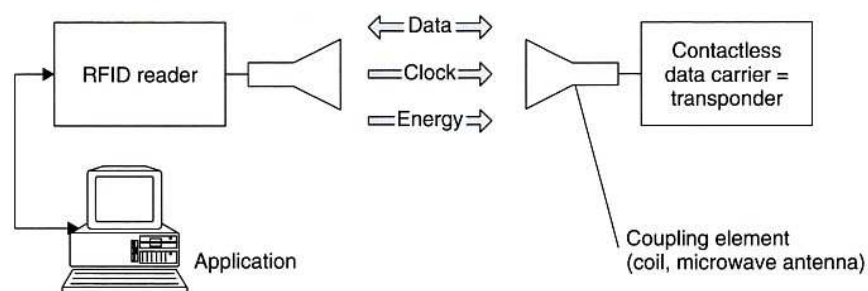


Figure 2.1 Reader and transponder in an RFID system

- The transponder which is located on the object to be identified and carries digital data
- The interrogator or the reader, which communicates with the tag and uses radio waves to capture the stored data

The reader typically contains an RF module (transmitter and receiver), a control unit and a coupling element to the transponder. It can be fixed or handheld and usually is fitted with an additional interface in order to forward the received data to another system.

The transponder consists of an integrated circuit (IC), which stores the actual data and a coupling element, which can be either an inductive coil or an antenna (e.g. dipole monopole, etc). The type of coupling element that is being used depends on the operating frequency of the RFID system and on the type of the transponder. In addition, according to the tag type and operating principle the transponder may also contain other electronic components. More details about the characteristics of an RFID tag will be discussed in Section 2.2.

2.1.2 Applications

Currently RFID finds a wide range of application in industry, supply chain, security, tracking and other expanding areas [3].

Some applications of RFID are, as shown in Figure 2.2:

Applications

- Supply chain
- Shipping
- Anti theft
- Access control
- Wireless pay systems
- Passport security
- Animal identification
- Libraries
- Human implants

Industries

- Aviation (baggage tracking, passenger registration, parts)
- Automotive
- Pharmaceutical
- Retail
- Inventory control
- Transportation
- Food industry
- Cargo management

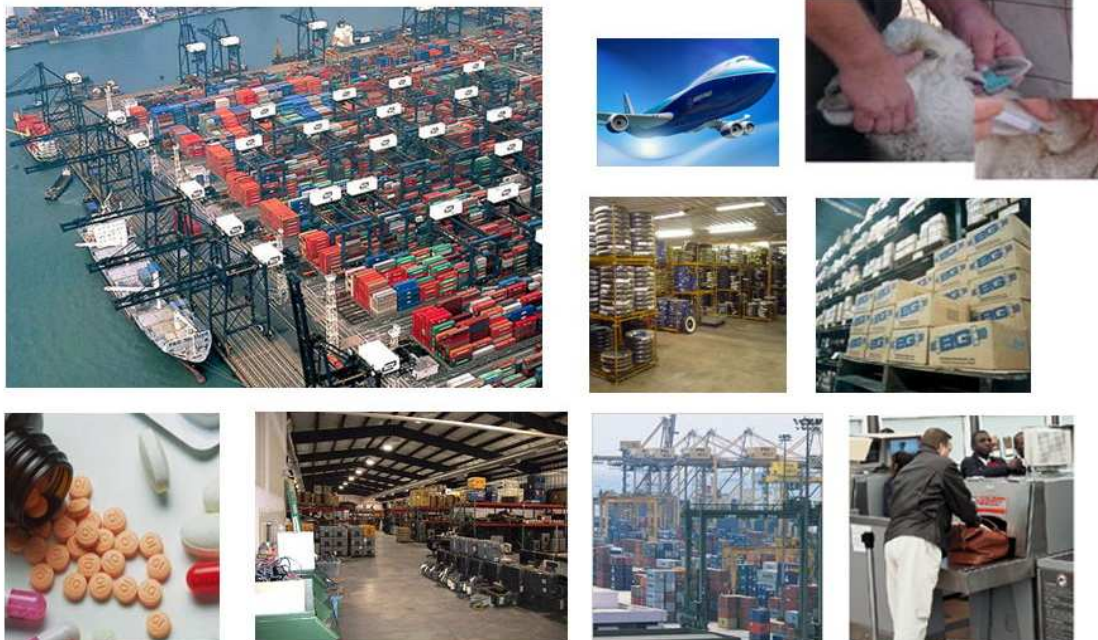


Figure 2.2 Various RFID applications

The use of RFID has shown a dramatic improvement in efficiency, productivity, security, organization, management and quality of services in the above industries. In fact it is becoming one of fastest growing sectors of the radio technology industry and conquers a bigger piece of the automatic identification market every day.

Furthermore, the exponential advancement in RFID technology and the numerous new insights in the subject can make feasible the realization of ubiquitous ad hoc wireless sensor networks and wearable electronics.

A wireless sensor network (WSN) consists of spatially distributed autonomous devices, as shown in Figure 2.3 that incorporate sensors to cooperatively monitor physical or environmental conditions at different locations. Inexpensive, low power consumption and flexible RFID tags can tackle the 3 major challenges that at present WSN face and are: cost, size and power consumption. In this way the beginning of WSN application in hot areas such as environmental monitoring and healthcare can be realized.

Wearable electronics utilize the flexibility, low power consumption, small size and cost that advancements in RFID promise for advanced military applications such as health monitor platforms on clothes, as shown in Figure 2.4.



Figure 2.3 Wireless Sensor Network Node



Figure 2.4 Wearable Electronics

2.1.3 Transponder types

RFID tags are differentiated based on the existence and the operation of a power supply [1]. There are three types of tags: passive, active and semi-passive:

Passive

Passive transponders are usually comprised of three elements: The IC or chip, the antenna or coil and the substrate on/in which they are integrated. Passive tags do not have their own power supply (e.g. battery) and therefore all power required for the operation of the transponder must be drawn from the (electric/magnetic) field of the reader. The antenna is used to absorb RF waves from the reader's signal and use the scavenged power to both turn on the IC and transmit the stored data back to the reader. Therefore the tag is only activated and can be read when it is near the reader.

Passive tags incorporate 3 very important advantages for RFID technology. First, they practically have an unlimited life time, since they contain no battery. Second they

are usually compact in size and can be flexible so that they can be easily attached to objects. Third, they have very low cost, approximately 5 cents per tag, and are easy to fabricate in mass production. However some of their disadvantages are that they have a small read range which varies from some centimeters to 10 meters and have a small memory capacity (usually 96bits).

Active

Unlike passive RFID tags, active RFID tags have their own internal power source, which is used to both power the IC and at the same time broadcast the response signal to the reader. This enables active tags to transmit at higher power levels than passive tags, allowing them to be more robust in "RF challenged" environments and have a very high read range, which varies from 30 meters to more than 300 meters. On the other hand they are larger in size than passive tags and have a much higher fabrication cost. Another disadvantage of active tags is the fact that the battery is depleted at some point and has to be replaced, which might prove out to be very challenging.

In addition, active RFID tags can be integrated with other electronic components. On-board electronics may consist of sensors, microprocessors and power amplifiers, all of which are powered by the tag's on-board power source. The electronics allow active RFID tags to be used in a wider range of applications than passive tags. For example, perishable food products may be tagged with sensors that collect data that can then be used to determine expiry dates and warn the end user that the item may be spoiled. Even though many products have expiration dates printed on them, these dates are valid only if the product is stored under the optimal conditions (temperature, humidity, exposure to light, etc.) for that type of product. Thus, the product may expire before the printed date if it is not stored properly. An RFID tag equipped with a temperature sensor might be able to predict the actual expiration date of a carton of milk, for example, which may be very different from the printed date.

Semi-Passive

Semi-passive tags are similar to active tags in the way that they have their own power source, but the battery only powers the microchip and is not used for transmitting the signal back to the reader. The communication with the reader is performed in the same manner as in passive tags, which will be described in Section 2.2.1.1. Semi-passive tags incorporate a much smaller battery than active tags and have at the same time a longer life time. However their read range is lower than active tags, but higher than passive tags.

2.2 RFID Transponder Characteristics

2.2.1 Operating principles

An RFID transponder can exchange information with the reader in two basic ways: Either via inductive coupling or via electromagnetic backscatter [2]. These two operating principles are described below:

2.2.1.1 Inductive Coupling

In inductively coupled RFID systems the antenna of both the transponder and the reader is a coil. Inductively coupled transponders are almost always passive and consist of the IC, which stores the data and a coil that functions as the antenna and is directly attached to the IC. The coil of the transponder and the coil of the reader are coupled by the generated changing magnetic flux, much like a transformer, as shown in Figure 2.5.

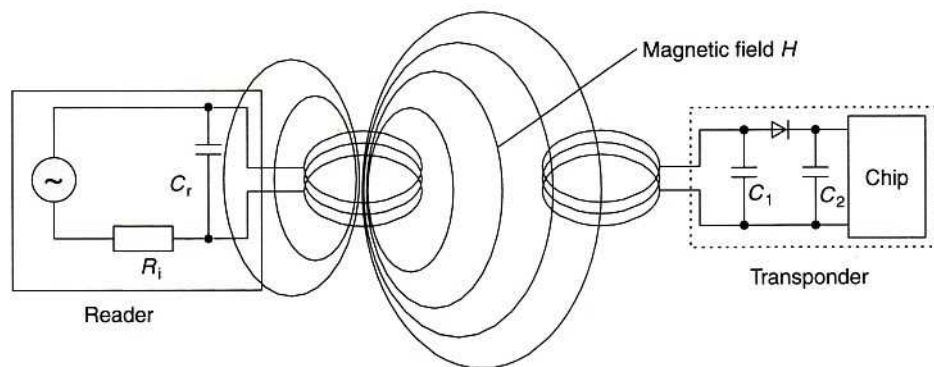


Figure 2.5 Operation principle of an inductively coupled transponder

The operation frequency of inductively coupled transponders is less than 100MHz (usually 13.56MHz) and therefore the corresponding wavelength at these frequencies is many times larger than the distance between the tag and the reader ($\lambda=22.1\text{m}$ for 13.56MHz). As a result, an inductively coupled tag operates always in the near field of the reader. The near field of an antenna is reactive and stores energy in the volume around it. This is the reason why a coil is used as the coupling element.

Inductively coupled passive tags are very easy to fabricate and have a very low cost, but at the same time a very short range of less than 1m because the field energy decreases proportionally to $\frac{1}{r^3}$ (where r is the distance from the tag). These types of tags are widely used in contactless smart cards in transportation as shown in Figure 2.6 below:

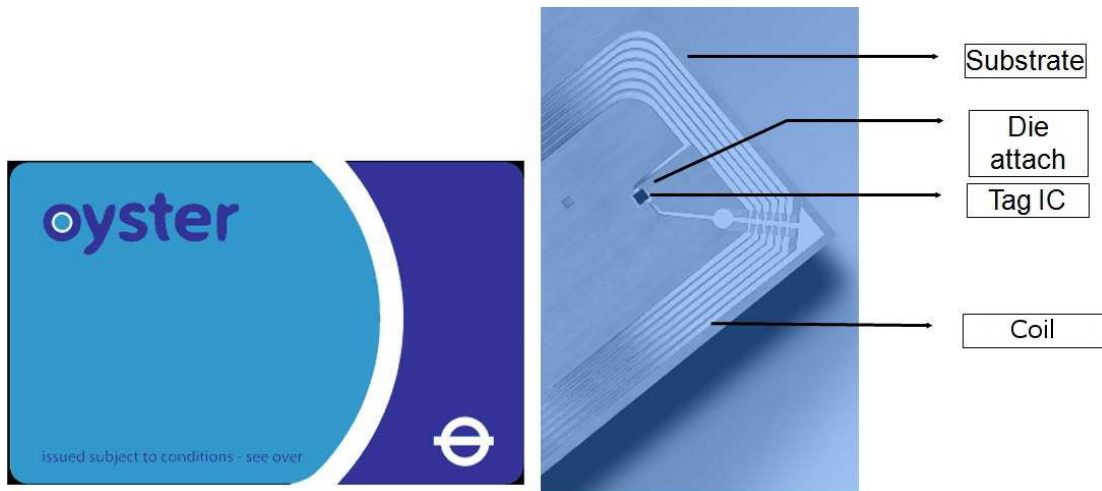


Figure 2.6 Example of an inductively coupled passive RFID transponder used in London underground transportation system. Left: Oyster card casing. Right: RFID transponder inside Oyster card.

2.2.1.2 Electromagnetic backscatter

RFID tags that communicate with the reader via backscatter consist always of an antenna instead of a coil which can be a dipole, monopole or other. The operating frequency is higher than 100MHz and therefore the corresponding wavelength is small ($\lambda=30\text{cm}$ for $f=1\text{GHz}$). As a result backscatter transponders operate in the far field of the reader, since the near-far field boundary is $\lambda/2\pi$. The reader antenna radiates travelling waves in its far field that carry power away from the antenna and are received as TEM waves from the tag's antenna. The tag's antenna reflects this energy back to the reader establishing in this way the two way communication as illustrated in Figure 2.7

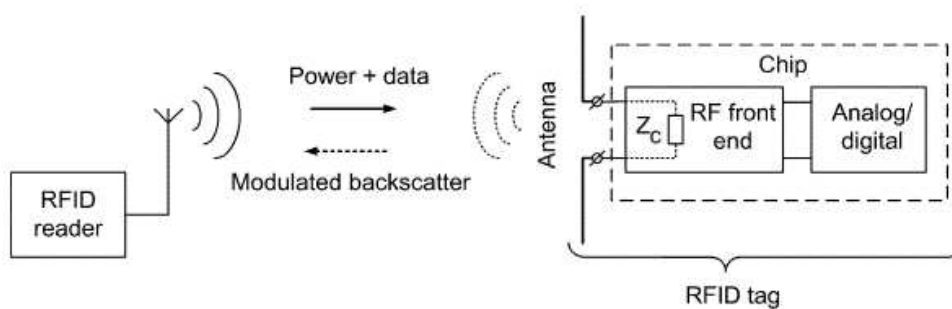


Figure 2.7 Operating principle of a backscatter transponder

Tags that operate via backscatter can be passive or active. Passive back-scattered RFID systems operate in the following way: The reader transmits a modulated signal with periods of unmodulated carrier, which is received by the tag antenna. The RF voltage developed on antenna terminals during unmodulated period is converted to dc. This voltage powers up the chip, which sends back the information by varying its

front end complex RF input impedance, modulating in this way the back-scattered signal. The passive backscatter operation principle is detailed in Figure 2.8.

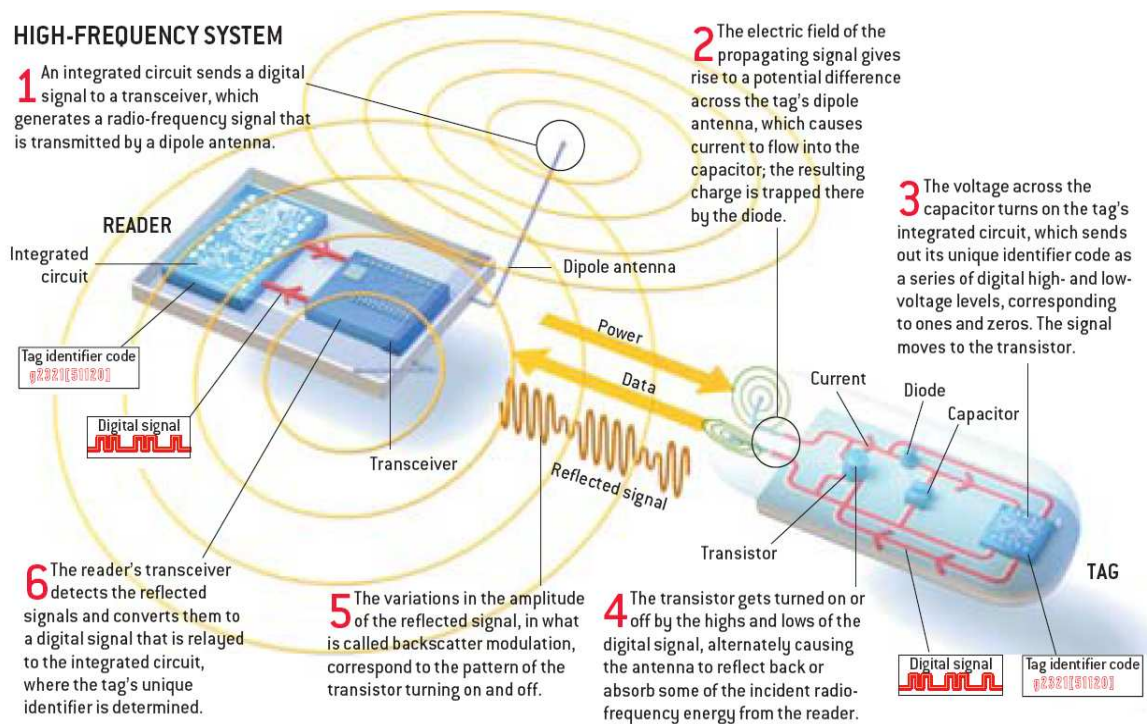


Figure 2.8 Analysis of the backscatter operating principle of a passive RFID tag

Passive backscattered tags are as easy to fabricate have the same low cost as inductively coupled tags. However they feature a higher read range that varies from 3m to 10m. An example of a passive backscattered transponder operating in the UHF frequency range [11] is illustrated in Figure 2.9.

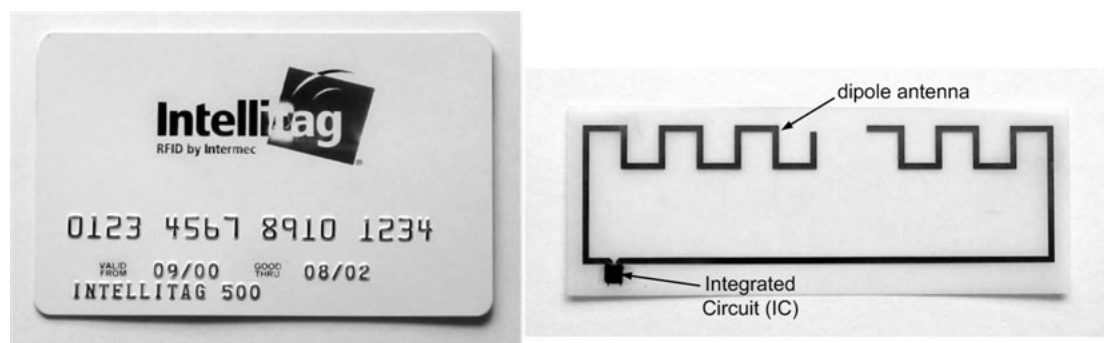


Figure 2.9 Intellitag card and passive UHF RFID transponder that operates via backscatter

In the case of an active tag that operates via backscattering, the signal from the reader is used only for activating the tag or programming it. The tag's integrated power source is responsible for powering up the IC and sending a signal back to the reader.

2.2.2 Operating frequency ranges

RFID systems are operated in a wide range of differing frequencies, as we have described. The operating frequencies of RFID transponders are summarized in Figure 2.10.

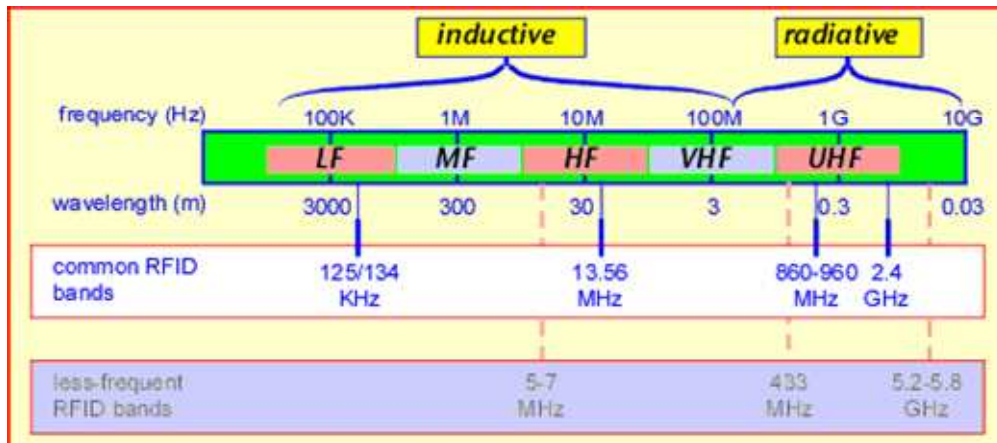


Figure 2.10 Available RFID operation frequencies in the RF band.

Although RFID systems operate in many frequency ranges, tags that operate in the UHF frequency band have received a great interest and rapid development in the last years and see the widest use because of their many attractive features such as:

- High read range (3m to 300m)
- Both passive and active tags can be incorporated in a system
- High data rates (40 – 640kpps)
- Already a protocol (EPC Gen-2) has been established
- Multitag tracking from a single reader (1500tags/s) is available
- Each country has its own frequency allocation shown in Figure 2.11

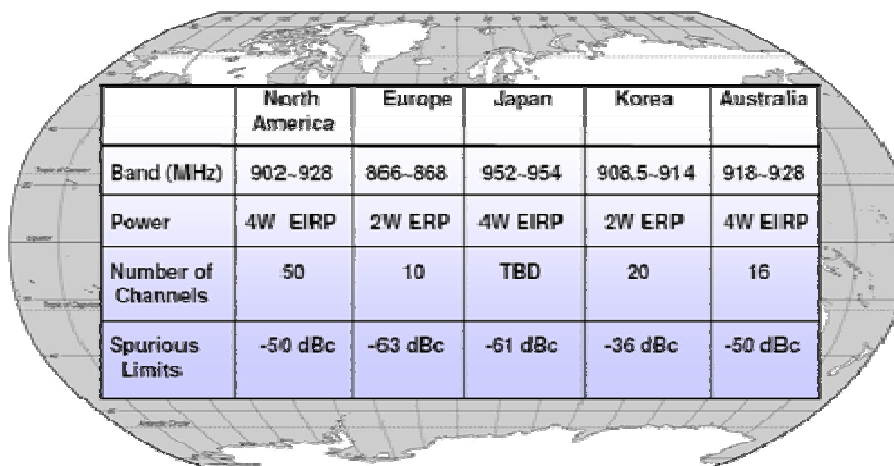


Figure 2.11 Frequency allocations of UHF RFID tags

2.3 RFID Tag Antenna Design

2.3.1 Dipole and monopole antenna theory

The most commonly used antennas in RF applications and especially in RFID are dipoles and monopoles. Therefore, some fundamental principles on the radiation characteristics of a $\lambda/2$ dipole and a $\lambda/4$ monopole antenna will be highlighted in this section [4].

2.3.1.1 $\lambda/2$ dipole

A $\lambda/2$ dipole antenna, depicted in Figure 2.12, is composed of two conductive parallel straight arms with length $\lambda/4$ each. Usually a dipole is fed by a parallel wire transmission line in its midpoint. The length (d) of this antenna is approximately equal to half of its wavelength ($d \approx \lambda/2$) in the operating frequency as the name itself suggests. In this configuration, the dipole antenna resonates when $d = 0.96\lambda/2$. This means that the complex input impedance of the dipole, which varies with frequency, becomes entirely real (resistive), and approximately 73Ω . In this specific frequency, which depends on the dipole length, the radiation of the antenna is maximized. Figure 2.13 shows the radiation pattern for the half wavelength dipole antenna.

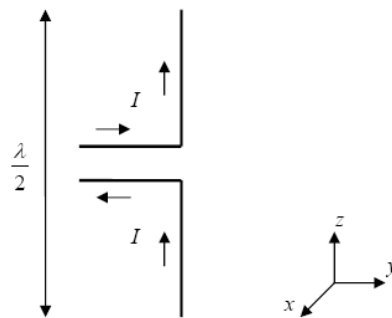


Figure 2.12 A theoretical $\lambda/2$ dipole antenna

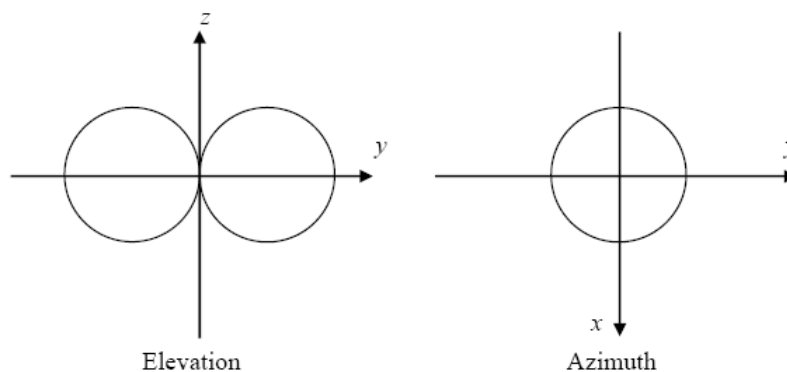


Figure 2.13 Radiation patterns of a $\lambda/2$ dipole.

2.3.1.2 $\lambda/4$ monopole

An ideal monopole antenna results from placing a $\lambda/4$ conducting wire over an infinite ground plane and applying the image theory. According to image theory if a conductor of length $d/2$ with a current I is placed vertically over an infinite ground plane, as shown in Figure 2.14, then an image of the conductor with length $d/2$ and the same direction of current flow is created symmetrically below the ground plane. As a result the combination of the element and its image radiates identically to a dipole of length d except that the radiation occurs only in the space above the ground plane. Thus, a half wavelength dipole can be approximated by a quarter wavelength monopole (with $d/2=\lambda/4$). It has however to be noted, that the resonance input impedance of an ideal $\lambda/4$ monopole antenna in the same frequency is half of that of a $\lambda/2$ dipole and is approximately 37Ω . The radiation pattern of an ideal monopole antenna is depicted in Figure 2.15.

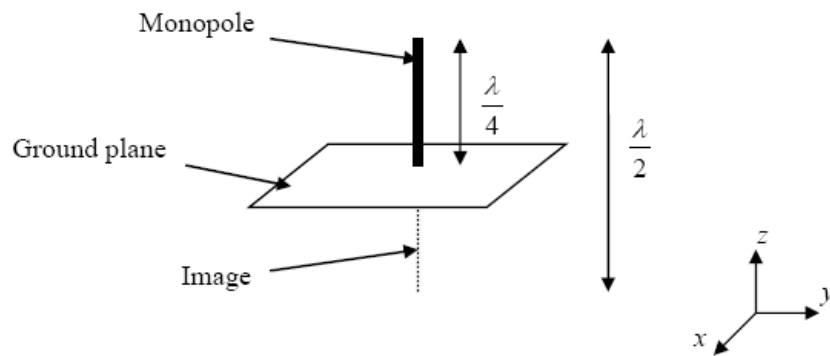


Figure 2.14 Theoretical $\lambda/4$ monopole antenna

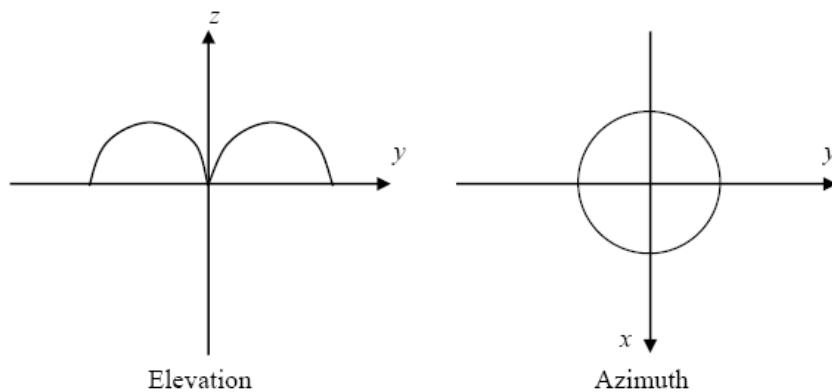


Figure 2.15 Radiation patterns of an ideal $\lambda/4$ monopole antenna

When however the ground plane of a monopole antenna is not infinite, but has dimensions comparable to the dimensions of its radiating element, the electromagnetic field is also expanded below the ground plane. As a result, the elevation radiation pattern of the monopole antenna is similar to that of the dipole as illustrated in Figure 2.16:

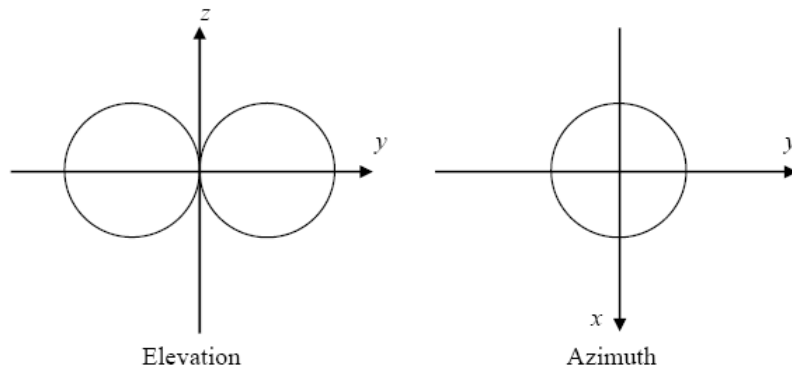


Figure 2.16 Radiation patterns of a $\lambda/4$ monopole antenna with finite ground plane

2.3.2 Antenna design process

A generalized RFID tag antenna design process [3] that will be followed in this thesis in chapters 3, 4 and 5 is illustrated on a flow chart shown in Figure 2.17.

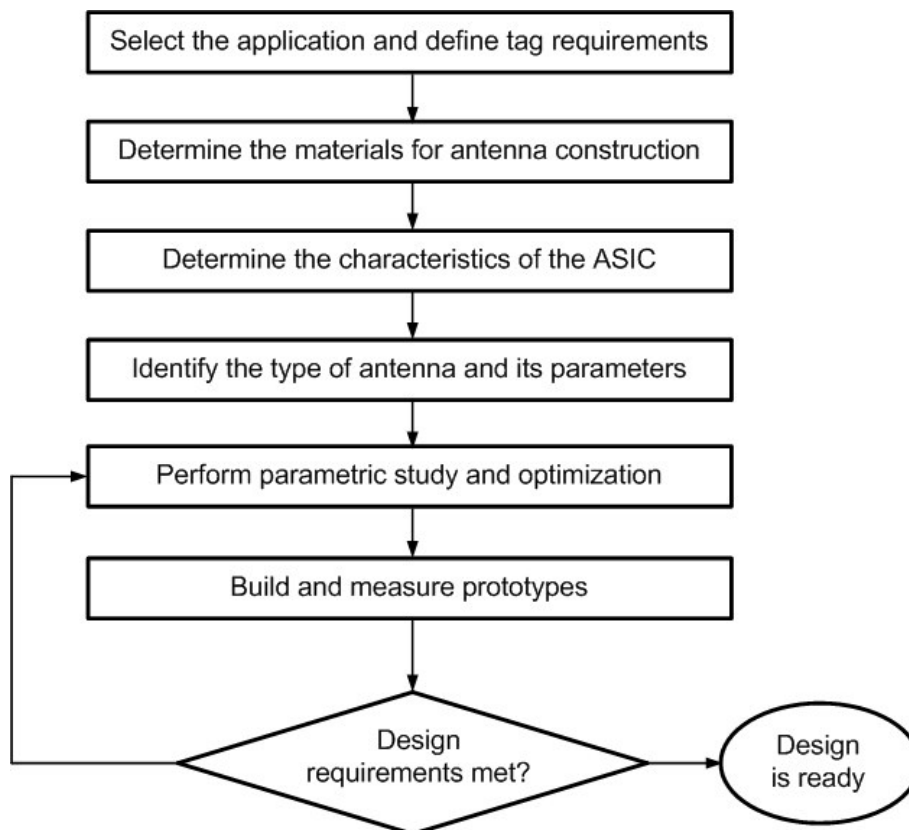


Figure 2.17 RFID tag antenna design process

First the desired application has to be determined in order to define the requirements of the tag. Parameters such as the type of the tag (passive or active), operation frequency, use of other electronics (e.g. sensors), size and cost will all be determined by the application. Second, the tag requirements are translated into the needed materials for the antenna construction. The substrate and antenna trace materials have to be carefully decided, so that the requirements can be met. Third, the characteristics of the heart of the transponder, the ASIC (Application Specific Integrated Circuit) have to be decided. The modules of which it will be composed of (e.g. power amplifiers, rectifiers, modulating circuits, etc) and the complex impedance in its output are some of the IC's characteristics. Now based on the previous requirements, the antenna characteristics can be determined. The input impedance, gain, directivity, radiation pattern, efficiency, polarization, frequency and bandwidth of operation will define the final type and design of the antenna.

The antenna performance is simulated using 3D electromagnetic modeling and simulations tools that utilize the method of moments (MoM). The antenna is first modeled and simulated. Then parametric study and optimization is performed by monitoring the antenna radiation pattern, input impedance and directivity until the desired design requirements are met in simulation. The simulation software that was used for the antenna design in this thesis was 3D EM solver Ansoft HFSS v10.0

In the last step of the design process, prototypes are built using the antenna materials that were determined and their performance is measured extensively. The obtained experimental results are compared with simulation and if the design requirements are satisfied, the antenna design is ready. Otherwise, the design is further modified and optimized until requirements are met.

2.3.3 Examples of RFID antennas

As has been described in Section 2.3.2, the design of an RFID antenna is defined by many requirements. However, most RFID antennas have some common characteristics. Printed, compact and single layer antennas are usually preferred for their ease of design, optimization and fabrication. A cross section of these types of antennas is depicted in Figure 2.18. Common substrates that are used for RFID tags, when a rigid tag is required are FR4, Duroid, and high electrical permittivity plastics. For flexible tag fabrication, common materials are PET (Polyethylene Terephthalate), LCP (Liquid Crystal Polymer) and paper. It is noted that the dielectric parameters of FR4 are $\epsilon_r=4.4$, $\tan\delta=0.01$ and of paper: $\epsilon_r=3.4$, $\tan\delta=0.08$. As for the antenna trace materials, copper, aluminum or silver ink are most commonly used.

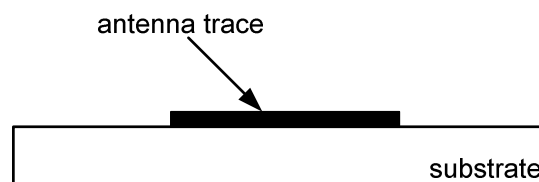


Figure 2.18 Cross-section of a single layer, printed RFID antenna

It is essential to note that 90% of RFID tag antennas are dipoles [2]. The length of a dipole antenna should be approximately $\lambda/2$. However in UHF frequencies the free space wavelength is $\lambda=0.33\text{m}$ (for $f=900\text{MHz}$), which results in too large dimensions for an RFID antenna. For this reason certain miniaturization techniques (e.g. meandering, folding) have to be followed: decreasing the antenna size while the radiation characteristics are retained.

An example of a typical antenna design for a UHF RFID passive tag [3] is depicted in Figure 2.19. Meandering allows the antenna to be compact and to provide omnidirectional performance in the plane perpendicular to the axis of the meander. The optimization of the antenna is accomplished by trimming the lengths of the meander trace bar in order to obtain the desired antenna characteristics defined by the requirements.

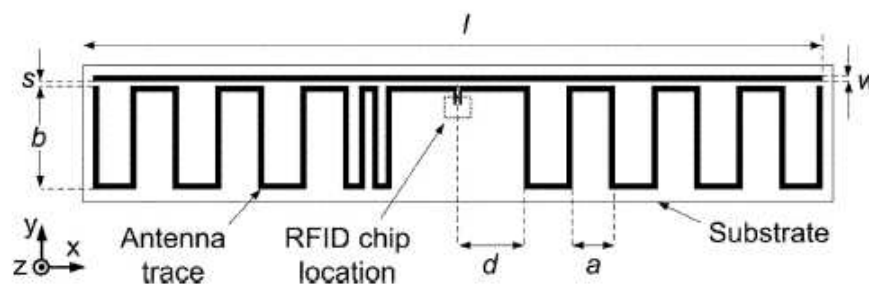


Figure 2.19 Geometry of a meandered RFID dipole antenna

Other types of RFID antennas are single layer monopole configurations. Examples of such antennas for UHF RFID applications are depicted in Figure 2.20. It is observed from Figure 2.20, that although all 3 designs are monopole antennas, they have different configurations. These antennas are composed of the same 3 elements: The radiating element, the feeding line and the ground planes. The ground plane and feeding line configuration is the same for the 3 antennas in contrast to the radiating element which is different. The antenna depicted on the left of Figure 2.20 has the simplest configuration [21]. It composes of a planar rectangular radiating element. Its dimensions and the height from the ground plane are optimized to achieve the required antenna characteristics. The radiating element of the antenna shown in the middle of Figure 2.20 is also rectangular as the former, but has two slots embedded [24]. The optimization of this type of antenna is achieved by varying the dimensions of the two slots. Finally the antenna shown on the right of Figure 2.20 composes of a meandered radiating element with an extended conductor line which is trimmed to achieve optimization [20].

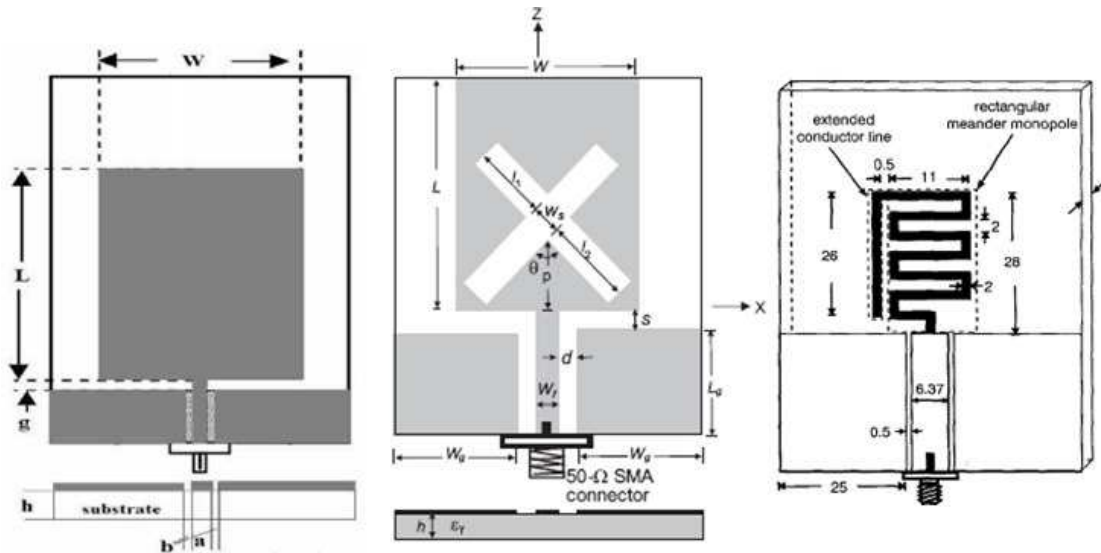


Figure 2.20 Examples of planar monopole RFID antennas. Left: Rectangular monopole configuration. Middle: Rectangular slotted monopole configuration. Right: Meander line monopole configuration.

Other antenna designs [2] are illustrated in Figure 2.21. It is observed that an antenna configuration can have any kind of shape and geometry including very arbitrary ones.

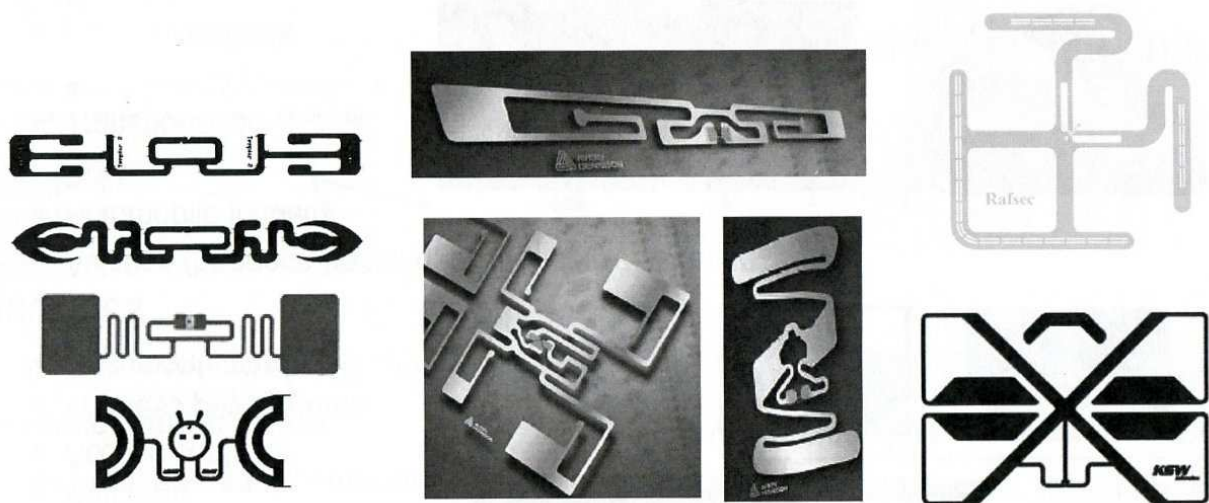


Figure 2.21 Different types and configurations of RFID antennas

2.4 State of the Art in RFID

In this section some of the latest developments in RFID technology are presented and some state of the art transponders are explained.

2.4.1 Miniaturized transponders

In the construction formats for inductively coupled passive RFID tags mentioned previously, the coil is separate from the chip and is bonded to the transponder IC in the conventional manner. An extreme miniaturization of the RFID transponder is possible by integrating the antenna coil on to the chip (coil-on-chip) [1], as shown in Figure 2.22. This is performed by a special microgalvanic process that can take place on a normal CMOS wafer. In this way the size of an entire RFID transponder can be minimized to a chip with dimensions just $3\text{mm}\times 3\text{mm}$.



Figure 2.22 Coil-on-chip miniaturized RFID transponders

2.4.2 Flexible, paper based transponders

Another very significant development in RFID tags involves integrating an entire active RFID module with temperature sensing capabilities on flexible substrates utilizing conductive inkjet printing technology [9]. In detail, flexible, low cost substrates such as LCP and paper are utilized for RFID applications. The tag antenna is fabricated on the paper substrate using direct write inkjet printing technology. The implementation of the antenna trace is achieved by spraying silver ink nano-particles on to the paper substrate. This technique will be analyzed in detail in Chapter 4. In addition, a temperature sensor along with the other electronic components (IC's resistors, batteries, switches etc), which are required for the active tag operation, are integrated on to the paper. The components are mounted on the paper substrate using silver epoxy and are connected together using circuits that are formed by silver ink conductive traces which are also inkjet-printed on the paper. The fabricated RFID platform is depicted in Figure 2.23.

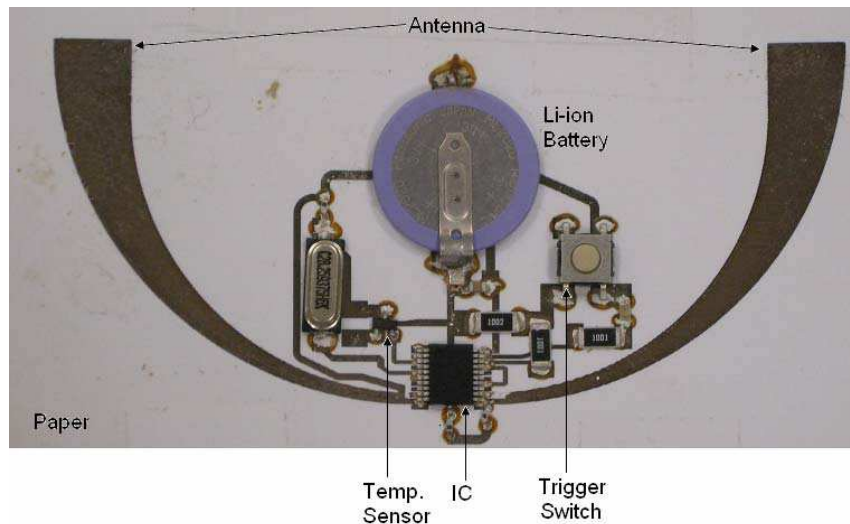


Figure 2.23 RFID-enabled wireless sensor platform on paper substrate using inkjet printing technology

2.4.3 Tags with power scavenging circuits

As has been emphasized in the previous sections an active RFID transponder has the highest range and the most capabilities compared to the other types of tags. However it requires its own power source to power the IC and transmit a signal back to the reader. Due to the fact that the power source is usually a battery, an active tag has some limiting disadvantages. The battery has a limited life time and has to be replaced. To seek and replace however a tag's battery in a ubiquitous wireless sensor network with thousands of RFID nodes placed arbitrary in the environment, is nearly impossible. For this reason active RFID tags are used less frequently than passive and only in limited applications (e.g. military applications).

However, the latest research in RFID technology involves the development of power scavenging circuits used as a power source in active tags and thus eliminating the need for a battery. Power scavenging technology has many forms. The most common ones that are being developed in RFID are:

Solar

Solar panels are used to scavenge the solar energy. The solar energy is converted into electrical, stored in a capacitor and in this way the necessary power is provided to the tag. Solar power scavenging circuits are easy to design and fabricate, have an acceptable efficiency and meet the power requirements of a typical RFID transponder. They do however have the disadvantage of requiring to be exposed under the sun at all times to function and increase the profile of the tag.

Piezoelectric

Piezoelectric power scavenging circuits utilize mechanical energy, convert it into electrical and provide the required energy to the tag. They show good efficiency, but have the disadvantage of requiring an external mechanical force. A possible

application would be in tire pressure monitoring RFID tags where the mechanical movement of the wheels is utilized to create the electrical energy.

Electromagnetic

In electromagnetic power scavenging technology a type of antenna called rectenna is used to scavenge the electromagnetic energy in the UHF frequencies, rectify it and convert it into DC power which is stored in a capacitor. This form of power scavenging can enable the tag to operate in any environment that there is some EM energy in the UHF frequency band. However it is very inefficient and difficult to implement, while increasing the tag cost and profile.

2.4.4 Other developments in RFID

Finally some other latest developments in RFID include [2]:

- New RFID ICs for passive tags with better sensitivity (the lowest amount of power that can activate them)
- Techniques to determine tag location and movement
- Tags with sensor capabilities (temperature, pressure, humidity, movement, vibration, light)
- UHF near field RFID
- Ultra-wide band RFID systems (capable of operating in the universal UHF RFID frequency band and in higher frequencies)
- Tags with multiple antennas (placing 2 same antennas with linear polarization perpendicular to each other increases tag performance by 40%)
- Multi-static reader antenna configurations
- Novel portal and conveyor belt solutions

CHAPTER 3

Antenna Design

3.1 Introduction

It has been highlighted that the performance of the RFID antenna is critical for the operation and the range of an active RFID transponder. Antenna design is therefore very important and has to be analytically detailed. Since the good impedance matching of the antenna to the load is the most important requirement, a theoretical background on impedance matching is thoroughly discussed in the beginning of this chapter. Next the antenna requirements are defined and the antenna configuration is described. Then the design process is outlined, while the antenna is simulated and optimized to meet the defined requirements. In the end of the chapter the simulation results are presented, proving that the antenna meets the requirements in simulation.

3.2 Impedance Matching

The two main components of a typical active UHF RFID transponder are: 1) The integrated circuit (IC or ASIC: Application Specific Integrated Circuit) that stores the identification data, controls the communication with the reader and performs other operations 2) The antenna that radiates the signal of the IC's output. However an active RFID tag consists also of an input circuit and an output circuit, which are connected to the IC. Each of these circuits includes different electrical components, such as:

Input Circuit

- Power sources (batteries, power scavenging devices, etc.)
- Sensors (temperature, humidity, light, etc...)
- Switches (for the control of the transponder)
- LED's (for the operation check of the transponder)

Output Circuit

- Integrated Power Amplifiers
- Lumped Components (resistors, capacitors, coils)

The block diagram of an active UHF RFID tag is shown in Figure 3.1 below:

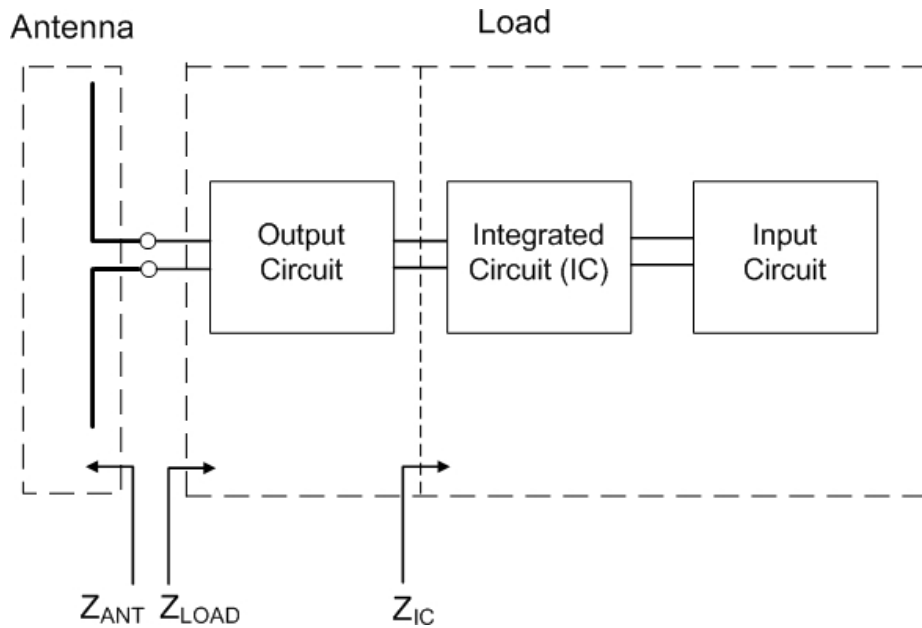


Figure 3.1 Block diagram of an active UHF RFID tag

In order to maximize the performance of the transponder, maximum power must be delivered from the antenna to the IC. However as shown in Figure 3.1 the antenna is not directly connected to the IC, but to the IC's output circuit that interferes between the IC and the antenna. As a result, in order to satisfy this requirement, the RFID antenna has to be matched to the Output Circuit or the load of the tag.

For years antennas have been designed primarily to match either 50Ω or 75Ω loads. In RFID however, the antenna has to be directly matched to the tag's load [1]. Adding an external matching network with lumped elements is usually prohibited due to cost, fabrication and size issues. As shown in Figure 3.1, looking into the antenna the antenna displays complex input impedance Z_{ANT} at its terminals. The transponder's load also displays complex impedance Z_{LOAD} , when looking into the opposite direction of the antenna into the output circuit. The load's impedance is depended on the IC's impedance Z_{IC} and can be calculated if the output circuit is known or it can be measured. The IC's input impedance is different for every IC and is also complex, but can only have negative reactive values (its imaginary part is always capacitive). The equivalent circuit of the antenna-load is shown in Figure 3.2, where V_s is the voltage across the antenna which is induced from the receiving signal.

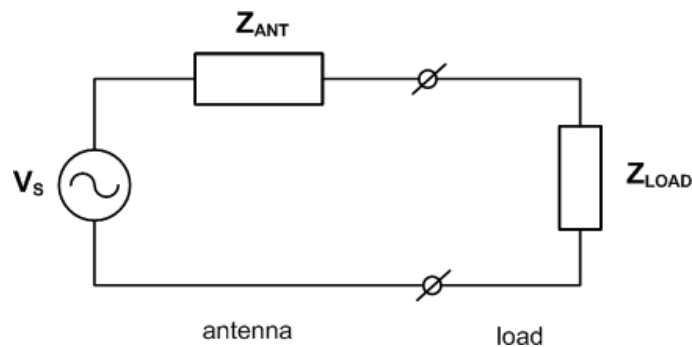


Figure 3.2 Antenna-Load equivalent circuit

In order to ensure, as described above, maximum power transfer from the antenna to the load, the input impedance of the antenna must be conjugately matched to the tag's load impedance in the operating frequency of the tag [11], verifying Equation 1. In other words, the real part of the antenna input impedance must be equal to the real part of the load's impedance and the imaginary part of the antenna input impedance must be equal to the opposite of the imaginary part of the load's impedance [16].

$$Z_{ANT} = Z_{LOAD}^* \Leftrightarrow R_A = R_L \text{ and } X_A = -X_L \quad (1)$$

if $Z_{ANT} = R_A + jX_A$ and $Z_{LOAD} = R_L + jX_L$

Kurokawa [15] described a concept of power waves traveling between the generator and load and introduced the following definitions for the power wave reflection coefficient s shown in Equation 2 and the power reflection coefficient $|s|^2$ shown in Equation 3.

$$s = \frac{Z_{LOAD} - Z_{ANT}^*}{Z_{LOAD} + Z_{ANT}} \quad (2) \quad |s|^2 = \left| \frac{Z_{LOAD} - Z_{ANT}^*}{Z_{LOAD} + Z_{ANT}} \right|^2, \quad 0 \leq |s|^2 \leq 1 \quad (3)$$

The power reflection coefficient $|s|^2$ shows what fraction of the maximum power available from the antenna is not delivered to the load [12]. As a result, achieving maximum power transfer from the antenna to the load is translated into minimizing the power reflection coefficient $|s|^2$. It has to be noted that both the impedance of the antenna and the load vary with frequency. For this reason $|s|^2$ can be minimized in a single frequency. Consequently this is chosen to be the operation frequency of the RFID tag. The value of $|s|^2$ changes with frequency and therefore it displays in every frequency what fraction of the maximum power is not delivered to the load. For that reason the return loss of an RFID antenna is defined as the value of the power reflection coefficient $|s|^2$. The frequency response of the return loss (s_{11}), as defined above, will be utilized to evaluate the performance of the proposed antenna and define its operation bandwidth.

It is observed from this analysis that the antenna is not operating at resonance, since the imaginary part of its input impedance is not zero at the operating frequency. This is a fundamental difference between common antenna design and RFID antenna design. The most important requirement in RFID antenna design is that the antenna is directly matched to the load, which has complex impedance, in order to achieve maximum power transfer between them. In other words the antenna is designed neither to resonate, nor to be matched to a 50Ω load. The antenna's self-resonance happens at the frequency, where the real part of its input impedance is maximized, while at the same time the imaginary part equals zero. At this frequency the power that is transmitted by the antenna is maximized. The resonance of the antenna when matched to a 50Ω load happens at the frequency, where the real part of its input impedance equals 50Ω and its imaginary part equals zero. The different antenna's

resonances, in respect to the antenna's and load's impedances (Z_A and Z_L) are shown in Figure 3.3.

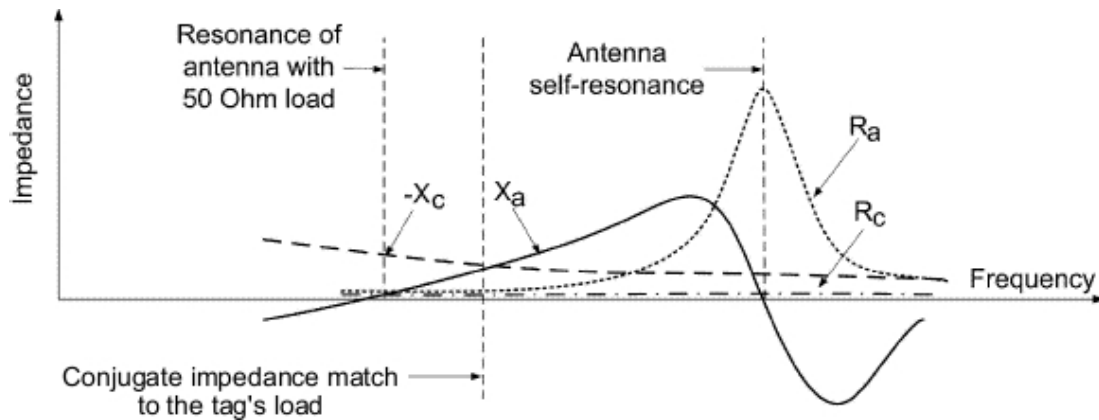


Figure 3.3 Antenna impedance and load impedance as functions of frequency for a typical RFID tag

3.3 Antenna Requirements

The proposed antenna must achieve specific design goals in order to be integrated with the RFID tag and operate efficiently. As has been discussed in Section 3.2 the antenna is designed for the specific IC that the RFID tag is using. In our application the IC has an operation frequency of 904.5MHz, at which communicates with the reader. As a result the first requirement of the RFID antenna is that it operates at the unlicensed UHF frequency band around 900MHz and resonate close to 904.5MHz. It is also important that the antenna operates in the North America (902-928MHz) and Europe (866-868MHz) UHF frequency bands so that the tag features operability both in USA and Europe. This requirement demands a bandwidth of operation of at least 866-928MHz. Another antenna requirement emerges from the fact that the tag must be able to communicate with the reader in any orientation. As a result, it is essential that the antenna has an omnidirectional radiation pattern in the azimuthal (x-z plane).

As has been emphasized before the antenna must be directly matched to the tag's load. This means that the input impedance of the antenna must be conjugately matched to the impedance of the load. In our application the load of the RFID transponder has a complex impedance of: $Z_{LOAD} = 37.31 + j65.96 \Omega$. As a result the value of the antenna impedance must be approximately equal to $Z_{ANT} = 37.31 - j65.96 \Omega$ at the tag's operation frequency (904.5MHz).

It is also essential that the antenna has positive directivity, gain close to zero and efficiency higher than 80%. This is necessary so that the EIRP (Equivalent Isotropic Radiated Power) of the antenna ($EIRP = P_t G = P_t e D$) is as high as possible in order to increase the tag's read range.

Finally the antenna must be linearly polarized. Most readers' antennas are circularly polarized, while tags' antennas are usually linearly polarized [2]. Circularly

polarized tag antennas are avoided, because the rotation of the circularly polarized RF wave radiated by the antenna might be inverted, due to ground reflection and multipath effects. This would result into $PLF=0$ (polarization loss factor) between the tag antenna and the reader's antenna and no power would be received from the tag's antenna. However linearly polarized waves received by a circularly polarized reader's antenna results always in a $PLF=-3dB$ [4]. The antenna requirements are now fully determined and are summarized in Table 3.1.

Table 3.1 Antenna Requirements

Antenna Parameter	Design Goal
Operation Frequency	904.5 MHz
Operation Bandwidth	866-928 MHz
Radiation Pattern	omnidirectional on the azimuthal plane x-z
Input Impedance	$\approx 37.31 - j65.96 \Omega$
Directivity	≥ 0 dBi
Gain	≈ 0 dBi
Efficiency	≥ 80 %
Polarization	linear

3.4 Antenna Configuration

3.4.1 Antenna geometry details

The geometry of the proposed printed monopole antenna is shown in Figure 3.4. The antenna is designed on a paper substrate with thickness of 0.254mm, relative permittivity $\epsilon_r=3.5$ and loss tangent $\tan\delta=0.08$. The substrate has width $W=75$ mm and length $L=100$ mm including the feeding line.

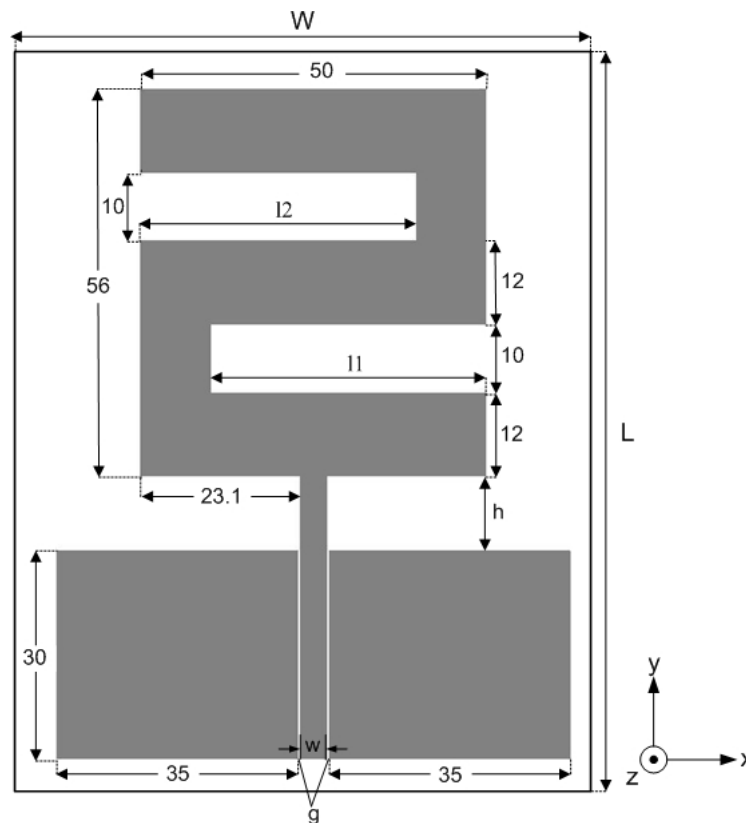


Figure 3.4 Configuration of the proposed printed monopole antenna

The proposed monopole antenna configuration shown in Figure 3.4 is composed of 3 parts:

- 1) The radiating element: The Z shaped part of the antenna above the ground planes. The radiating element radiates and receives the RF signals and its configuration affects all of the antenna parameters.
- 2) The ground planes: The two rectangular areas below the radiating element compose the ground of the monopole geometry. The ground planes are responsible for creating a symmetrical image of the radiating element in respect to the x-z plane. Their size affects the radiation characteristics of the antenna and is critical for the antenna performance.
- 3) The feeding line: The part below the radiating element comprises the feeding line of the antenna. The feeding line consists of a central conductor strip, which carries the RF signal and also two ground planes in either sides of the feeding strip.

The parts of the antenna are depicted in Figure 3.5 below:

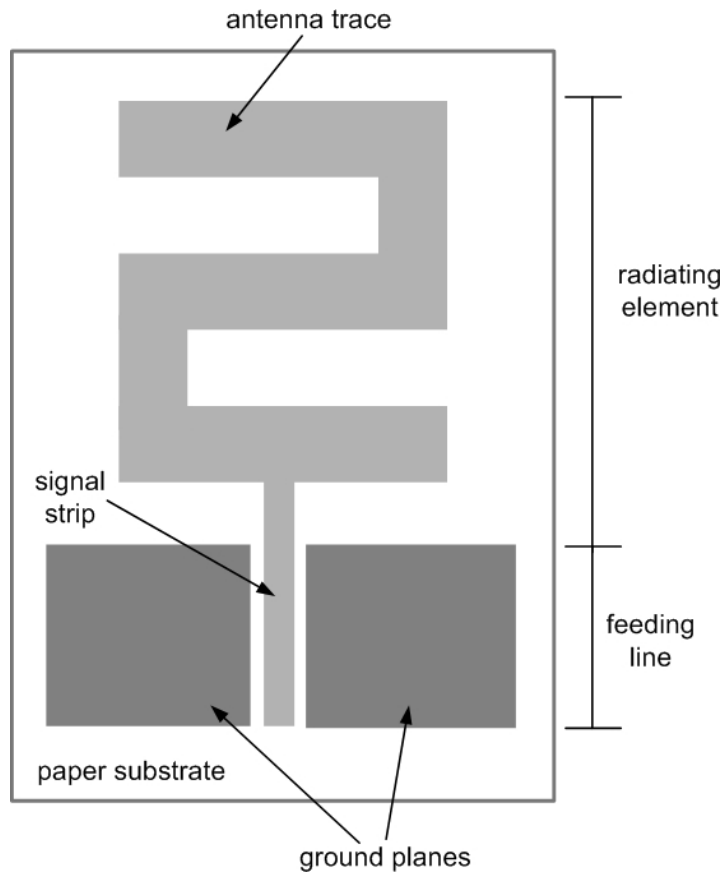


Figure 3.5 Parts of the proposed monopole antenna

3.4.2 Ground plane and monopole antenna advantages

The most commonly used antennas for RFID applications are half-wavelength dipole antennas [1]. However, in this paper, a monopole antenna is proposed, due to its many attractive features in comparison to a dipole antenna [4]. First, the input impedance of a resonating monopole antenna is approximately 37Ω , which is half of that of a dipole. This value is very close to the real part of the tag's load impedance in our application and therefore the impedance matching will be simplified.

Another advantage of monopole antennas is that they have a wider bandwidth than dipole antennas. The impedance of an IC varies with frequency and the input power applied to the chip, thus increasing the return loss in frequencies away from the centre frequency. In addition, fabrication deviations of not only the antenna, but also of the IC shift the centre frequency of the tag's operation. As a result the matching of the antenna to the load is being made more challenging. If however a broadband antenna is utilized, then the impedance matching to the load is achieved in a wider range of frequencies.

The most important advantage of the monopole is however that it composes of a ground plane. The ground plane makes easier the integration of the antenna with the other electronic components of the tag (sensors, power sources, IC's) and reduces at the same time the cross-talk and the interference between them. In addition the ground plane shields the electronic components from the antenna radiation, minimizing in this way the coupling between them. The ground plane acts also as a radiating surface,

increasing the directivity of the antenna. Finally the monopole antenna does not require a differentially fed input signal like a dipole, due to also the existence of the ground plane, which makes more efficient the connection to the load, since the IC's output is single-ended.

3.4.3 Feeding line

A coplanar waveguide (CPW) transmission line is used for feeding the antenna, because of its simple single layer metallic structure and its little radiation loss compared to a microstrip line [16]. A 50Ω CPW transmission line proved to be very difficult to implement on a paper substrate, because the design resulted in either too large signal strip, or too small gap spacing. For this reason the characteristic impedance of the feeding line was chosen to be $Z_o=60\Omega$. As a result, the CPW line composes of a central conductor strip with width of $w=3.8\text{mm}$ and gap spacing between the signal strip and the ground $g=0.3\text{mm}$, as shown in Figure 3.4. The overall length of the transmission line is 30mm which corresponds to 40° impedance transformation from the input impedance of the radiation element to the input impedance of the antenna on the normalized Smith Chart.

3.4.4 Radiation element

The antenna is designed based on a rectangular radiating element with width of 50mm and length of 56mm. The rectangular element is the extension of the signal strip of the feeding line and has a spacing of $h=11\text{mm}$ from the ground plane. It has to be noted, that the monopole antenna is designed, considering the feeding line and the rectangular surface as a single radiating element. Two rectangular slots are embedded into the radiating element from both side edges, resulting in a meander-like, Z-shaped antenna, as shown in Figure 3.4. Both slots have a width of 10mm and lengths of $l_1=l_2=40\text{mm}$. The length of the slots is optimized in order to achieve the impedance matching of the antenna to the load. The impedance matching process is discussed in Section 3.5.2.

3.5 Design Process

As has been mentioned before, the operation frequency of the antenna is 904.5MHz. The respective wavelength in free space at this frequency is:

$$\lambda_o = \frac{c_o}{f} = 33.167\text{cm}. \text{ The wavelength is much greater than the thickness of the}$$

antenna trace on the substrate and for this reason the antenna trace is considered as a perfect conductor in the design process.

To achieve the required design goals mentioned in Section 3.3, the antenna must be optimized [3]. However there is an inevitable tradeoff when trying to meet all the requirements. For this reason impedance matching will be achieved in the end, since it is the most important requirement. Firstly we will try to achieve that the antenna is operating at the desired frequency (904.5MHz). Secondly we will try to optimize the

radiation of the antenna by ensuring that the antenna has a omnidirectional radiation pattern in the x - z plane. In the end we will try to accomplish the matching of the antenna to the load. The antenna performance will be verified in simulation and if the design goals are met, the design process will be complete.

3.5.1 Planar rectangular monopole antenna

The first step in the design process is to design a typical planar rectangular antenna, as shown in Figure 3.6, which resonates around the frequency of 900MHz and has an omnidirectional radiation pattern in the azimuth plane and a directional pattern with 2 nulls in the elevation plane [21]. This type of radiation pattern will ensure that the RFID antenna is radiating as a theoretical linear wire monopole antenna with finite ground planes, as defined in Section 2.3.1.2. The planar rectangular UHF monopole antenna will be used only as a starting point for the design process.

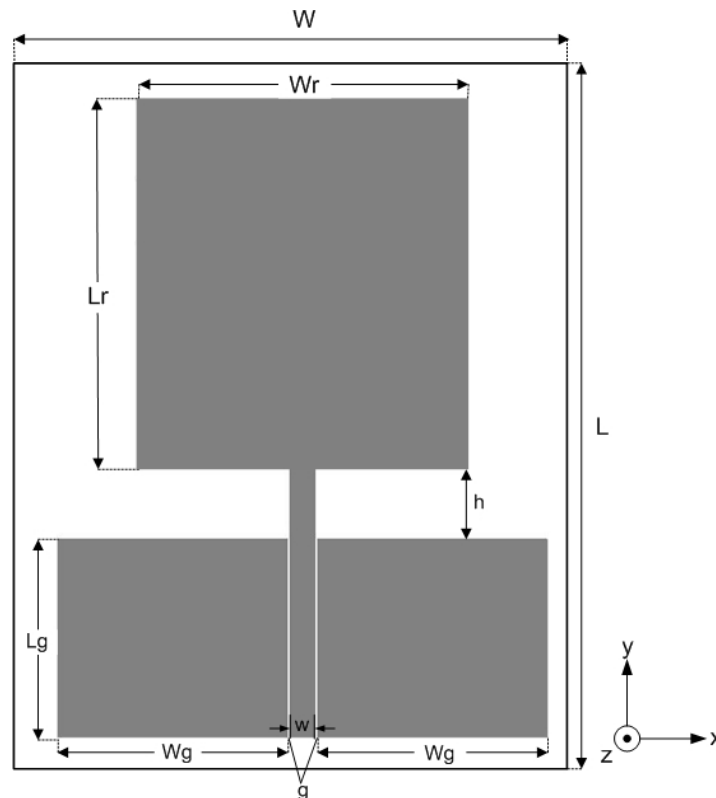


Figure 3.6 Planar rectangular UHF monopole antenna configuration

First the dimensions of the rectangular monopole antenna have to be determined. It has been noted that the CPW feeding line of the proposed antenna has width $w=3.8\text{mm}$, gap spacing $g=0.3\text{mm}$ and length $L_g=30\text{mm}$. Therefore the length of the ground planes is also $L_g=30\text{mm}$. The width of the ground planes is chosen to be $W_g=35\text{mm}$ and a typical value [22] for the height of radiating element from the ground is chosen $h=11\text{mm}$. The height h of the radiating element from the ground has

a major influence on the performance of the antenna, as it modifies the radiation pattern and the antenna impedance. Increasing it, guided waves of the antenna are transitioning more efficiently into free-space waves and the impedance becomes more capacitive. Maximizing it however, results into thick and difficult to mount RFID tags. For that reason a typical value is selected.

It is essential now to determine the dimensions of the rectangular radiating element. A typical value for the width of the rectangular element is chosen $Wr=50\text{mm}$. As in the theoretical ideal linear wire monopole antenna the resonance is defined by its length, in the same way the length of the monopole defines the resonant frequency of the antenna. As a result, the length Lr of the rectangular element is determined by Equation 4 defined in [4], [21]. Equation 4 is an empirical formula for calculating approximately the resonant frequency of a planar monopole antenna given its dimensions. This equation is derived by equating the area of the planar rectangular radiating element to that of a cylindrical wire of height l (which is the same as the rectangular monopole's height Lr), with equivalent radius r given by (5). Due to the fact that the antenna must have a resonance around 900MHz, Equation 4 has to be solved in respect to l to find the value of l that makes the rectangular monopole antenna to resonate around 900MHz. For this reason, we set in (4) $f=0.9\text{GHz}$.

$$f = \frac{7.2}{(l+r+h) \cdot k} \quad (4) \qquad 2\pi rl = L \cdot W \quad (5)$$

where the lengths l, r, h are in cm, the resonant frequency f in GHz and k is an empirical constant $k=1.1$

Solving (5) for $l=Lr$ we find $r=0.796\text{cm}$. Using r in (4) and solving in respect to l , we find $l \approx 5.6\text{cm}$. As a result the length of the rectangular element must be $Lr = 56\text{mm}$

Based on these configuration dimensions, the performance of the planar UHF rectangular monopole antenna is simulated at the required centre frequency of 900MHz. The frequency response of the return loss is shown in Figure 3.7 and the normalised radiation intensity radiation pattern in the azimuth (x-z plane) and elevation (y-z) plane at the simulation frequency is depicted in Figure 3.8. It is observed from the return loss simulation results that the resonant frequency of the planar antenna is close to 900MHz. Furthermore, the radiation pattern is omnidirectional in the azimuth plane and directional with 2 nulls in the elevation plane. As a result the requirements for the preliminary design are satisfied.

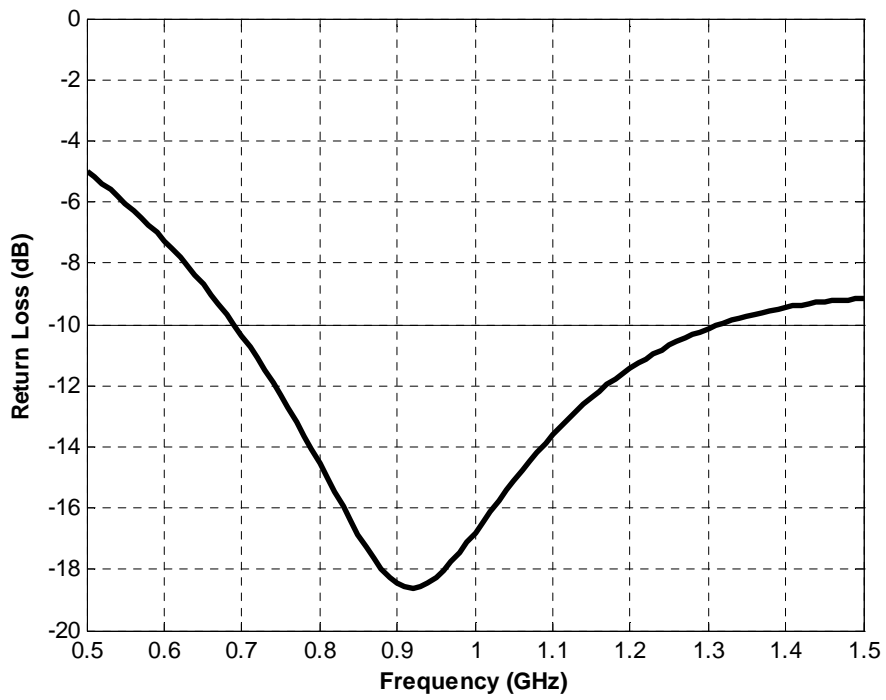


Figure 3.7 Return loss versus frequency of the planar UHF rectangular monopole antenna

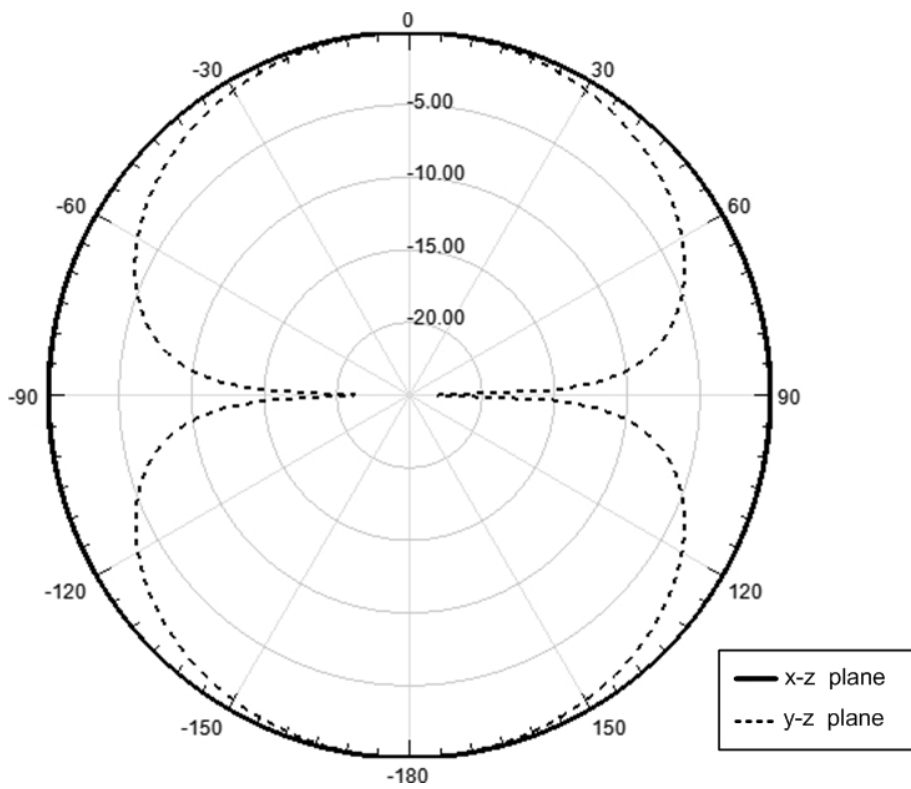


Figure 3.8 Normalized radiation patterns of the planar UHF rectangular monopole antenna

3.5.2 Impedance matching

The planar rectangular configuration that has been designed satisfies the radiation requirements for the proposed RFID antenna. However, as has been emphasized in Section 3.2, it is designed to match a 50Ω load and not the tag's load which has complex impedance. It is therefore necessary to optimize the antenna, changing the values of some of its parameters (dimensions), to achieve the required impedance matching.

In order to match the antenna to the load, the lengths of the two slots $l1$ and $l2$ respectively were parameterized in simulation and optimized so that the input impedance of the antenna approximates the value of $Z_{ANT} = Z_{LOAD}^* = 37.31 - j65.96 \Omega$. The parameters h, g, w, Lg, Wg, Lr, Wr , are not changed. By observing the variations of the antenna input impedance in respect to the different combinations of the lengths $l1$ and $l2$, we can determine the values that achieve the best matching. In Figure 3.9 - Figure 3.12, the real and imaginary part of the antenna input impedance versus frequency is depicted with different lengths of $l2$ ($l2=15, 25, 35, 45$ mm) when $l1$ is fixed in every variation at 15, 25, 35 and 45mm respectively. The value of the desired antenna input impedance ($Za=Ra+jXa=37.31-j65.96$) is also shown in the impedance plots.

It can be seen in Figure 3.9 - Figure 3.12 that increasing the length $l1$ the resistance and reactance curves are shifted to the left. The resistance curves have a local maximum and the reactance curves a local minimum. In order to achieve maximum bandwidth, the minimum of the reactance curve must be close to the operating frequency. By comparing Figure 3.11b and Figure 3.12b we observe that the reactance plots minimums approach the operating frequency 904.5MHz for a value of length $l1$ that is between $l1=35$ mm and $l1=45$ mm. Now we investigate the antenna input impedance at the operating frequency 904.5MHz while varying the length $l2$ when $l1$ is fixed at $l1=40$ mm, as shown in Figure 3.13

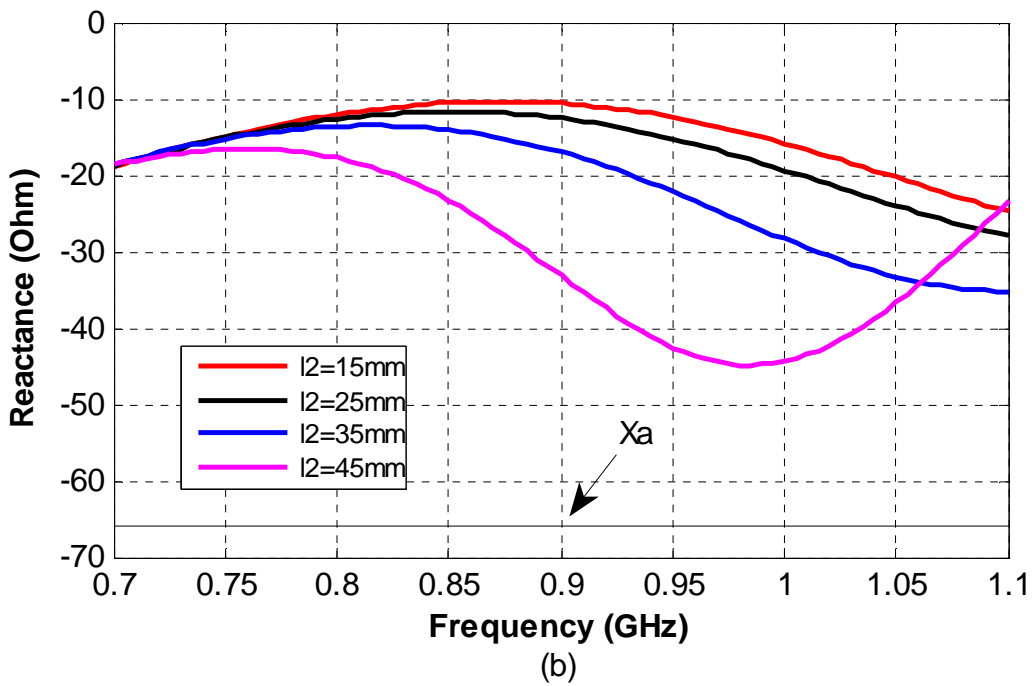
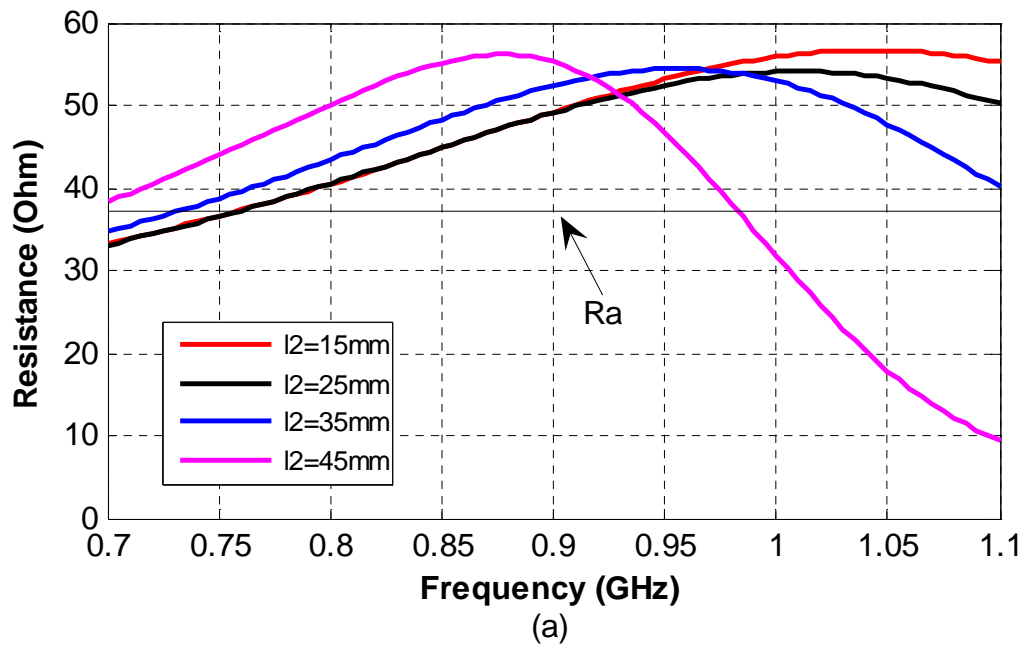
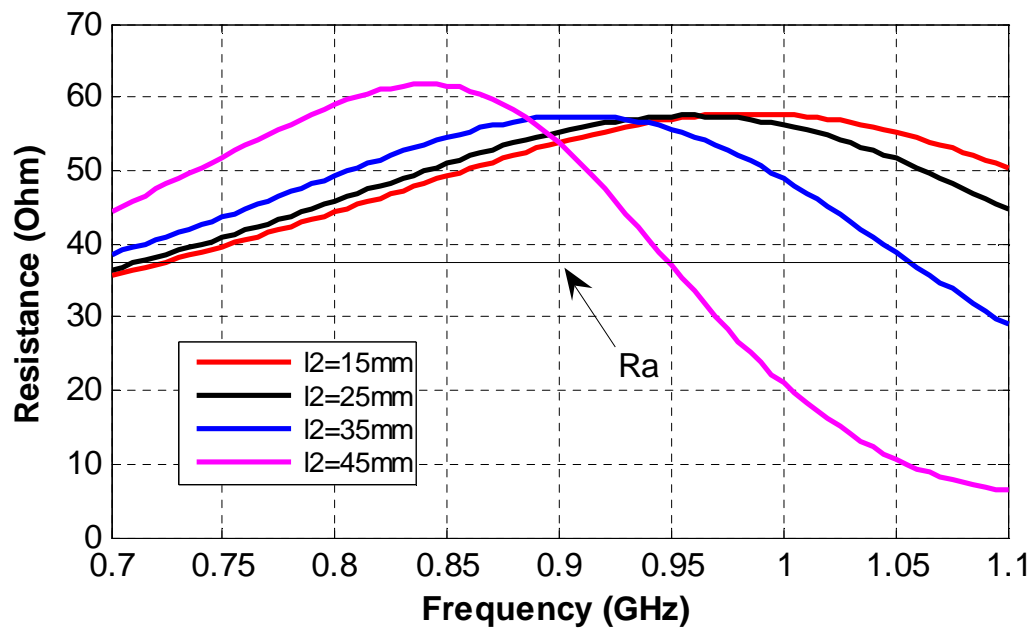
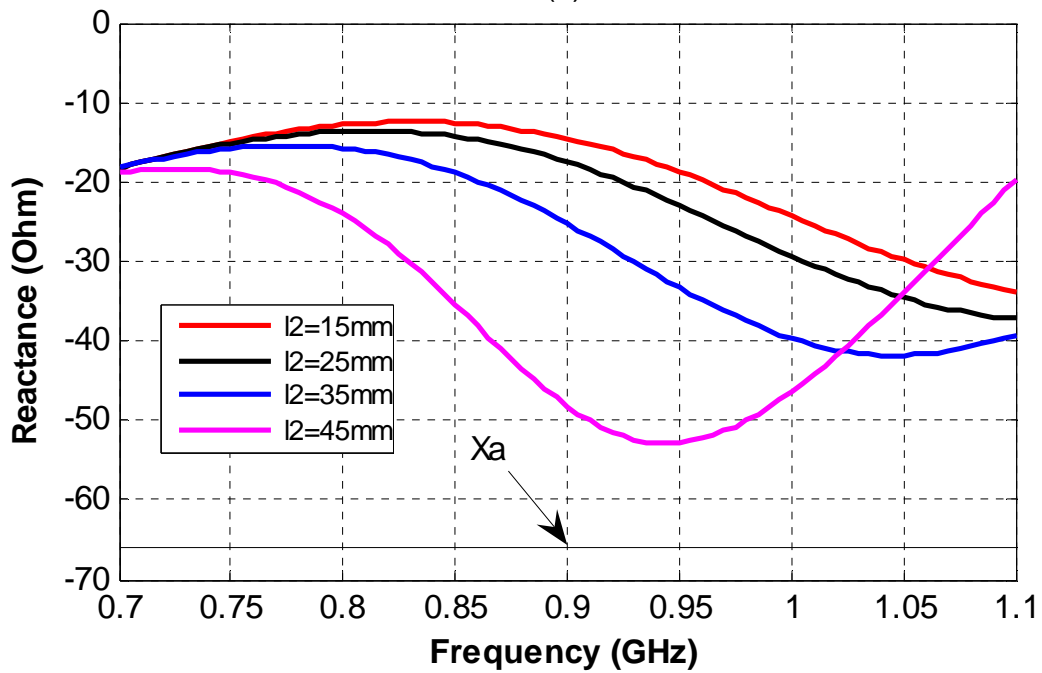


Figure 3.9 Simulated input impedance for different lengths l_2 of the slot with $l_1=15\text{mm}$
 (a) Resistance R
 (b) Reactance X

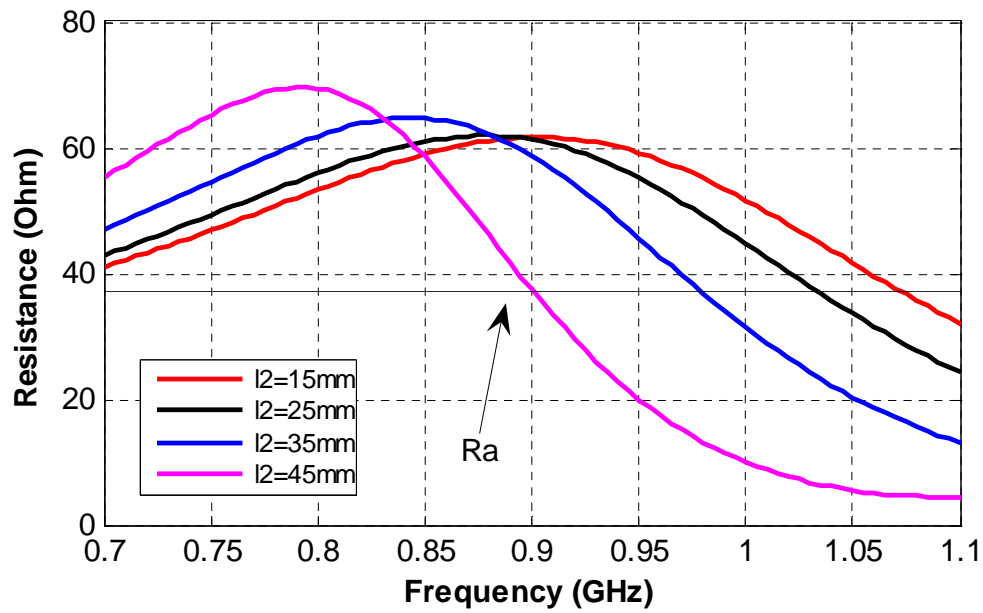


(a)

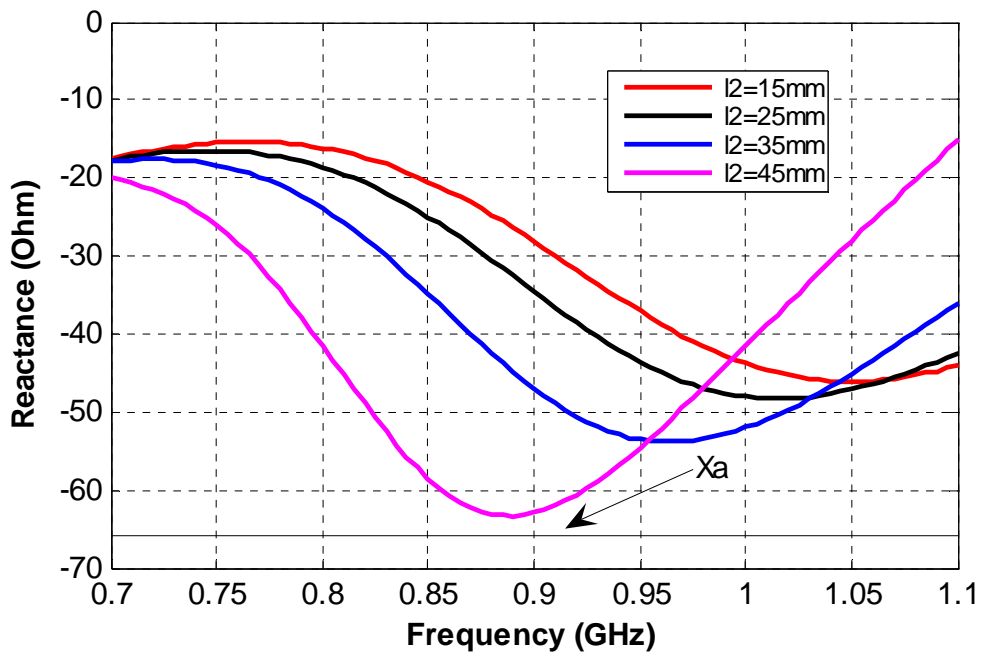


(b)

Figure 3.10 Simulated input impedance for different lengths l_2 of the slot with $l_1=25\text{mm}$
 (a) Resistance R
 (b) Reactance X



(a)



(b)

Figure 3.11 Simulated input impedance for different lengths l_2 of the slot with $l_1=35\text{mm}$
 (a) Resistance R
 (b) Reactance X

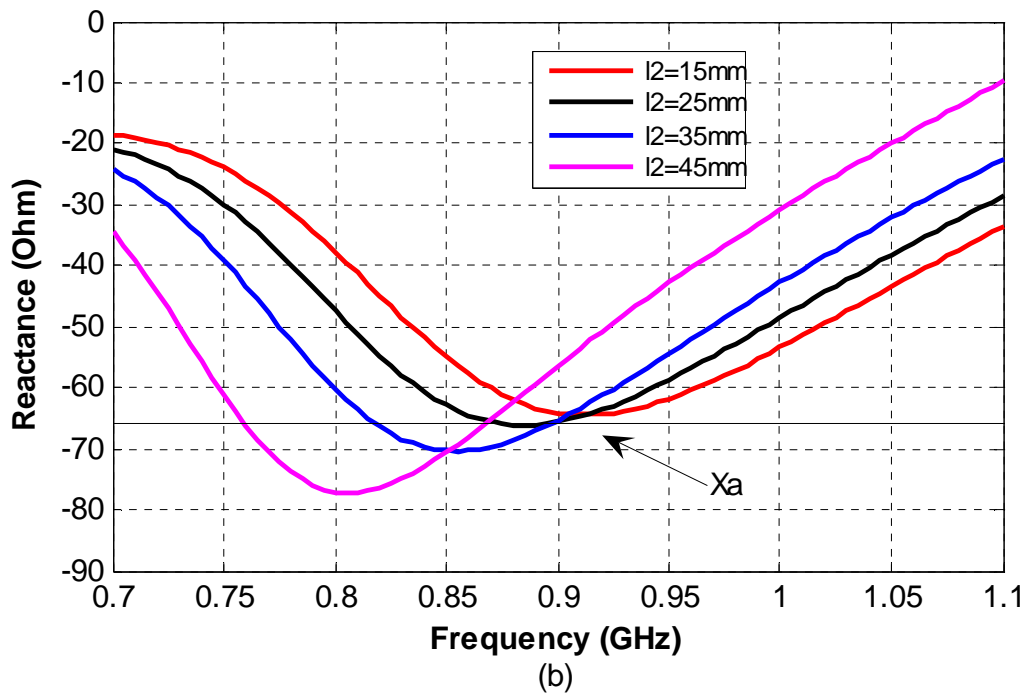
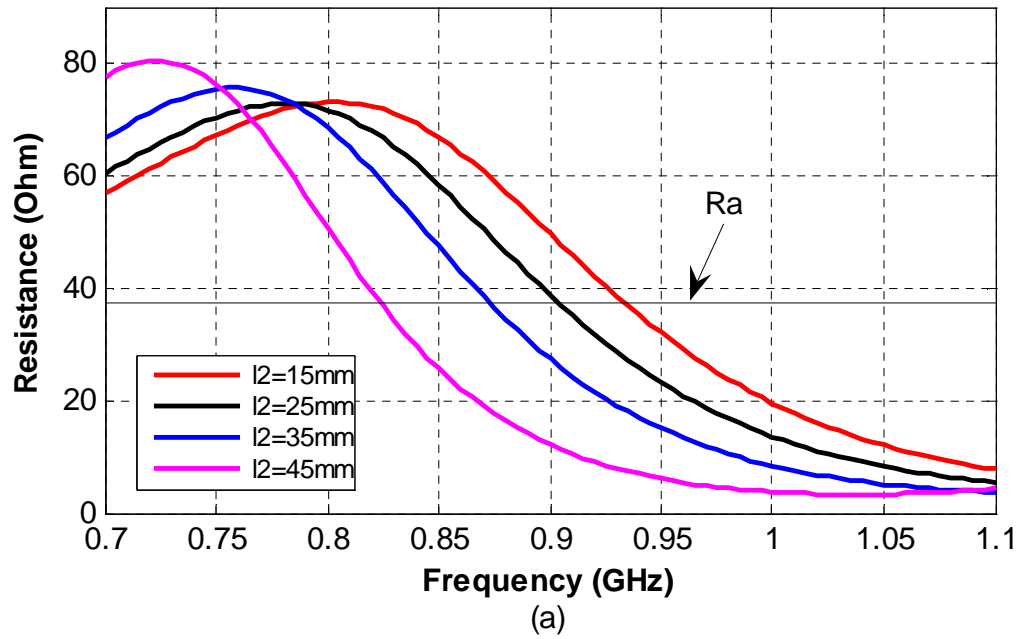


Figure 3.12 Simulated input impedance for different lengths l_2 of the slot with $l_1=45\text{mm}$
 (a) Resistance R
 (b) Reactance X

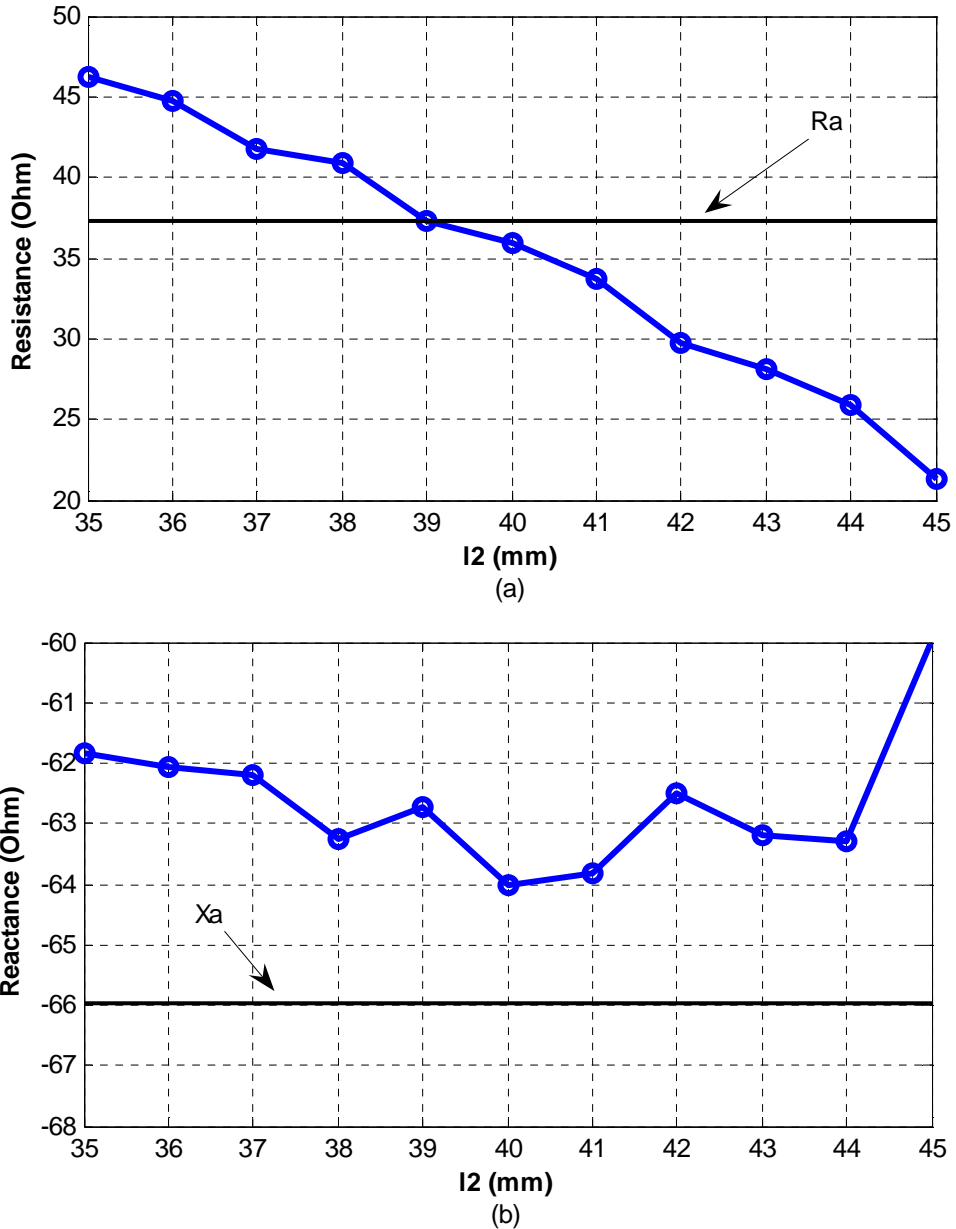


Figure 3.13 Simulated input impedance at the operating frequency 904.5MHz versus slot length l_2 with $l_1=40$ mm
 (a) Resistance R
 (b) Reactance X

We observe in Figure 3.13 that the length l_2 for which the input impedance of the antenna is closest to the desired value ($37.31 - j65.96 \Omega$) is $l_2=40$ mm. When $l_1=l_2=40$ mm the antenna input impedance that is obtained from the simulation is $Z_a = 37.5 - j65.2\Omega$. With the determined parameters combination the monopole antenna is successfully matched to the load and maximum power is transferred from the IC to the antenna.

3.6 Simulation Results

It is observed that the required input impedance and radiation characteristics are achieved. In the following paragraphs the antenna performance, with the determined parameters (dimensions) is simulated, verifying that the antenna requirements are satisfied.

3.6.1 Input impedance

The real and the imaginary part of the antenna input impedance is plotted in Figure 3.14 below. The desired antenna input impedance $Z_a = R_a + jX_a$ is also depicted:

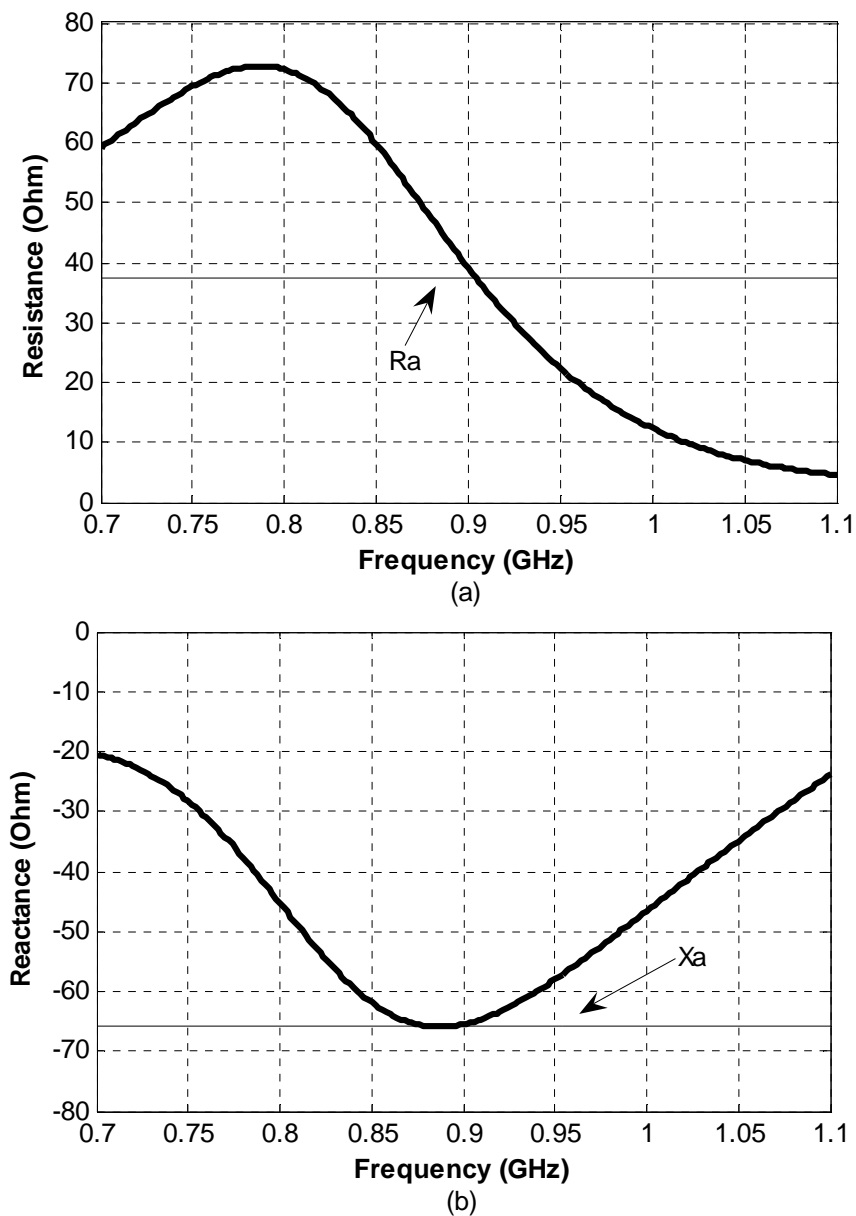


Figure 3.14 Simulated input impedance vs frequency of the proposed UHF monopole antenna
(a) Resistance R
(b) Reactance X

3.6.2 Return loss

It is critical that we investigate the power reflection coefficient when the antenna is connected to the load. The calculation of the return loss from the simulated results is described in Section 3.2. The simulated frequency response of the return loss of the proposed antenna when connected to the load is depicted in Figure 3.15.

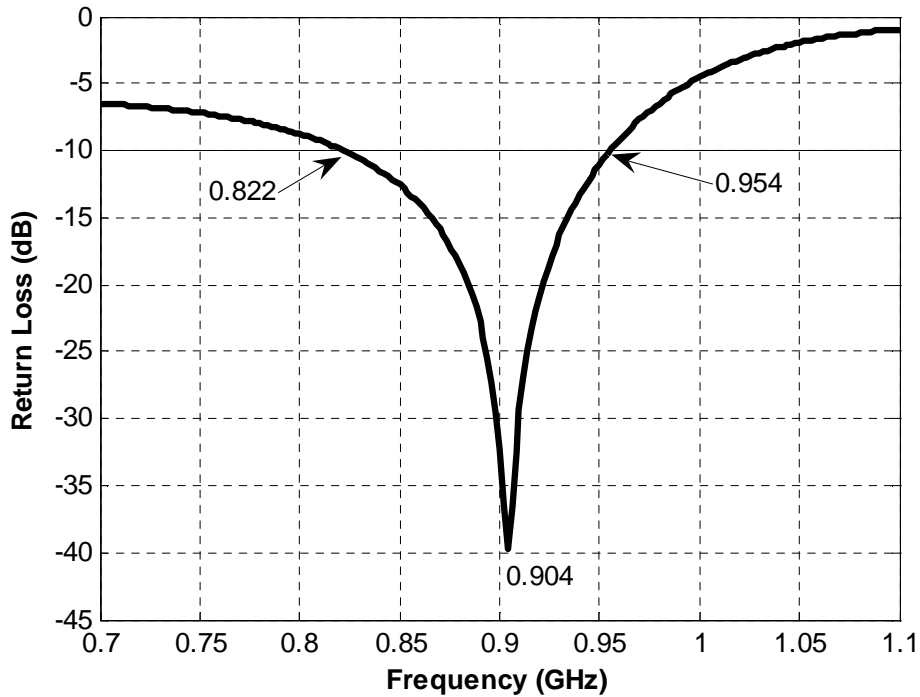


Figure 3.15 Frequency response of the return loss of the proposed antenna

It is seen from the above plot that the antenna has a resonance at 904MHz, very close to the IC's operation frequency, and a -10dB impedance bandwidth of 132MHz (822 – 954MHz) corresponding to 14.6% around the center frequency. The simulated antenna bandwidth covers the global RFID UHF frequency band.

3.6.3 Radiation pattern

The normalized two-dimensional radiation intensity radiation patterns of the proposed UHF monopole antenna for the azimuth (x-z plane) and the elevation (y-z plane) at the resonant frequency 904.5 MHz are depicted in Figure 3.16.

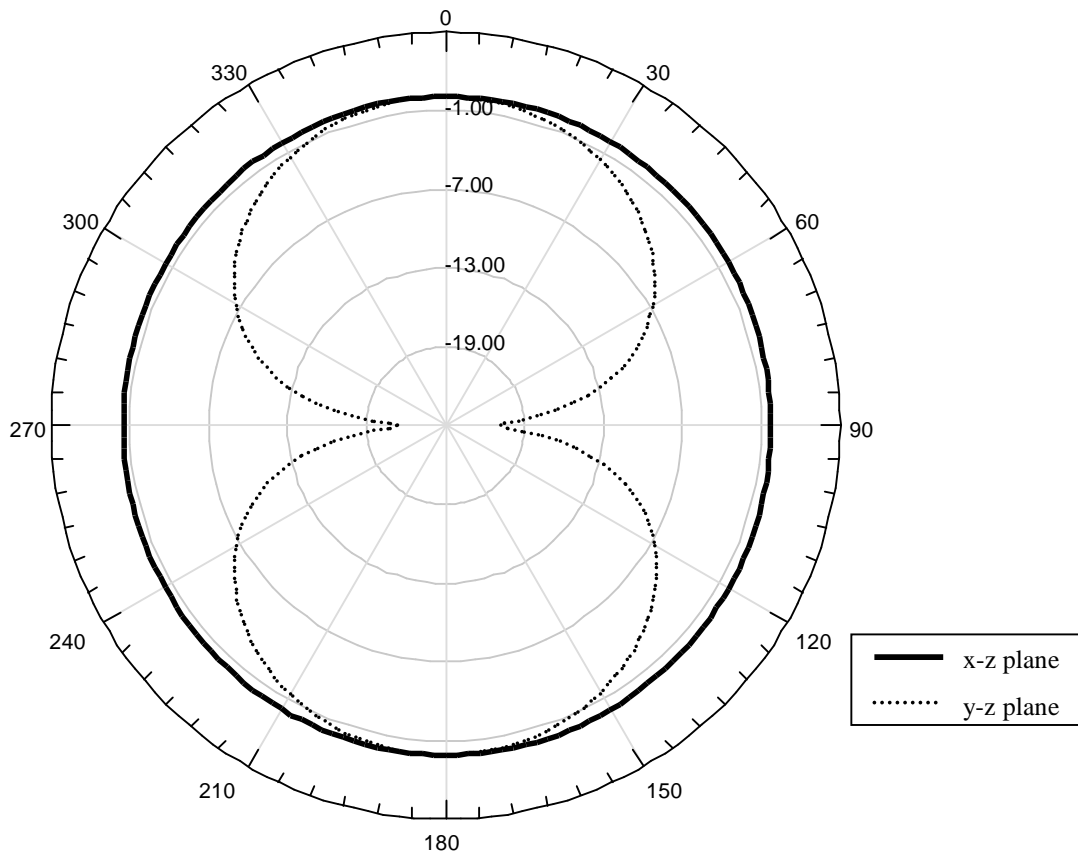


Figure 3.16 Two dimensional normalized radiation patterns of the proposed monopole antenna

It is clearly seen from Figure 3.16 that the antenna demonstrates a radiation pattern similar to a classic dipole antenna, displaying an omnidirectional radiation pattern on the horizontal x-z plane and a directional pattern with 2 nulls in the vertical y-z plane. The three dimensional normalized radiation intensity radiation pattern of the antenna has also been simulated and is illustrated in Figure 3.17.

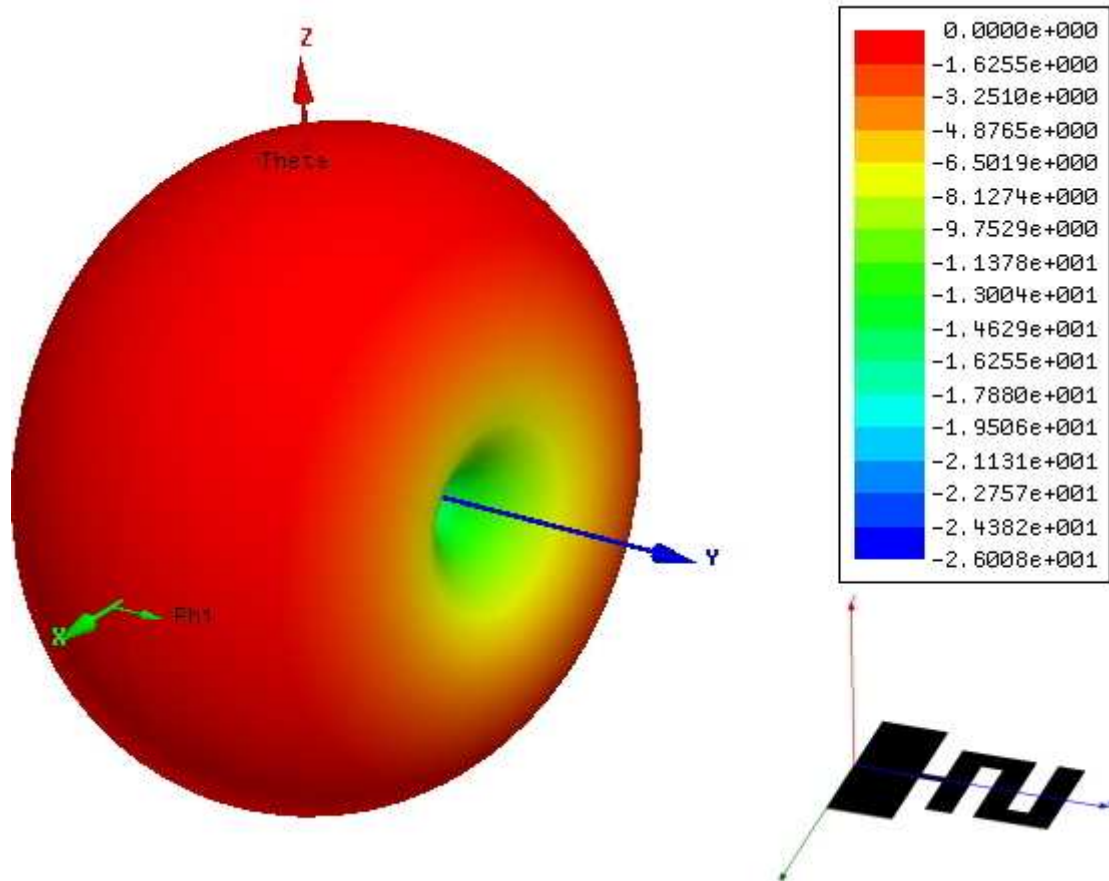


Figure 3.17 Three dimensional normalized radiation pattern of the proposed antenna

3.6.4 Directivity, Efficiency and Gain simulation

The directivity of the antenna has also been simulated in order to further verify the performance of the antenna. The frequency response of the directivity of the monopole antenna is shown in Figure 3.18:

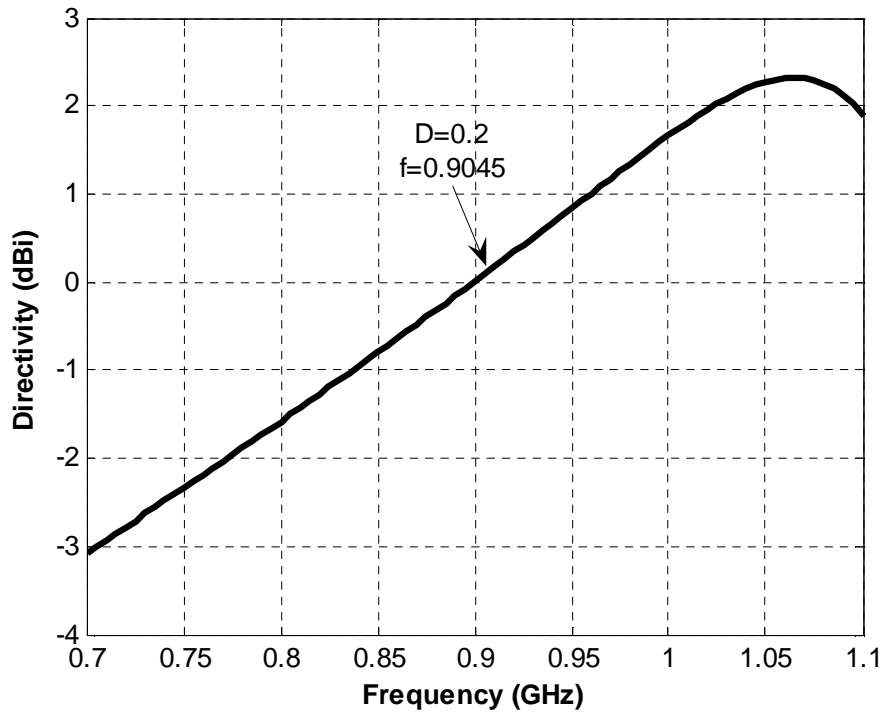


Figure 3.18 Directivity versus frequency of the proposed monopole antenna

It is obtained from Figure 3.18 that the directivity of the antenna at the operating frequency is 0.23dBi. We also observe that the directivity of the antenna increases as the frequency increases. This is expected, because as the frequency increases the wavelength decreases and as a result the electrical length of the antenna increases. It is known [4] that the directivity increases when the electrical length of the antenna increases.

The efficiency e and the gain G of the antenna were also simulated and the results along with the other simulated antenna parameters at the operating frequency are shown in Table 3.2:

Table 3.2 Simulated monopole antenna parameters at the centre frequency 904.5MHz

Parameter	Value
D	0.23 dBi
e	88.7 %
G	-0.42 dBi
Z_{ANT}	$37.5 - j65.2 \Omega$
Return Loss	-38.4 dB

3.6.5 Current distribution

The simulated current distribution of the proposed antenna is presented in Figure 3.19. The current pattern depicts the magnitude of the surface current at the operating frequency on the conducting antenna trace of the design. It is observed from Figure 3.19 that the current is distributed mainly along the edges of the two embedded slots. This explains why varying the length of the slots affects the input impedance of the antenna and its radiation characteristics. In addition the current path is forced to be extended along the edges of the slots, following the meander-like shape of the antenna. As a result, the electrical length of the antenna is increased and consequently its directivity and gain.

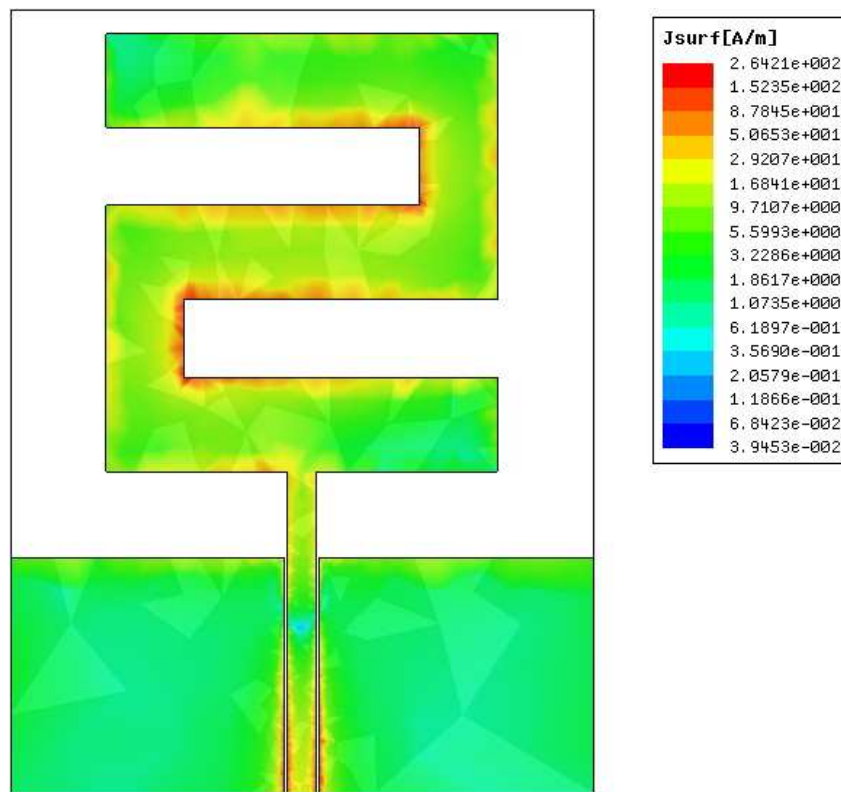


Figure 3.19 Simulated current distribution of the proposed antenna at the operation frequency of 904.5MHz

CHAPTER 4

Prototype Fabrication

4.1 Introduction

The proposed monopole antenna was fabricated on a flexible paper substrate using inkjet-printing technology. In this chapter, first we discuss the benefits of using paper as a substrate for high-frequency applications and present a method for paper RF characterization. Then we give details about the inkjet printing technology and outline the fabrication process of this technique. Finally we present an alternative method for implementing the antenna on a flexible paper substrate using thin copper tape.

4.2 Paper Substrate Advantages

There are many aspects of paper that make it one of the best organic-substrate candidates for UHF and microwave applications, such as antenna fabrication [6], [7]. Paper has excellent dielectric characteristics. Its dielectric constant is close to air's meaning electromagnetic power can penetrate easily even if the RFID is embedded in the substrate. The high demand and the mass production of paper make it widely available and at the same time the lowest cost material ever made. From a manufacturing point of view paper can undergo large reel-to-reel processing, as shown in Figure 4.1, thus mass fabricating RFID inlays on paper becomes more feasible. Paper also has low surface profile and with appropriate coating it is suitable for direct write methodologies, such as conductive inkjet printing, instead of the traditional metal etching techniques. Such a fast process can be used efficiently to print electronics on the surface of paper substrate or even embedded in a multilayer fashion. In addition, paper can be made hydrophobic as shown in Figure 4.2, and/or fire-retardant by adding certain textiles to it, which easily resolve any moisture absorbing issues that fiber-based materials such as paper suffer from. Moreover, paper is one of the most environmentally-friendly materials. One of its biggest advantages is its high biodegradability with respect to other ceramic substrates, such as FR-4, requiring only months to turn into organic matter in land-fills.



Figure 4.1 Reel-to-reel mass paper production



Figure 4.2 Magnified droplet of water sitting on a paper substrate

It has to be noted that paper is also suitable for integrating other electronic components (sensors, integrated circuits, power sources) and making in this way feasible the implementation of a complete RFID tag module on paper, as discussed in Section 2.4.2. Last but not least paper is a flexible substrate enabling the implementation of flexible antennas and wearable electronics as shown in Figure 4.3 and Figure 4.4 respectively.

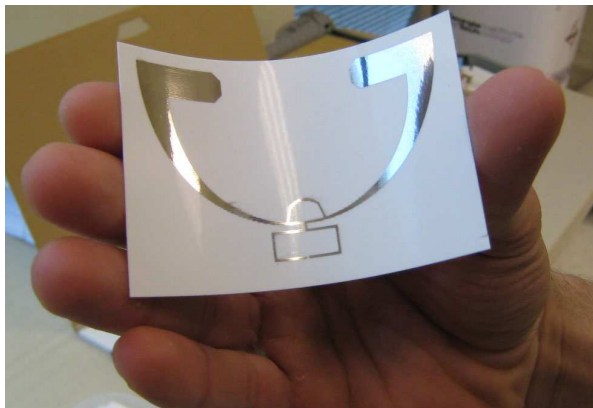


Figure 4.3 Inkjet printed antenna on flexible paper substrate



Figure 4.4 Wearable RFID tag on wrist for medical monitoring

4.3 Dielectric Characterization of the Paper Substrate

RF characterization and the knowledge of the dielectric properties of the paper substrate become necessary for the design and modeling of any high frequency structure such as RFID antennas on paper. The two most important electrical parameters used to characterize an RF/microwave substrate are the dielectric constant and the loss tangent. Dielectric constant (ϵ_r) determines the characteristic impedance

of circuitry, such as transmission lines, the wavelength in the dielectric medium and affects the performance of the antenna. Loss tangent ($\tan\delta$) determines the amount of loss in the dielectric medium and hence determines if a substrate is appropriate for a certain application depending on its power level requirements. The most precise method for determining these parameters of paper in the UHF band and higher frequencies is the microstrip ring resonator method. This method has been studied and performed by [5], [6] and an outline is presented here.

In order to measure the dielectric constant (ϵ_r) and loss tangent ($\tan\delta$) of paper in the frequency range of up to 2 GHz, two microstrip ring resonator structures (A and B) are designed and fabricated on a 3 sheet and 9 sheet thick photo paper substrate respectively. Typical Kodak photo paper with thickness $260\pm 3\mu\text{m}$ is used to fabricate the structures. Since the conductivity of silver ink varies with the curing temperature and duration (curing will be discussed in Section 4.4.5), an 18 μm thick copper foil was selected as the metallic material and was heatbonded on both sides of the paper substrate, in order to accurately model and de-embed the conductive loss of the microstrip circuit. A calibration method named Through Reflect Line (TRL) was utilized to de-embed the effects of the input and output feeding lines. For this reason TRL lines were designed to be a quarter-wavelength long at different frequencies over the range of measurement. Typical SMA coaxial connectors were also used to feed the ring resonator structure and the TRL lines. Figure 4.5 shows a layout of the ring resonator along with the dimensions for the microstrip feeding lines, the gap in between the microstrip lines and the microstrip ring resonator, the width of the signal lines, and the mean radius r_m . Figure 4.6 displays the fabricated ring resonators along with the TRL lines.

The ring resonator produces insertion loss (S_{21}) results with periodic frequency resonances. In this method, ϵ_r can be extracted from the location of the resonances of a given radius ring resonator while $\tan\delta$ is extracted from the quality factor (Q) of the resonance peaks along with the theoretical calculations of the conductor losses. Measurements of S_{21} were done over the frequency range of 0.4 GHz to 2.5 GHz using a typical Vector Network Analyzer (VNA) and are shown in Figure 4.7.

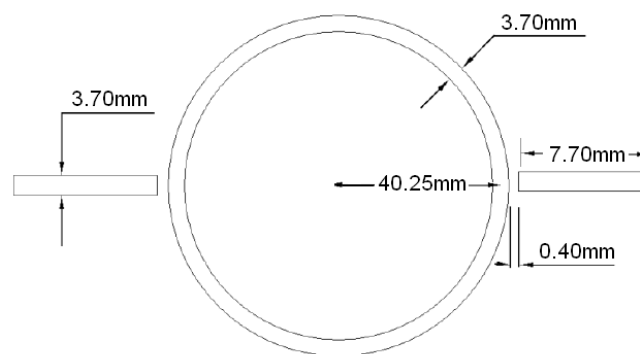


Figure 4.5 Microstrip ring resonator configuration diagram

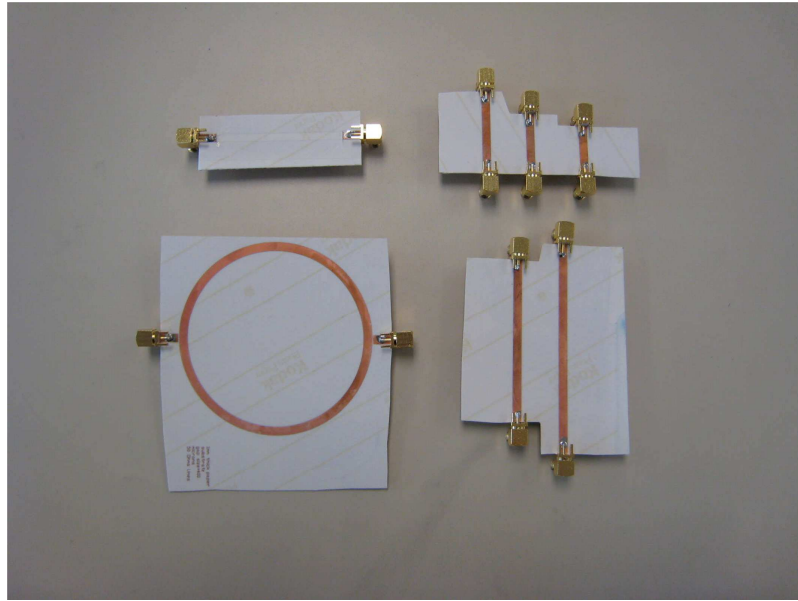


Figure 4.6 Photo of fabricated microstrip ring resonators and TRL lines bonded to SMA connectors

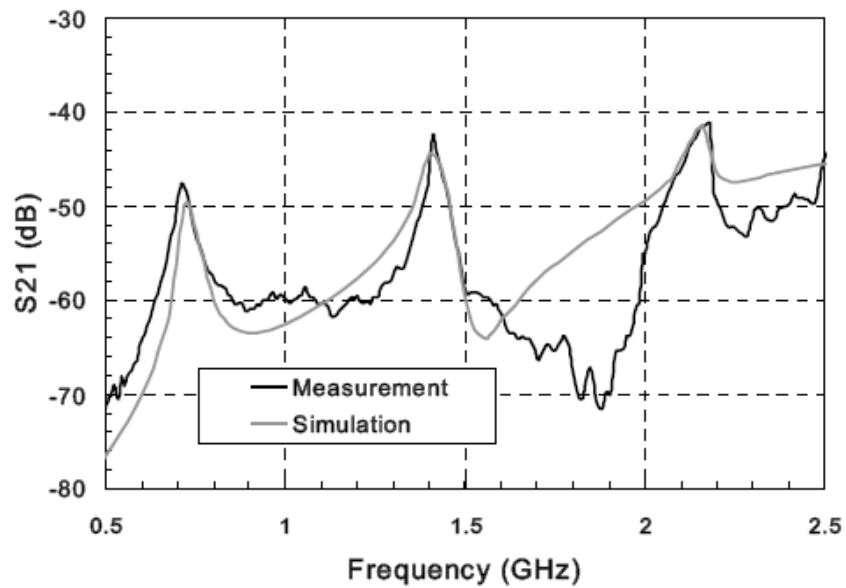


Figure 4.7 Measured and simulated S_{21} results of ring resonator configuration A

4.3.1 Dielectric constant

In order to extract the dielectric constant, the desired peaks were first obtained from Figure 4.7: The dielectric constant ϵ_r can be extracted from (6), (7):

$$\epsilon_r = \frac{2 \times \epsilon_{eff} + M - 1}{M + 1} \quad (6)$$

$$\epsilon_{eff} = \left(\frac{n \times c}{2 \times \pi \times r_m \times f_o} \right)^2 \quad (7)$$

where:

ϵ_{eff} : the effective relative permittivity

f_0 : the n^{th} resonant frequency

c : the speed of light in vacuum

r_m : the mean radius of the ring resonator

M : a function of the dimensions of the microstrip

The values of the dielectric constant extracted at the three resonating modes' frequencies for each ring resonator are shown in Figure 4.8. The lowest value obtained in the frequency range of 0.5–2.5 GHz, was $\epsilon_r = 3.2$ and the highest was $\epsilon_r = 3.5$ with a slight decrease with increasing frequency. For our application where the operating frequency is 904.5MHz the dielectric constant of paper substrate is found $\epsilon_r=3.4$

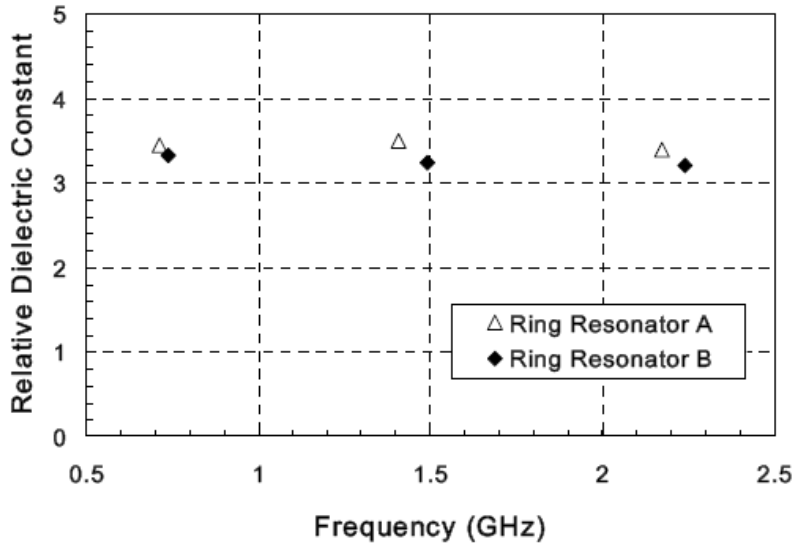


Figure 4.8 Extracted relative dielectric constant ϵ_r of paper versus frequency

4.3.2 Dielectric loss tangent

The extraction of the loss tangent was performed by calculating the theoretical values of conductor and radiation losses. This is done in order to isolate the dielectric loss α_d from the total loss α_o since the ring resonator method gives the total loss at the frequency locations of the resonant peaks. The loss tangent is a function of α_d (in Nepers/m) according to (8):

$$\tan \delta = \frac{\alpha_d \alpha_o \sqrt{\epsilon_{eff} (\epsilon_r - 1)}}{\pi \epsilon_r (\epsilon_{eff} - 1)} \quad (8)$$

where λ_0 is the free-space wavelength and ϵ_r and ϵ_{eff} are defined in Section 4.3.1

The loss tangent extracted from ring B at the three different resonating frequencies is shown in Figure 4.9. The measured values vary from 6×10^{-2} to 8×10^{-2} versus frequency. In order to verify the ring resonator measurement method, another simulation-based transmission line (TL) method was utilized. A microstrip line with length 74.8mm and width 2.53mm was fabricated on the same paper material. Simulation results for conductor and radiation losses, a_c and a_r respectively, of the microstrip line were subtracted from the total loss a_0 . This was done by simulating a microstrip line with no dielectric loss in HFSS, extracting a_r and a_c and then subtracting these effects from the total measured loss. The TL method results are also plotted in Figure 4.9, showing good agreement with the microstrip ring resonator method. For our application were the operating frequency is 904.5MHz the dielectric loss tangent of paper substrate is found $\tan\delta=0.08$.

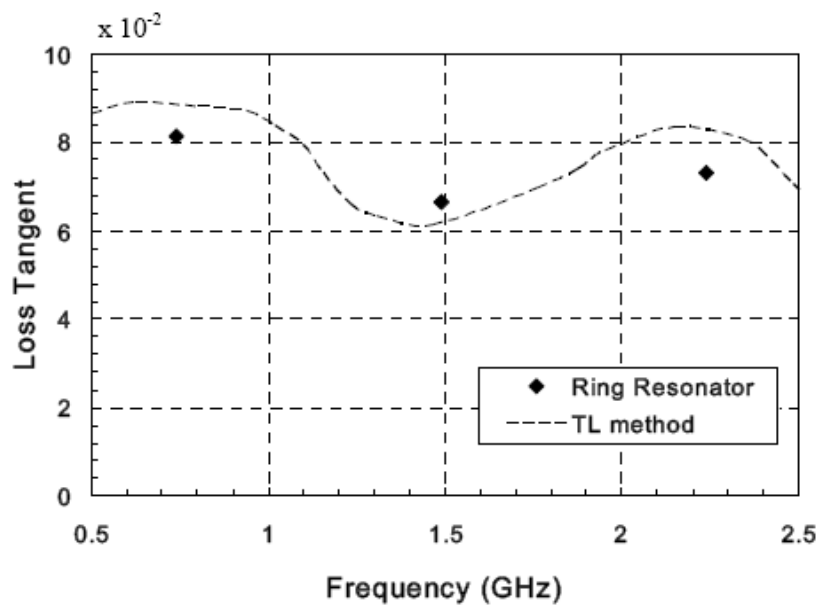


Figure 4.9 Paper loss tangent $\tan\delta$ versus frequency measured with the microstrip ring resonator method and the TL method

4.4 Conductive Inkjet Printing Technology

Inkjet printing is a direct-write technology for fabricating electronic circuits and RF structures [8], [9]. In inkjet printing the design pattern is transferred directly to the substrate. As a result there is no requirement for photolithographic masks as in traditional etching techniques for fabricating circuits which are widely used in industry. A specialized inkjet-printer is used to deposit a conductive silver ink on to the paper substrate. The ink contains silver nano-particles and is sprayed from a piezoelectric ink-jet nozzle forming in this way a conductive paste into the desired position.

4.4.1 Inkjet printing technology advantages

Inkjet printing features many advantages compared to traditional fabrication techniques [6]. Traditional etching fabrication procedures are subtractive methods. In these techniques the entire surface of the substrate is covered with the conductive material and the desired pattern is created by removing its complimentary unwanted metal from the surface. However in inkjet printing the conductive silver ink is sprayed in the form of single ink droplets from the printer's nozzles to the desired position; therefore, no waste is created, resulting in an economical fabrication solution. This makes inkjet printing also an environmentally friendly process, because no toxic chemicals are used as in common etching procedures. In addition printing is a simple, fast and safe process that is completely controlled from the designer's computer and does not require a clean room environment. The savings in fabrication/prototyping time that inkjet printing brings to RF/wireless circuits are very critical to the ever changing electronics market of today's verifying its feasibility as an excellent prototyping and mass production technology for next generation electronics especially in RFID applications.

4.4.2 Inkjet printer details

The Inkjet Printer used to print the proposed UHF monopole antenna is a "Dimatix Materials Printer DMP-2800 Series", made by Fujifilm and is depicted in Figure 4.10 below.



Figure 4.10 Dimatix Materials Inkjet Printer DMP-2800 Series

The printer is composed of many components and embedded systems, which are all required for the efficient printing process [27], [29]. The most important parts of the printer are explained below and are visible when the top glass lid of the printer is open, as shown in Figure 4.11:

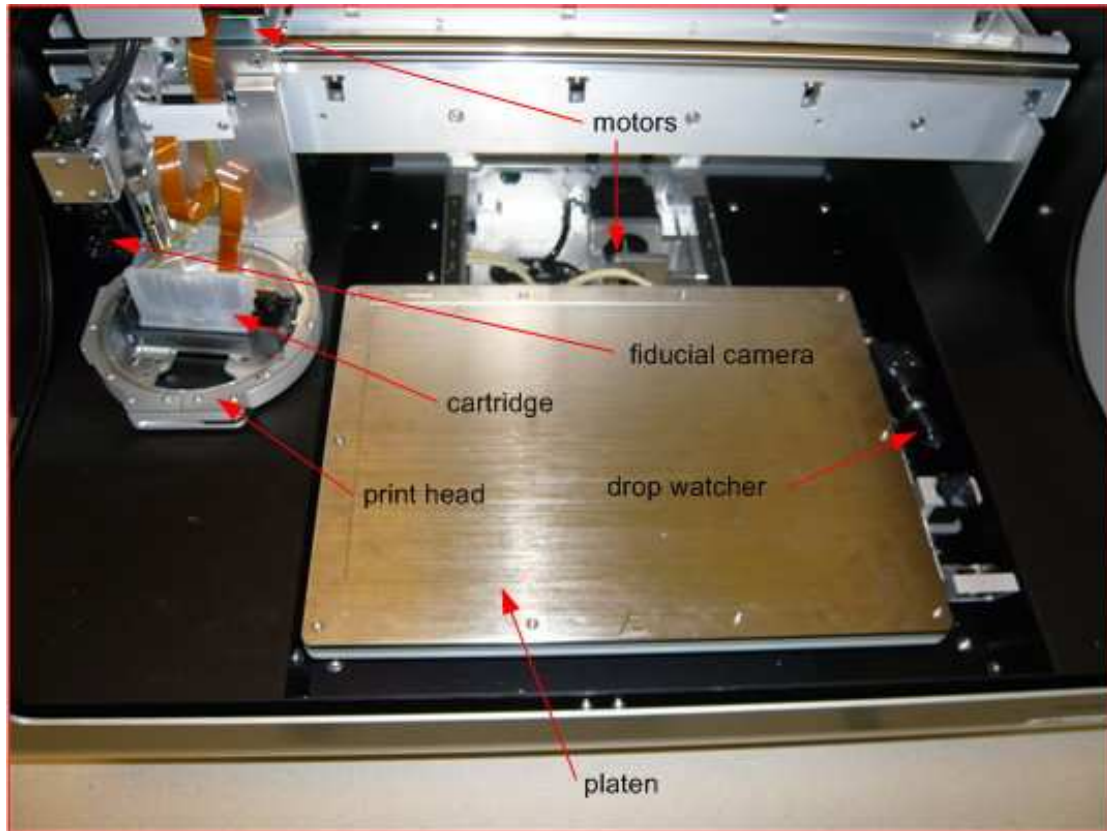


Figure 4.11 Different parts of the inkjet printer

platen

A heated vacuum platen is used for holding the paper substrate. Tiny holes are embedded in the metallic plate and create air vacuum, so that the substrate is attached firmly on the plate. The platen can be heated up to 60° C, sintering the substrate during the inkjet printing. The sintering process removes excess solvent and material impurities from the ink depositions and increases bonding between the silver ink and the paper substrate.

print head

The print head holds the print cartridge and the fiducial camera. The print head moves horizontally in the x-axis by one motor while the platen moves vertically in the y-axis by the other motor. In this way it is possible to print bar by bar just like a conventional inkjet printer.

cartridge

The print cartridge is a low cost, user-fillable, piezo-based inkjet cartridge, shown in Figure 4.12. It composes of a 1.5mL ink reservoir, which can be heated up to 70° C to ensure that the ink flows smoothly. At the bottom it has 16 nozzles with 254µm spacing in a single row, from which the conductive ink is jetted. The type of cartridge determines the resolution of the printer. A 10pL “DMC-11610” cartridge has a

nominal drop volume of 10pL, where a highly accurate 1pL “DMC-11601” cartridge can achieve 20 μ m gap spacing between printed lines. The former cartridge is used when large areas, such as ground planes, are printed to increase their conductivity. The latter cartridge is utilized when high precision printing is required, such as printing traces to connect the pads of an IC, or planar transmission lines with small gap spacing. The low accuracy cartridge achieves however a thicker printed trace, and thus higher conductivity in contrast to the high accuracy cartridge. It has to be noted that when filling the high accurate cartridge, the silver ink has to be filtered first in order to remove any large aggregates or particles.

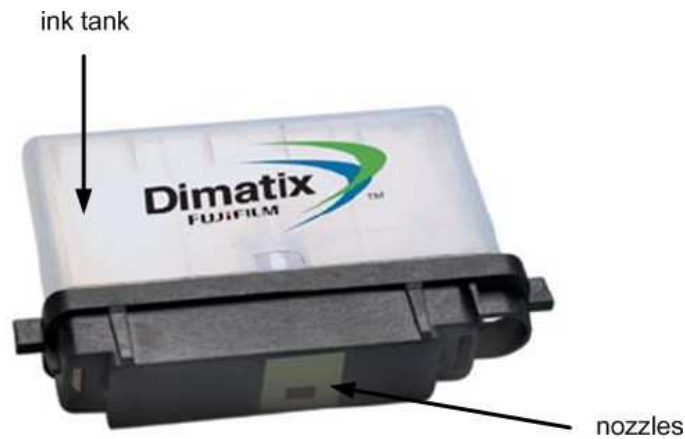


Figure 4.12 Inkjet-printer cartridge

fiducial camera

The fiducial camera is a high definition macro camera that is mounted on the print head. It provides a close-up view of the paper substrate enabling the inspection of printed patterns. In addition using the fiducial camera other operations can be performed, such as: positioning a print origin to match substrate placement, cartridge alignment, measurement of features and locations. More information about the fiducial camera can be found in the Appendix. In Figure 4.13 an image captured with the fiducial camera showing an example of the high accuracy of the printer is illustrated.

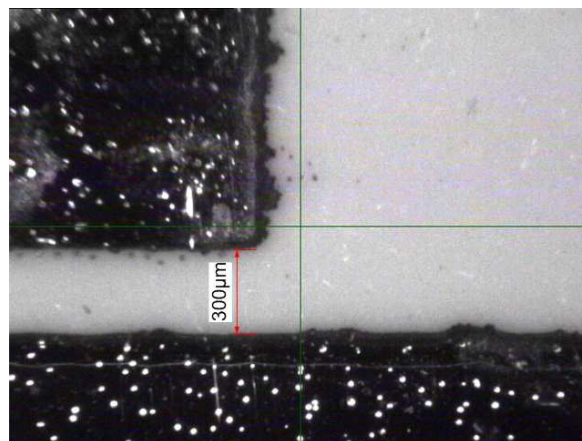


Figure 4.13 Image of a printed silver ink conductive trace captured by the fiducial camera

drop watcher

The drop watcher is a built in drop jetting observation system, that composes of a high-speed camera and a lens system. It is used to verify that all nozzles are firing properly the ink droplets. A common problem that exists with silver ink cartridges is that the ink often clogs and is not being sprayed out of the nozzle. In this case the drop watcher can be used to identify the nozzles that are not functioning properly. Then the voltage across them can be increased through the software, so that the clogged and excessive ink can be fired from the nozzle and normal nozzle operation can be achieved again. In Figure 4.14 an image captured with the drop watcher is illustrated, where six nozzles are firing a single silver ink droplet each.

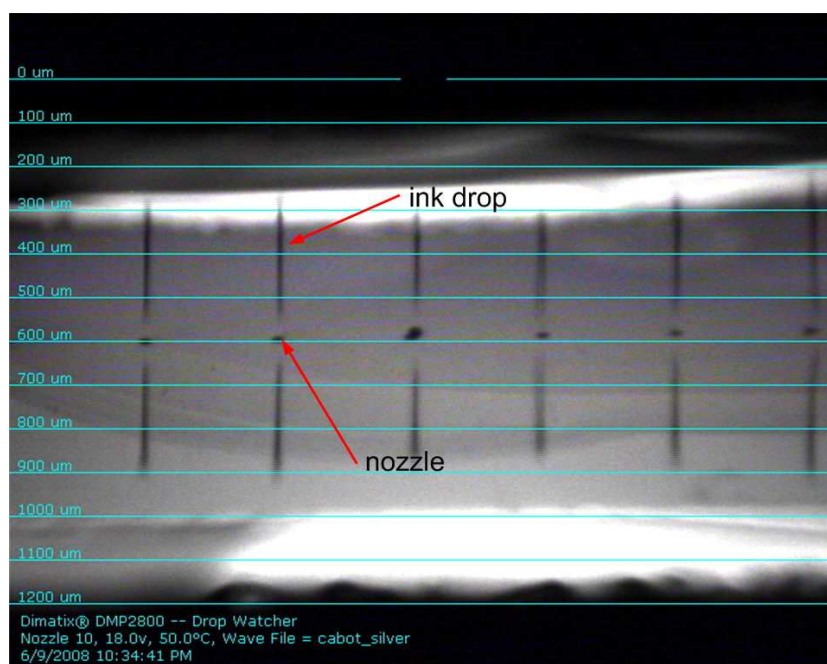


Figure 4.14 Image captured with the drop watcher camera that depicts the cartridge nozzles while jetting silver ink drops

cleaning pad

The cleaning pad is placed below the print head, when the print head is in its original position (it is not visible in Figure 4.11). During the printing process excessive ink is concentrated around the cartridge nozzles, which may result into ink clogging and deterioration of the printing. For this reason a special textile replaceable pad is used to clean the cartridge nozzles. In fact special cleaning cycles can be set up and must be executed several times during printing. This is achieved by the cartridge moving every fixed amount of time over the cleaning pad to clean itself.

The data sheet of the DMP-2800 Series inkjet printer is cited in Appendix.

4.4.3 Silver ink and inkjet system

The material that is being used as an ink to print a pattern on the substrate is silver ink. Silver ink is composed of silver conductive nano-particles, as shown in Figure 4.15. Before use, it is stored in liquid form in temperature lower than 3° C. The ink is loaded into the cartridge reservoir using a syringe. After the ink is sprayed on to the substrate, it becomes a solid paste with low conductivity. In order to increase its conductivity the silver ink must be cured. Curing is a heating process described in Section 4.4.5.

Silver ink is sprayed from the cartridge nozzles on to the paper substrate. The operation of the jetting system, illustrated in Figure 4.16, is based on voltage applied at the orifice of each nozzle. The spraying of silver ink droplets is controlled, by the automatic adjusting of the voltage in the charge electrode and across the deflection plates. When the nozzles are not jetting a voltage is still applied so that the ink is contained at the edge of the nozzles and is not dripping down to the substrate. Manual setting of the nozzle voltage can be applied through the printer's software in order to control the thrust and speed of the ink drops.

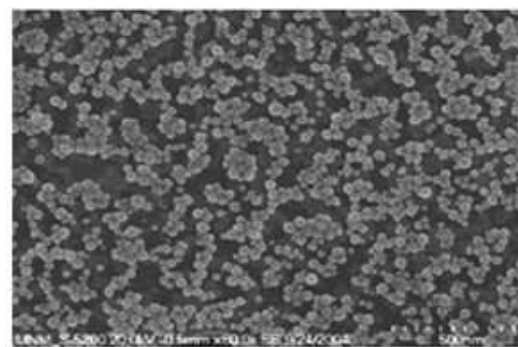


Figure 4.15 Nano-sized silver ink

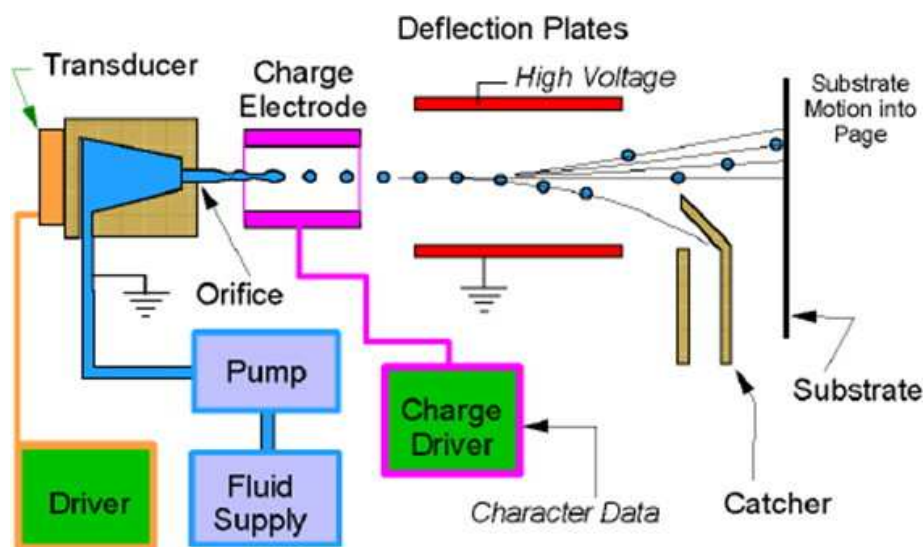


Figure 4.16 Inkjet mechanism of silver ink droplets sprayed from the cartridge nozzles

4.4.4 Antenna printing process

The printing process of the antenna is completely controlled from a PC connected to the printer and is summarized in the following 9 steps:

- 1) The design pattern to be printed is saved as a black and white image in a Gerber file format (*.gbr).
- 2) The Gerber file is opened in the included with the software program called “Gerber Magic”. After verifying that all dimensions and traces of the design are correct the file is saved as a Bitmap file (*.bmp).
- 3) The printer’s software program is opened. In the first screen dialog the appropriate settings file for the desired accuracy cartridge (10pL or 1pL) is required to be selected. The settings for each cartridge can be modified according to the user’s preference and saved in a file so that can be loaded and applied any time. The desired cartridge is filled with silver ink and is placed on the print head.
- 4) The design pattern bitmap file is opened through the tools menu and is previewed in the printing area. A reference point is set in the printing area that determines the upper left starting print origin point in the design pattern. The bitmap file with the placed reference point is saved as a Pattern file (*.ptf).
- 5) In the second screen dialog the substrate is required to be loaded. It is aligned in the metallic platen and tape is placed at its edges so that it remains firm attached to the platen. It is very important to ensure that the paper is not lifted from the platen, because the print head moves very close to the paper substrate. Then the air vacuum is turned on and the desired platen temperature is selected. In our case the temperature was set at 50° C
- 6) The drop watcher application is opened and all nozzles are verified that operate properly through the high speed camera. If a nozzle is not firing, the input voltage is increased until the ink is unclogged.
- 7) The fiducial camera application is opened and a print origin is positioned on the substrate, which defines the upper left starting point of the printing area. In this way the reference point placed in the design pattern and the print origin placed in the fiducial camera application are matched and the design is printed properly.
- 8) The basic settings have now been modified. The printer has also some more advanced settings such as cartridge angle, custom cleaning cycles, ink temperature, nozzle deactivation and others which were not altered.
- 9) In the final screen the print pattern is previewed and the printing process can be initiated by pressing the print button.

A prototype of the proposed monopole antenna was fabricated following the above procedure and is shown in Figure 4.17. The 10pL low precision cartridge was used to print the radiating element of the monopole and its grounds, except from the part of the ground that was near the feeding line gap where accuracy was needed. Five layers were printed with the 10pL cartridge to ensure maximum conductivity. The high precision cartridge was used to print seven layers of the CPW transmission line of the antenna where the gap spacing between the central conductor and the ground is only 0.3mm. A close up image of the overlap between the printed ink layers using the 10pL cartridge captured with the fiducial camera is shown in Figure 4.18. An image of the CPW feeding line which was printed with the 1pL cartridge is illustrated in Figure 4.19. The difference in accuracy and thickness can be clearly seen between the two cartridges. It is essential to note that when a high accuracy cartridge is replaced by a low accuracy or vice versa the new cartridge must be aligned using the fiducial camera.



Figure 4.17 Prototype of the conductive inkjet-printed antenna

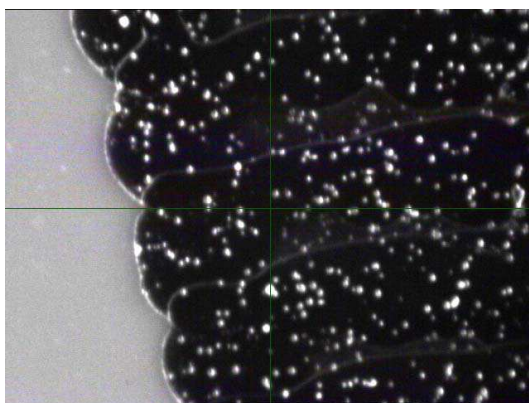


Figure 4.18 Multiple silver ink layers printed using the 10pL inkjet cartridge

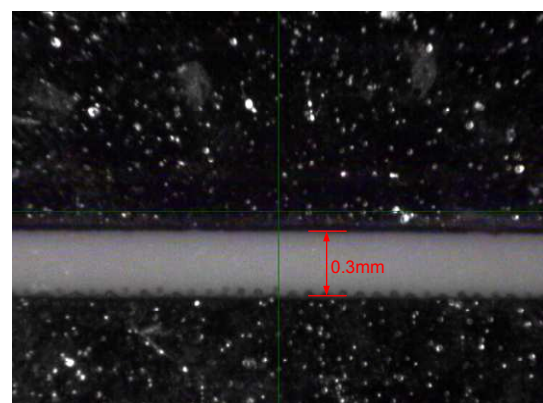


Figure 4.19 Close-up image of the CPW transmission line printed with the 1pL inkjet cartridge, showing the gap between the signal strip and the ground planes

4.4.5 Curing and assembly

After the printing of the antenna it is essential to cure the prototype in order to increase the conductivity of the silver ink. Curing is simply heating the fabricated antenna, so that the printed silver ink nano-particles melt and connect with each other. The curing is performed in a high precision industrial oven, shown in Figure 4.20, at a constant temperature of 100°C for 10 hours. The curing must be performed immediately after the printing, because the silver ink begins to oxidize which may result into permanent poor conductivity and low efficiency of the antenna trace. It has to be noted that the maximum temperature that paper can endure is 150°C.



Figure 4.20 Test Equity FS series industrial oven for performing curing of the prototype antenna

The conductivity of the silver ink varies from $0.4 \sim 2.5 \times 10^7$ Siemens/m depending on the curing temperature and duration time. Before the cure large gaps exist between the particles, resulting in a poor connection. After the cure, the high temperature has caused the particles to expand and the gaps between them to diminish. That guarantees a virtually continuous metal conductor, providing a good percolation channel for the conduction electrons to flow and consequently high conductivity. Figure 4.21 shows the difference of the printed silver ink nano particles before and after the curing process.

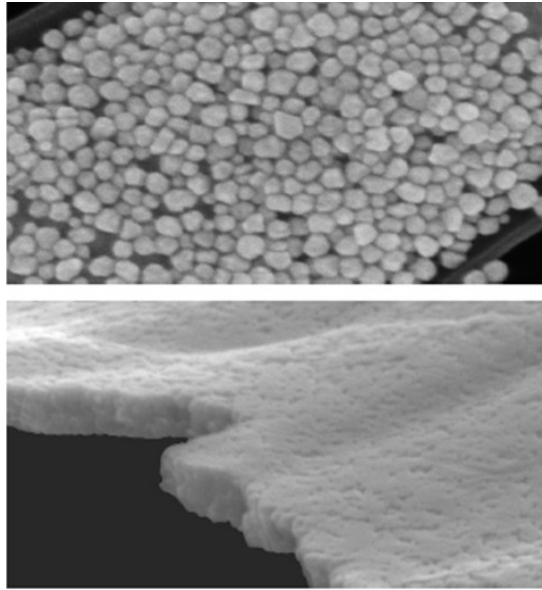


Figure 4.21 Images of a layer of printed silver ink before (top) and after (bottom)

Finally the prototype is assembled by attaching a typical SMA connector to the feeding line of the antenna. An adhesive has to be used in order to mechanically connect the SMA connector to the paper substrate and ensure conductive electrical contact between the connector and the printed silver antenna trace. However, given the low temperature tolerance of paper, and the relative weak adhesion of printed silver ink traces on paper, soldering cannot be used. For this reason a silver epoxy is utilized as an adhesive, in order to permanently attach the connector at the edge of the paper substrate and create an electrical connection. After the application of the silver epoxy, the structure is cured again in the oven at 120°C for 20 minutes, to harden the epoxy's texture and improve conductivity. In Figure 4.22 the completed fabricated antenna is shown and in Figure 4.23 a close up image of the SMA connector attached with epoxy to the printed silver trace is depicted.

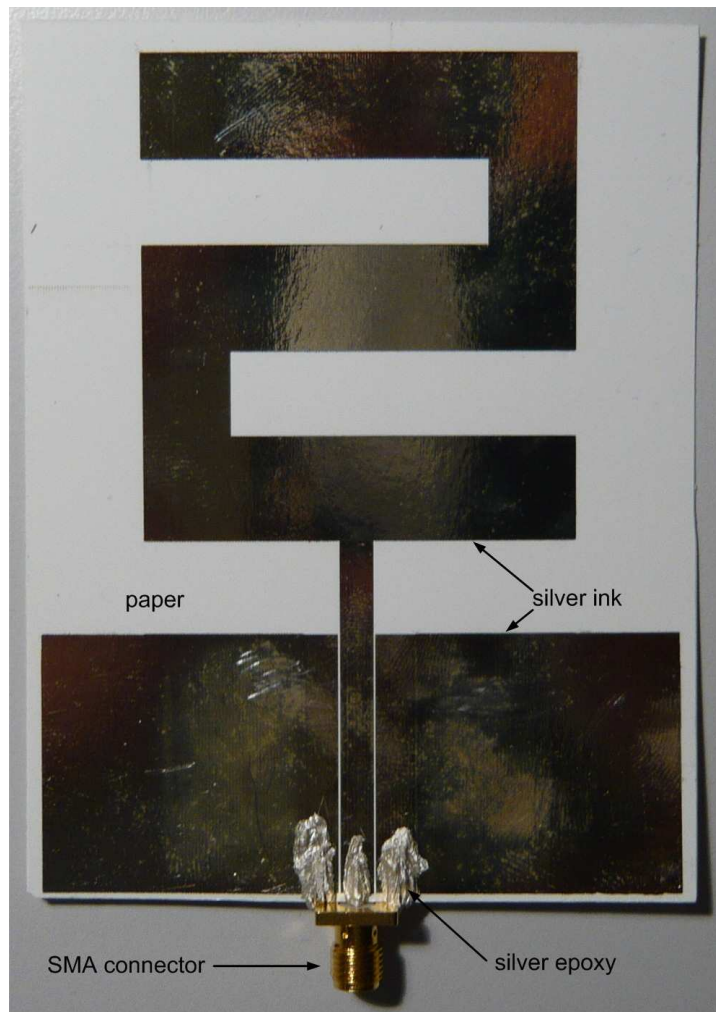


Figure 4.22 Prototype of the fabricated inkjet printed antenna on paper substrate with attached SMA connector

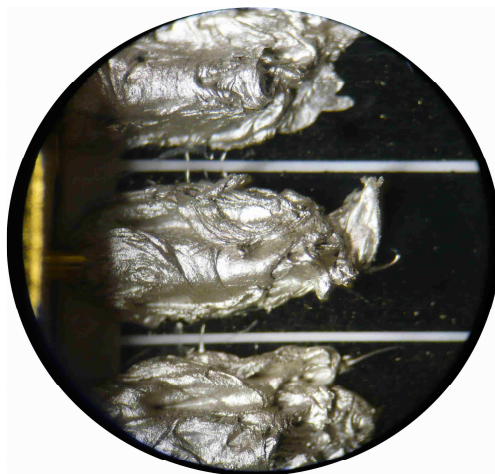


Figure 4.23 Close-up image of the SMA connector attached with silver epoxy to the printed silver antenna trace

4.5 Copper Tape Fabrication

In terms of evaluating the inkjet printing technique and verifying the agreement of the measured results with the simulation, the antenna was also fabricated using copper tape on a paper substrate, as shown in Figure 4.24. This fabrication method is a very simple and fast process, requiring only a thin copper tape, a scalpel and a precision electronic ruler. The process is completed in 4 steps:

- 1) The paper substrate is cut to the required size ($75\text{mm}\times 100\text{mm}$).
- 2) Strips of a self adhering copper tape are applied on to the substrate's surface (on the upper layer) in such way that each piece overlaps by $1/3$ with its next.
- 3) The exact antenna shape is marked on the copper layer using the precision ruler, based on the design's dimensions.
- 4) The complementary copper layer part of the antenna is cut out of the substrate using the scalpel, forming in this way the antenna trace.

Then the conductivity of the fabricated antenna is tested with a multimeter by checking that different copper strips are short circuited. Where an open circuit is detected, solder is applied to electrically connect the 2 parts. Finally a typical SMA connector is also soldered at the input of the feeding line of the antenna.

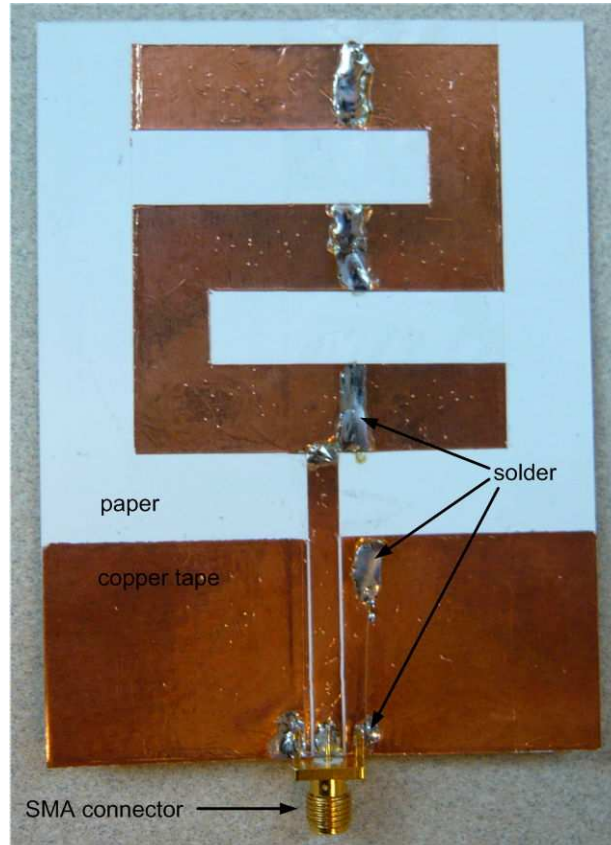


Figure 4.24 Prototype of the copper tape fabricated antenna with attached SMA connector

CHAPTER 5

Experimental Results and Discussion

5.1 Introduction

The performance of the fabricated UHF monopole antenna was experimentally tested in the PIREAS RFID/Sensors Lab. The return loss and the gain were measured and the obtained results were compared with the simulation to verify that the antenna satisfies the design requirements. In this chapter, first the experimental setup and process of the measurements are described. Then the return loss and gain measurements are presented and discussed. A table summarizing the antenna requirements and the simulated and measured results is provided at the end of the chapter for comparison and discussion.

5.2 Antenna Return Loss Measurement

The return loss of the proposed antenna is measured indirectly by first measuring its input impedance. The antenna is designed to be matched to the tag's load which has complex impedance. Attempting to measure directly the return loss of the antenna using a 50Ω coaxial cable as a transmission line, would produce incorrect results, since the return loss of the antenna has to be calculated in respect to the tag's load [3]. As a result the return loss of the proposed antenna has to be measured indirectly, by first measuring the input impedance of the antenna. Then the frequency response of the return loss can be calculated using the approach described in Section 3.2.

5.2.1 Experimental setup

The input impedance measurement of the inkjet printed and copper tape fabricated antenna was performed using the following equipment.

- ROHDE & SCHWARZ
ZVA 8 Vector Network Analyzer
300kHz ... 8 GHz
- Calibration Unit ZV-Z51
- Typical 3.5mm Coaxial Cable

5.2.1.1 Vector network analyzer calibration

First the Vector Network Analyzer (VNA) has to be calibrated using the Calibration Unit ZV-Z51. The calibration is essential so that the measurement reference plane is moved at the very end of the coaxial cable. One end of the coaxial cable is connected to port 1 of the VNA and the other is connected to port 1 of the calibration unit. The VNA is connected also with a USB cable to the calibration unit in order to control the calibration process. The calibration is performed through the Network Analyzer's embedded software and the calibration setup is depicted in Figure 5.1. The measurement frequency range, the type of cable, the port numbers and the type of the calibration unit are inserted into the software. When the calibration, which is fully automated, is complete the VNA is able to perform correctly s-parameters and input impedance measurements at the end of the coaxial cable connected to port 1.

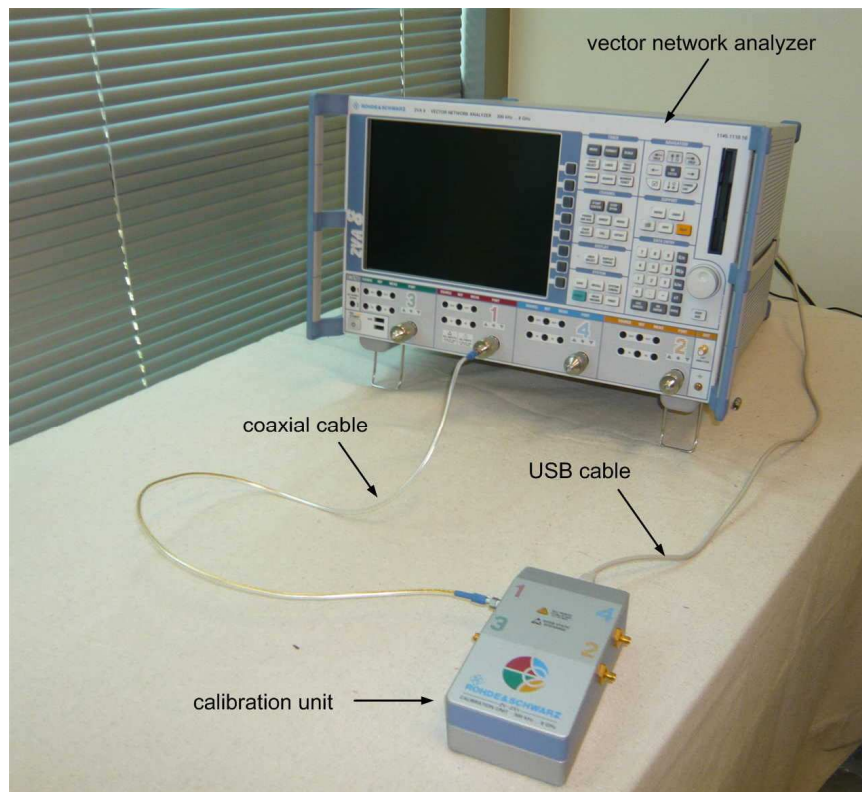


Figure 5.1 Vector network analyzer calibration setup

5.2.1.2 Input impedance measurement

Once the calibration is complete the actual input impedance measurement can be performed. The experimental setup is shown in Figure 5.2. The calibrated coaxial cable is connected to the SMA connector of the antenna. In order to minimize backside reflections the fabricated antenna was placed on a custom-made probe station using high-density polystyrene foam with low relative permittivity $\epsilon_r=1.06$ resembling that of free space. The network analyzer is set to measure the input

impedance at the end of the coaxial cable in the frequency range (700 – 1100 MHz) and a marker is placed at the operation frequency of the proposed antenna at 904.5MHz.

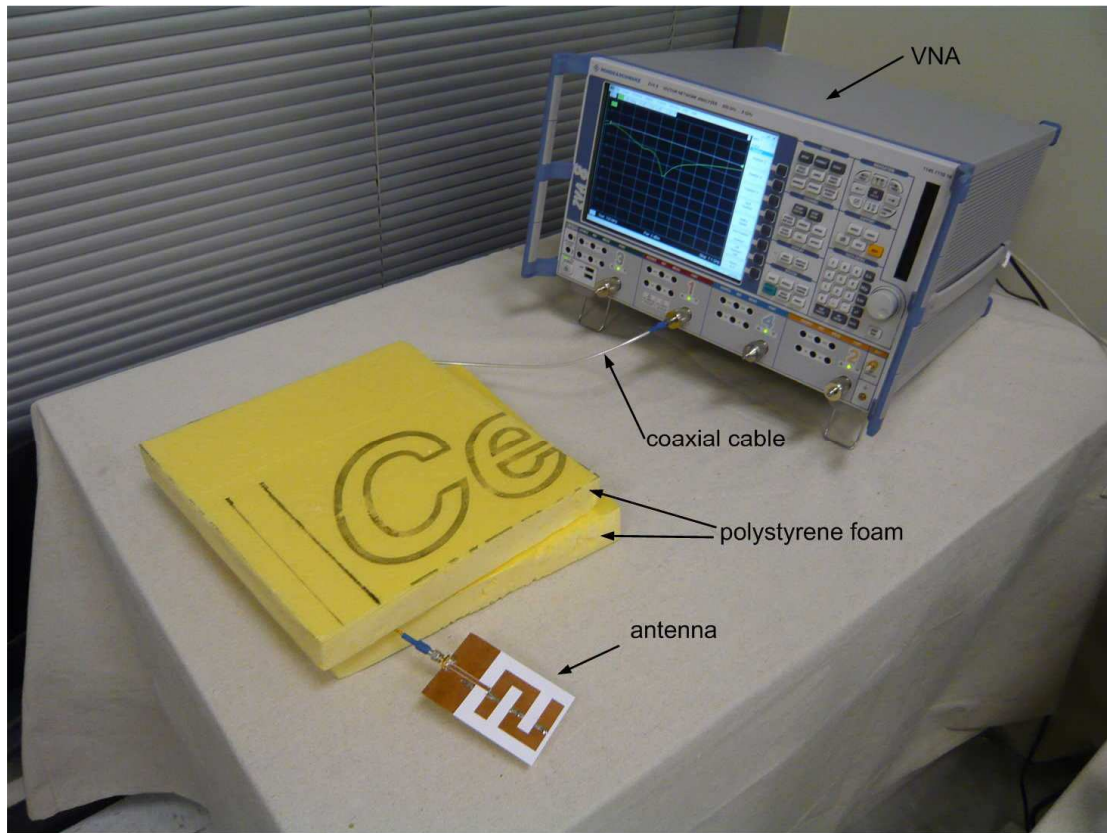


Figure 5.2 Antenna input impedance measurement setup

5.2.2 Input impedance measurement results

The resistive and the reactive part of the input impedance of the inkjet-printed and copper tape fabricated antenna are measured in the UHF frequency range as described in Section 5.2. The frequency response of the measured and simulated results is shown in Figure 5.3. In Table 5.1 is presented the simulated and measured input impedance of the fabricated antenna at the operation frequency. The conjugate input impedance of the load is also given for comparison.

Table 5.1 Simulated and measured input impedance of the proposed antenna at the operation frequency of 904.5MHz

	antenna input impedance at 904.5 MHz (Ohm)
simulation	37.5 – j65.2
inkjet-printed	36.2 – j61.5
copper	39.5 – j65.4
Z_{LOAD}^*	37.31 – j65.96

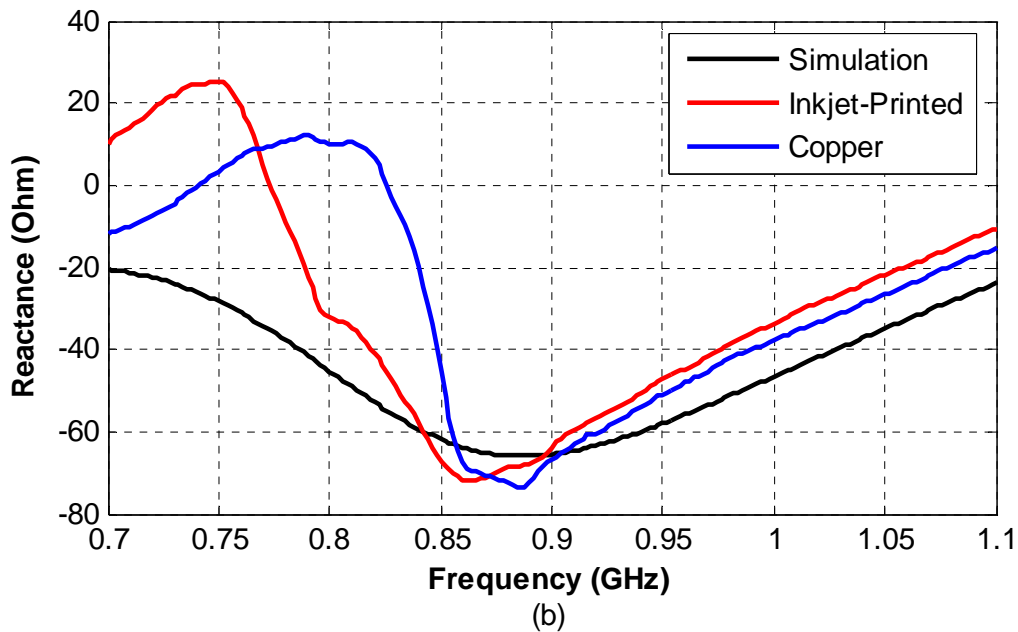
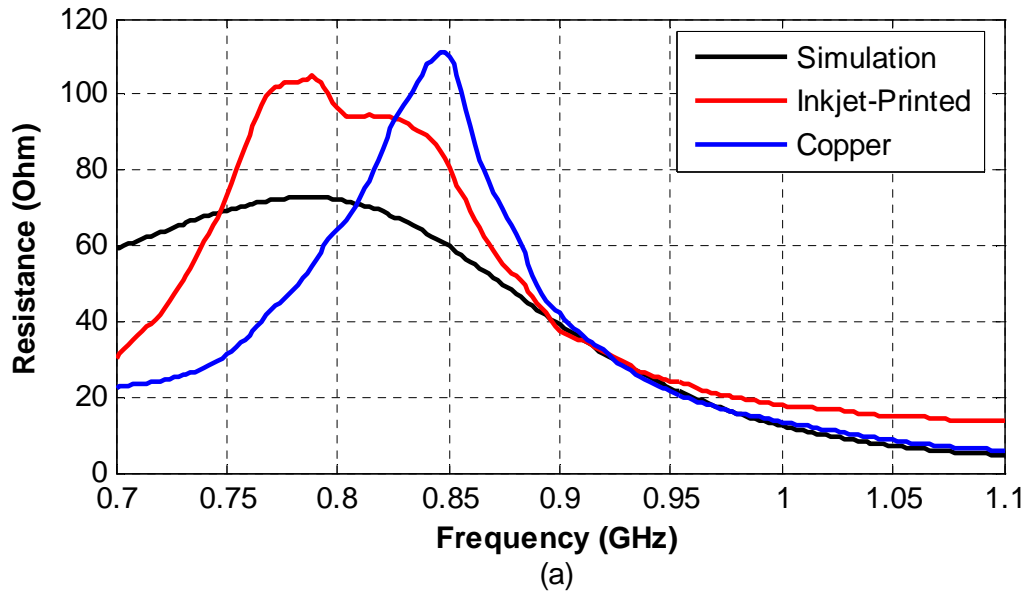


Figure 5.3 Simulated and measured input impedance versus frequency of the inkjet-printed and copper tape fabricated antenna
 (a) Resistance R
 (b) Reactance X

It can be seen from Figure 5.3 that there is a fairly good agreement between the simulated and the measured results. It is also observed that the resistance and reactance plots of both the copper and inkjet-printed antenna agree very well in the (900 – 1100 MHz) frequency range with the simulation plot; however there is a notable deviation from the simulation in the (700 – 900 MHz) frequency range. This comes from the fact that, as has been mentioned before, the dimensions of the ground plane are comparable with the wavelength in free space. For this reason at lower

frequencies the electrical length of the ground plane becomes significantly smaller and it does no longer simulate the existence of a theoretical infinite ground plane that an ideal monopole antenna has; in high frequencies however, where the wavelength is significantly smaller, the electrical length of the ground plane is larger and the radiation of the antenna approaches that of an ideal monopole.

5.2.3 Return loss calculation

The measured frequency response of the Return Loss of the inkjet-printed and the copper fabricated antenna is calculated based on the input impedance measurements and the analysis described in Section 5.2. The measured and simulated return loss is depicted in Figure 5.4.

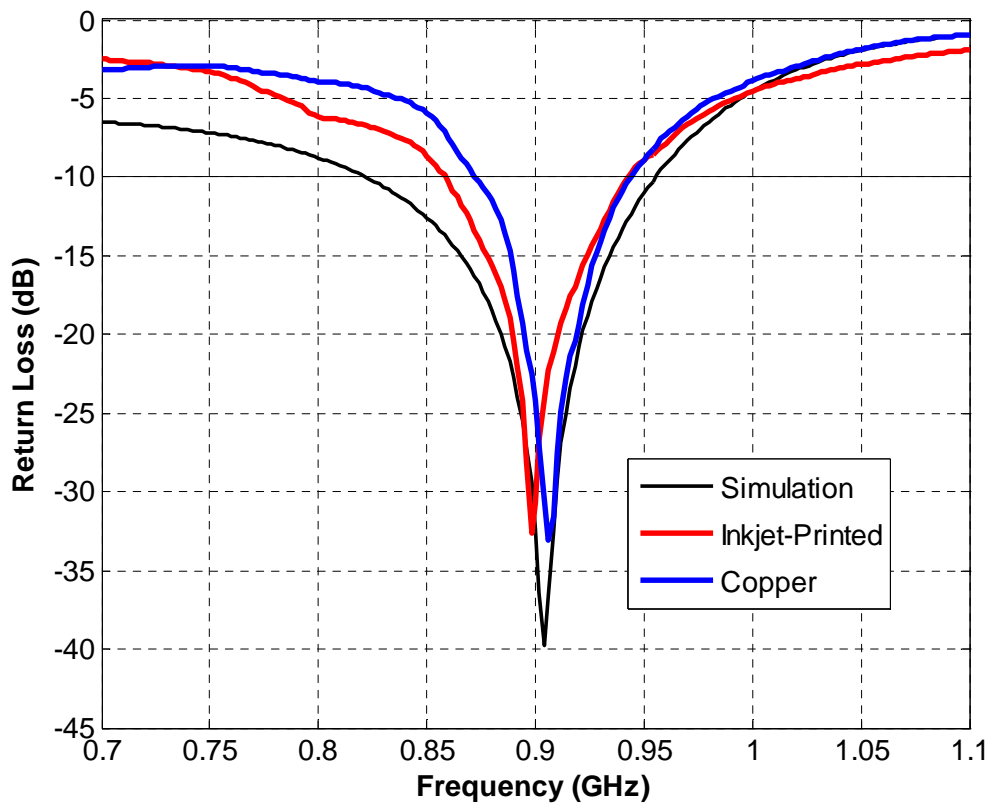


Figure 5.4 Measured and simulated frequency response of the return loss of the inkjet printed and copper tape fabricated antenna

It is observed from Figure 5.4 that the measured S_{11} plot of the inkjet-printed antenna is resonant at 898MHz with -10 dB impedance bandwidth of 82MHz (860 – 942MHz) corresponding to 9.1% around the center frequency. The copper tape fabricated antenna displays a return loss plot with center frequency at 906MHz and a bandwidth of 68MHz (874 – 942MHz) corresponding to 7.5% around the center frequency. The above results are summarized in Table 5.2.

Table 5.2 Antenna return loss comparison between experimental and simulated results

	simulation	inkjet-printed	copper
center frequency (MHz)	904	898	906
frequency range (MHz)	822 – 954	860 – 942	874 – 942
bandwidth (MHz)	132	82	68
bandwidth (%)	14.6	9.1	7.5
return loss at 904.5MHz (dB)	-38.4	-23.7	-31.9

It is observed from the obtained results that there is a good agreement between the simulation and the measurements. The power transmission coefficient is greater than 99% for the inkjet printed antenna, and greater than 99.9% for the copper tape fabricated antenna at the operation frequency. As a result almost all of the available power from the antenna is transferred to the load and the range of the RFID tag is expected to be large.

Observing the return loss measurement plot of the copper tape fabricated antenna, it is seen that there is a slight resonance shift from the desired antenna operation frequency and that the return loss bandwidth is narrow compared to the simulation. This discrepancy has occurred due to human errors at cutting copper tape, during the copper tape antenna fabrication process.

5.3 Antenna Gain Measurement

5.3.1 Experimental setup

The following equipment was used to carry out the gain measurements for the inkjet-printed and copper fabricated UHF monopole antenna:

- ROHDE & SCHWARZ
SMJ 100A Vector Signal Generator
- Tektronix RSA3408A DC – 8GHz
Real Time Spectrum Analyzer
- AN-400 Reader Antenna with gain $G_r=6\text{dBi}$
- Typical 3.5mm Coaxial Cable with attenuation=0.1dB

The equipment was set up as shown in Figure 5.5. The prototype antenna to be measured was treated as the transmitter and was connected with a coaxial cable to the Vector Signal Generator. The antenna (transmitter) was attached at a height of $h_t=1.60\text{m}$ on a piece of polystyrene foam using thin adhesive tape, as shown in Figure 5.6. Polystyrene foam was used to hold the antenna in place, simulating a free-space environment. If another material had been used, for example a metallic stand, reflections would have occurred, changing the performance of the antenna. The AN-400 antenna is an RFID reader antenna [26] and is treated as the receiver in the experimental setup. The receiver was connected with a coaxial cable to the Real Time Spectrum Analyzer and was positioned at a fixed place that had also a height of $h_r=1.60\text{m}$, as shown in Figure 5.7. Both distances were measured from the middle

point of each antenna to the ground. The distance between the transmitter and the receiver was measured $d=4.06\text{m}$.

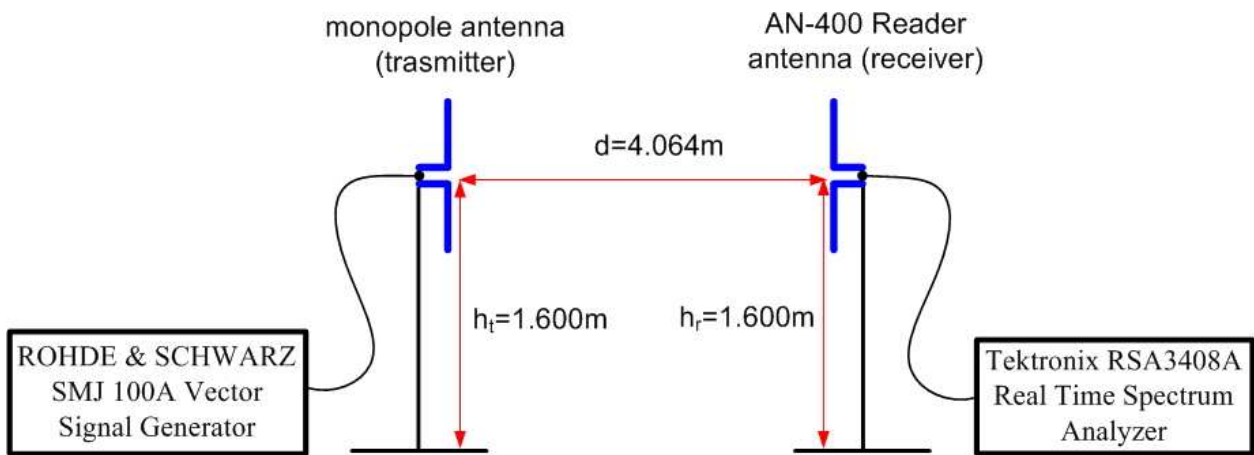


Figure 5.5 Gain measurement experimental setup

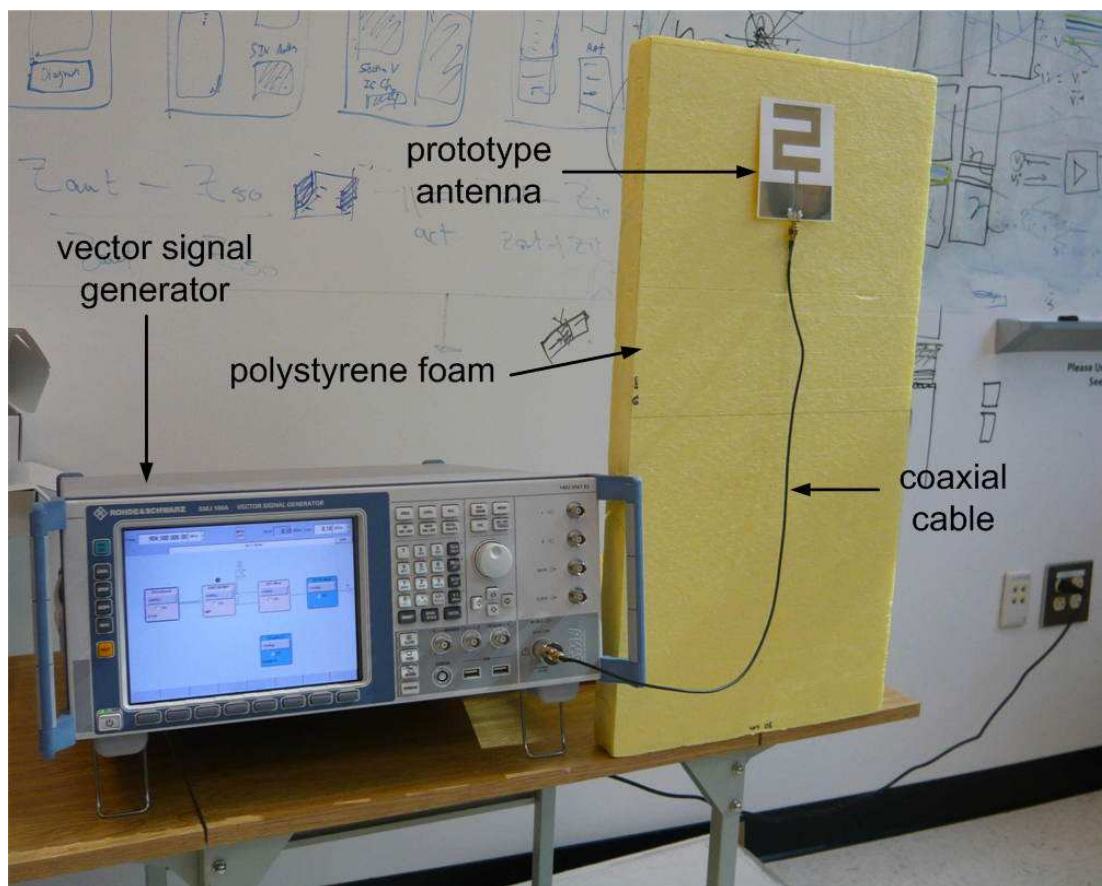


Figure 5.6 Prototype antenna (transmitter) and vector signal generator setup

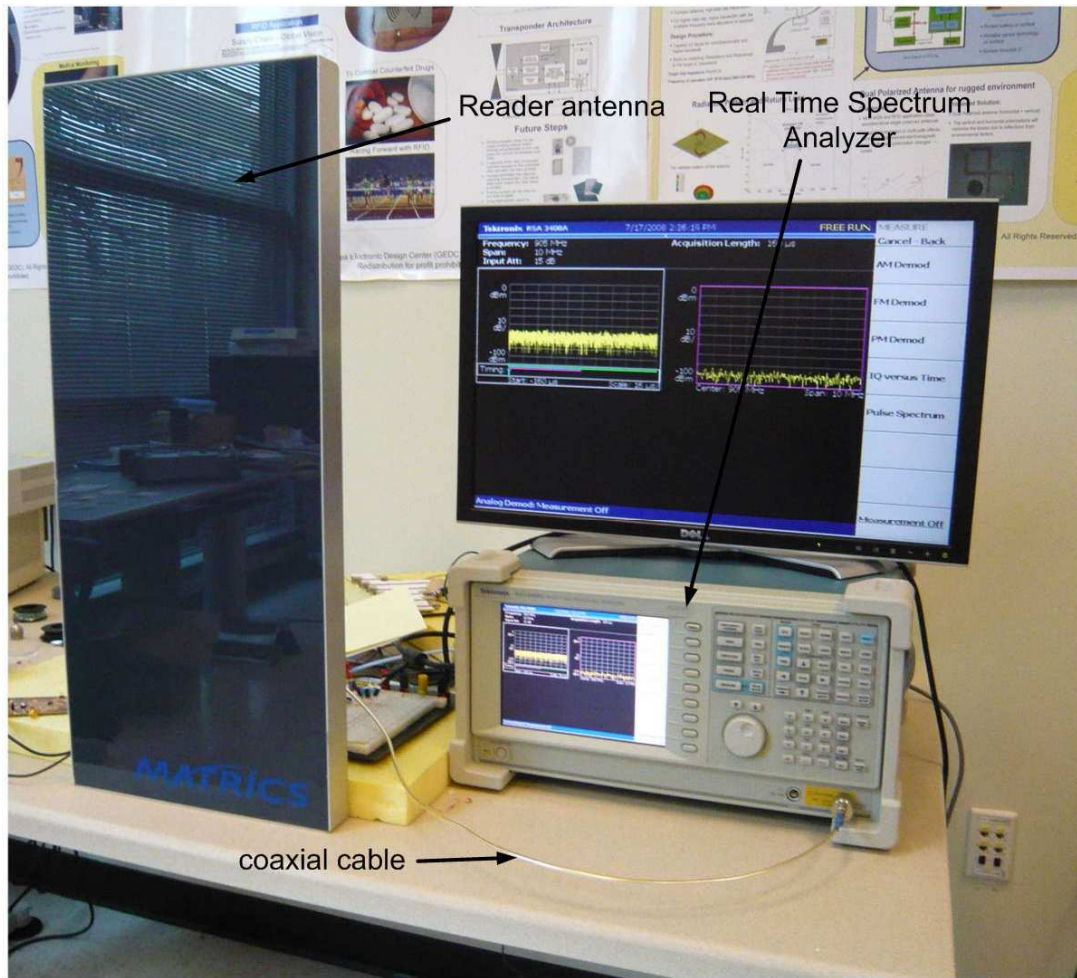


Figure 5.7 AN-400 RFID reader antenna (receiver) and real time spectrum analyzer setup

First it is essential to verify that the receiver is at the far field region of the transmitter [17]. The far field boundary is calculated using (9), Fraunhofer's far field equation, shown below:

$$R = \frac{2D^2}{\lambda} \quad (9)$$

where:

R : the distance from the prototype antenna at which its far field region starts

D : the largest dimension of the antenna

λ : the free space wavelength at the transmission frequency of 904.5MHz

The far field boundary for the monopole antenna is evaluated using (9) to be $R=6.0\text{cm}$. Therefore it is verified that the receiver is in the far field region of the monopole antenna. It is also essential to make sure that there is a clear line of sight between the two antennas and that no other objects are at a smaller distance from the antenna's far field boundary.

Finally it is critical to make sure that both antennas are placed in the optimum orientation with each other. Each antenna must be placed in the direction of maximum

radiation intensity or gain of the other. In this way the gain of the fabricated antenna can be measured correctly at the operating frequency and compared to the simulation.

5.3.2 Measurement process and results

The gain measurement is performed for both the inkjet-printed and the copper fabricated antenna. The Vector Signal Generator is set so that it transmits a continuous wave signal at the operating frequency of the antenna, which is at 904.5MHz with power $P_s=0.1\text{dBm}$. The Signal Generator is connected to the antenna, with a 50Ω coaxial cable with loss $L_c=0.1\text{dB}$. Therefore, the power at the end of the coaxial cable and before the input of the antenna is $P_t = P_s - L_c = 0\text{dBm}$.

In addition the antenna is not matched to the 50Ω coaxial cable, since it has complex input impedance. As a result there is another power loss in the antenna input because of power reflection, between the antenna and the 50Ω transmission line. The reflection coefficient ρ for the both inkjet printed and copper fabricated antenna is calculated by (10) taking into account their respective measured input impedance at the operating frequency.

$$\rho = \frac{Z_{ant} - Z_0}{Z_{ant} + Z_0} \quad (10)$$

where:

Z_{ant} : the measured input impedance of the antenna at the operating frequency

Z_0 : the characteristic impedance of the coaxial cable ($Z_0=50\Omega$)

ρ : reflection coefficient

The magnitude of ρ is found for the inkjet printed antenna $|\rho|=0.59$ and for the copper tape fabricated antenna $|\rho|=0.60$. The mismatch loss is evaluated for both antennas as: $L_m = (1 - |\rho|^2)_{dB} = 1.9\text{dB}$.

The input power after the losses is radiated from the proposed antenna (transmitter) into space and is received by the Reader Antenna (receiver). The reader antenna has gain of $G_r=6\text{dBi}$ and is matched to the 50Ω coaxial cable that connects it to the spectrum analyzer. Because the receiver antenna is circular polarized and the transmitter monopole antenna is linear polarized, a polarization mismatch exists in the wireless link between the two antennas. The polarization mismatch has to be accounted and is $L_p=3\text{dB}$ as described in Section 3.3. The accepted power from the reader antenna is measured by the spectrum analyzer, which was set to a center frequency of 904.5MHz with a resolution bandwidth of 36MHz. The measured accepted power results are the same for both antennas and are illustrated in Figure 5.8.

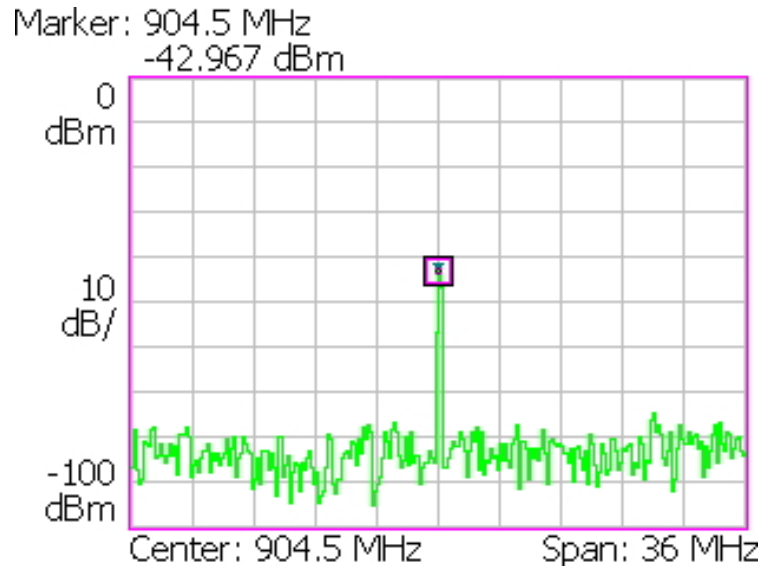


Figure 5.8 Received power at the AN-400 RFID reader antenna (receiver) terminals

5.3.3 Antenna gain calculation

In order to calculate the gain of the antenna from the measured results, a propagation model has to be applied. To determine which propagation model is suitable for our measurement setup, we have to investigate if any obstacles exist in the first Fresnel zone of our wireless link setup. Therefore, the maximum radius of the first Fresnel zone has to be calculated. The maximum radius of the first Fresnel zone is calculated by determining the radius of the Fresnel zone cross section from (11) at the midpoint between the transmitter and the receiver, as shown in Figure 5.9.

$$r = \sqrt{\frac{\lambda}{\left(\frac{1}{d_t} + \frac{1}{d_r}\right)}} \quad (11)$$

where:

r : the radius of the first Fresnel zone

λ : the wavelength of the transmitted signal in free space

d_t : the distance from the fresnel zone cross section to the transmitter

d_r : the distance from the fresnel zone cross section to the receiver

The radius r , when $d_t=d_r=2.03\text{m}$ is found $r=0.58\text{m}$. It is observed that r is lower than the heights of the transmitter and the receiver and since no object exists between them, the requirement of clearance of the first Fresnel zone is satisfied. As a result the free space loss model can be applied as the propagation model in the wireless link of the two antennas.

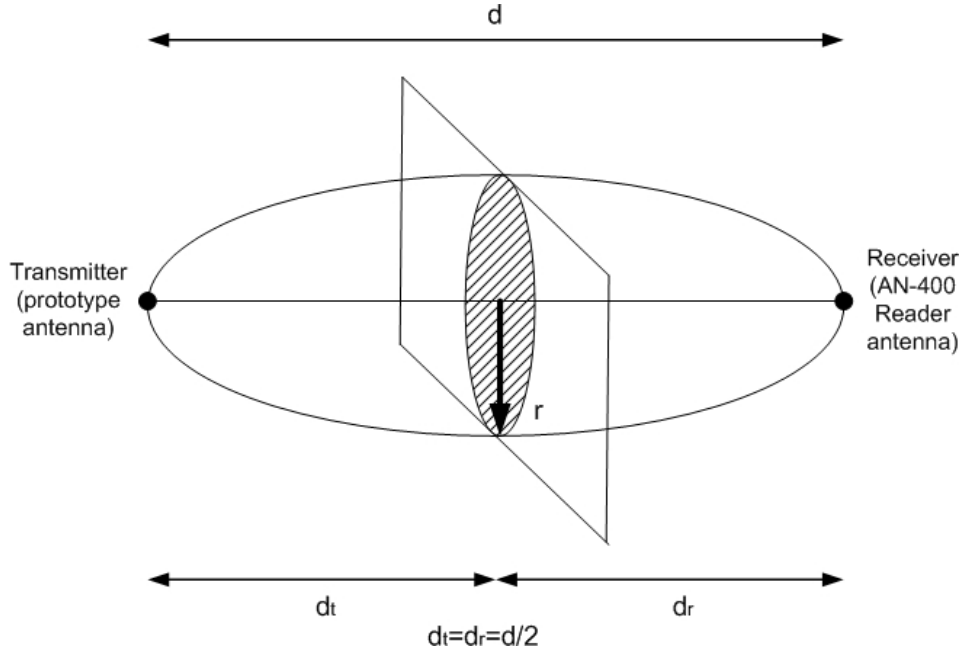


Figure 5.9 First Fresnel zone cross section at the middle point of the wireless link setup between the prototype antenna (transmitter) and the reader antenna (receiver)

Since the free space loss propagation model can be applied, the gain of each prototype antenna will be calculated using the Friis transmission equation [4]. The power received by an antenna is described by the Friis formula, which accounts for all antenna gains, path loss and losses in the system and is given for the current measurement by (12).

$$\frac{P_r}{P_t} = G_t G_r (1 - |\rho|^2) |\hat{\rho}_t \cdot \hat{\rho}_r|^2 \left(\frac{\lambda}{4\pi d} \right)^2 \quad (12)$$

where

P_t : the radiated power from the transmitter antenna

P_r : the received power from the receiver antenna

ρ : the complex reflection coefficient at the input of the transmit antenna

$\hat{\rho}_t$: polarization unit vector of the transmitter antenna

$\hat{\rho}_r$: polarization unit vector of the receiver antenna

The Friis formula can be written in a decibel form, as shown in (13) using the definitions given in Section 5.3.2:

$$P_r = P_t + G_t + G_r - L_m - L_p - 20 \log_{10} \left(\frac{4\pi}{\lambda} \right) - 20 \log_{10} (d) \quad (13)$$

It has to be noted that the polarization mismatch is given by $|\hat{\rho}_t \cdot \hat{\rho}_r|^2$ and equals the mismatch loss L_m in dB. From Equation 13 the gain for both the inkjet printed and the copper tape antenna is calculated: $G_t = -0.33$ dB.

5.4 Summary and Discussion

The obtained results, along with the results from the simulation are summarized in Table 5.3. In addition, the design goals that have been defined in Section 3.3 are also given for comparison: It has to be noted that the input impedance, directivity, gain, antenna efficiency and return loss are calculated at the required antenna operation frequency, at 904.5MHz. Since no radiation pattern measurements were carried out, the directivity and the efficiency of the monopole antenna could not be experimentally measured.

Table 5.3 Comparison of simulated and experimental results with the design requirements

Antenna Parameter	Requirement	Simulation	Inkjet-Printed	Copper Fabricated
Center Frequency (MHz)	904.5	904	898	906
Operation Bandwidth (MHz)	$\geq 866 - 928$	822 – 954	860 – 942	874 – 942
Bandwidth (MHz)	≥ 62	132	82	68
Bandwidth (%)	≥ 6.9	14.6	9.1	7.5
Input Impedance (Ω)	$\approx 37.3-j65.96$	37.5-j65.2	36.2-j61.5	39.5-j65.4
Directivity (dBi)	≥ 0	0.23	-	-
Gain (dBi)	≥ -1	-0.42	-0.33	-0.33
Efficiency (%)	≥ 80	88.7	-	-
Return Loss (dB)	≥ -15	-38.4	-23.7	-31.9

It is observed that the return loss and gain measured results are in close agreement with the simulation and therefore the antenna design requirements defined in the first step of the design process are satisfied. It is seen from the measured -10dB impedance bandwidth, that both the inkjet-printed and the copper tape fabricated antenna can operate efficiently across the USA (902 – 928MHz) UHF RFID frequency band. The inkjet printed antenna can operate also in the Europe (866 – 868MHz) UHF RFID band, satisfying the design requirements.

As a result the feasibility of modeling, designing and efficiently printing antennas on paper substrate is verified. Paper proved to be an excellent candidate as an antenna dielectric substrate material, since its dielectric loss doesn't decrease significantly the antenna gain, as seen from the gain measurements good results. The agreement of the inkjet printed antenna measured results with the simulation, qualifies the inkjet printing process as an efficient method for printing RF structures, such as antennas on paper substrate.

As mentioned in Section 5.2.3 there is a slight deviation of the measured return loss bandwidth results from simulation for the copper tape fabricated antenna. However, as mentioned also in Section 5.2.3, more than 99.9% of the input power is radiated by the copper tape antenna at the operation frequency resulting in excellent antenna performance. As a result the fact that the gain measurements proved to produce the same results for both antennas, also verify the good performance of the inkjet printing technique and high conductivity of the printed antenna. The high conductivity of the proposed inject printed antenna also verifies the need to print many layers of the antenna trace and proper cure the antenna.

CHAPTER 6

Conclusions and Future Work

6.1 Conclusions

The design and implementation of a novel conductive inkjet printed monopole antenna on paper substrate for UHF RFID applications has been presented. The operating principles and the applications of active RFID tags were summarized, highlighting their importance for the realization of ubiquitous wireless sensor networks. The proposed antenna was designed and optimized to meet specific design goals, including UHF operation, high directivity and impedance matching to the load of the RFID transponder. The inkjet-printing process of the antenna on to the paper substrate was detailed, emphasizing the importance of this technology as a fast and simple fabrication technique. Experimental measurements were performed on the antenna to determine its return loss in the UHF bandwidth and its gain in a wireless link setup. The measured results showed good agreement with the simulation, thus proving the realization of the inkjet printing technology as an efficient method for printing antennas on paper.

From this work, several conclusions are extracted. The single layer configuration of the proposed antenna proved to be suitable for the inkjet-printing fabrication process. If a double layer configuration was chosen, the implementation of the antenna would require two sheets of paper, since paper substrates can only be printed on one side. As a result, the assembly of two separate paper substrates would be necessary to create the double layer prototype, using fiducial marks and creating vias, which would make the fabrication process very challenging.

The monopole geometry showed good results, because of the use of the ground plane. The wideband characteristics of a monopole antenna were verified in the return loss measurements, where an almost 10% bandwidth was obtained. The existence of the ground plane was also utilized in the inkjet-printing technique, since the low-precision cartridge could be used and increase the conductivity of the antenna trace. If a dipole configuration [9] with thin antenna traces was chosen, the high precision, low conductivity cartridge would be required to accurately print the antenna. Finally, the printing of many layers was also found essential during the fabrication process to ensure maximum conductivity of the antenna trace.

The embedment of the slots in the radiation element was verified as a proficient technique for the antenna optimization. It provided an efficient way for tuning the input impedance of the antenna, in order to achieve impedance matching to the tag's load. The use of slots increased also the current path and therefore the electrical length of the antenna, resulting in a higher value of directivity. The return loss of the inkjet printed antenna at the operation frequency was found from the measurement results to be -23.7dB .

6.2 Directions for Future Work

6.2.1 Antenna further experimental measurements

Although the antenna characteristics have been verified from the return loss and gain measurements, further investigation of the antenna performance is essential for the complete prototype characterization. In particular:

It is essential to perform radiation pattern measurements for the azimuth and elevation plane in an anechoic chamber. In this way it will be possible to compare the obtained results with the simulation and verify the omnidirectional pattern of the antenna. In addition, the experimental value of the antenna directivity can be calculated from the measured radiation pattern. As a result the antenna efficiency can be estimated from the measured antenna directivity and gain. Comparison of the antenna efficiency experimental results to the simulation can further verify the antenna performance and the effectiveness of the inkjet printing fabrication process.

In addition, the performance of the antenna has to be investigated when attached to various materials. An RFID transponder is always attached to an object and therefore some kind of material is always in the near field of the antenna. The performance of a tag antenna changes in terms of radiation pattern distortion and gain decrease, when applied to materials, such as metal, water or wood [19]. Metal reflects the antenna RF radiation and water or wood absorbs it. It is possible to discover through the experimental study of the antenna material attachment that the antenna performance is deteriorated and no longer meets the design requirements. In this case techniques, such as input impedance tuning have to be utilized to improve the antenna performance and radiation.

6.2.2 Antenna further optimization

Although the proposed antenna showed good results and met the required design goals, it can be further optimized. The optimization can be performed in terms of:

Size: A more compact antenna that also achieves the same design requirements can be realized. The antenna can be made more compact by decreasing the dimensions of the feeding line, ground planes and radiating element.

Feeding line: The CPW feeding line of the antenna had a very small gap width ($g=0.3\text{mm}$), which made challenging the antenna fabrication, since a high-precision ink cartridge had to be used in the inkjet-printing process. The feeding line can be redesigned with larger gap width (e.g. 1mm), resulting however in different transmission line characteristic impedance. The antenna transmission line can have any characteristic impedance, as long, as the desired impedance is achieved at the input of the antenna.

Embedded slots: Due to the fact that the embedment of slots resulted in an efficient way of impedance matching, other types and positions of slots can be considered. For example, circular or square slots with vertical or horizontal orientation can be investigated.

Impedance Matching: Another way to optimize the antenna design process would be to determine the parameters of the antenna configuration that affect independently the resistive and the reactive part of the antenna input impedance. In this way the

antenna could be matched to any load with any impedance just by changing its parameters, so that the desired antenna input impedance is achieved. It has to be first ensured that the other antenna characteristics still meet the design requirements.

Other antenna geometries: Different antenna geometries, such as slot antennas and other monopole antennas can be investigated in terms of optimizing the antenna performance.

APPENDIX



Materials Printer & Cartridges DMP-2831 & DMC-11601/11610

Datasheet

System Description

- Flat substrate, xyz stage, "ink jet" deposition system
- Low cost, user-fillable piezo-based ink jet print cartridges
- Built-in drop jetting observation system
- Fiducial camera for substrate alignment and measurement
- Variable jetting resolution and pattern creation PC-controlled with Graphical User Interface (GUI) application software
- Capable of jetting a wide range of fluids
- Heated vacuum platen
- Cartridge cleaning station
- Includes PC, monitor, and software



Mechanical System

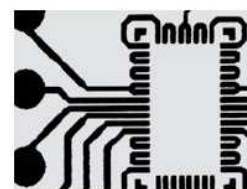
- Printable area
 - Substrate < 0.5 mm thickness: 210 mm x 315 mm (8.27 in x 12.4 in)
 - Substrate 0.5 - 25 mm thickness: 210 mm x 260 mm (8.27 in x 10.2 in)
- Repeatability: $\pm 25 \mu\text{m}$ (± 0.001 in)
- Substrate holder
 - Vacuum platen
 - Temperature adjustable; ambient to 60° C
- System Footprint: 673 mm x 584 mm x 419 mm (26 in x 23 in x 16 in)
- Weight approximately 43 kg (95 lbs)
- Power 100-120/200-240 VAC 50/60 Hz 375 W maximum
- Operating range 15-40° C at 5-80% RH non-condensing
- Altitude up to 2000 m
- Safety and EMC compliance
 - Safety: NRTL Certified to EN 61010-1, UL 61010-1, CSA 22.2 No. 61010-1
 - EMC: EN61326-1 Class A, FCC Part 15 Class A



Drop Watcher View

Fiducial Camera

- Allows substrate alignment using reference marks
- Allows positioning a print origin or reference point to match substrate placement
- Provides measurement of features and locations
- Provides inspection and image capture of printed pattern or drops
- Provides cartridge alignment when using multiple cartridges
- Allows matching drop placement to previously patterned substrate



Fiducial Camera View

Cartridge

- Type: Piezo-driven jetting device with integrated reservoir and heater
- Usable Ink Capacity: Up to 1.5 ml (user-fillable)
- Materials Compatibility: Many water-based, solvent, acidic or basic fluids
- Number of Nozzles: 16 nozzles, 254 μm spacing, single row
- Drop Volume: 1 (DMC-11601) and 10 (DMC-11610) picoliter nominal



Control PC and Application Software

- Pre-loaded patterned templates
- Pattern preview
- Editors: Pattern, piezo drive waveform, cleaning cycle, substrate setting
- Bitmap (1 bit) files accepted
- Optional Gerber (RS-274X) file import

Replaceable Items

- Print cartridge with one-time user-fillable reservoir
- Cleaning station nozzle blotting pad
- Drop watcher fluid absorbing pad



FUJIFILM Dimatix, Inc. • 2230 Martin Avenue • Santa Clara, CA 95050 • USA

Tel: (408) 565-9150 • Fax: (408) 565-9151

E-mail: infomdd@dimatix.com • URL: www.dimatix.com

REFERENCES

- [1] K. Finkenzeller, "RFID Handbook: Fundamentals and Applications in Contactless Smart Cards and Identification", John Wiley and Sons LDT, Second Edition, 2003
- [2] K. V. S. Rao, Raj Mittra, "Design of RFID Tags and Systems", Short Course & Workshop Series, *IEEE International AP-S Symposium*, July 2008
- [3] K. V. S. Rao, P. V. Nikitin and S. Lam, "Antenna design for UHF RFID tags: a review and a practical application", *IEEE Transactions on Antennas and Propagation*, vol. 53, no. 12, pp. 3870-3876, Dec. 2005
- [4] C. Balanis, "Antenna Theory, Analysis and Design", 3rd edition. New York: Wiley, 2005
- [5] L. Yang, and M. M. Tentzeris, "Design and Characterization of Novel Paper-based Inkjet-Printed RFID and Microwave Structures for Telecommunication and Sensing Applications", *IEEE Intentional Microwave Symposium*, accepted, June, 2007
- [6] L. Yang, A. Rida, R. Vyas and M. M. Tentzeris, "RFID Tag and RF Structures on Paper Substrates using Inkjet-Printing Technology", *IEEE Transactions on Microwave Theory and Techniques*, Vol.55, No.12, Part 2, pp.2894-2901, December 2007
- [7] Rida, L. Yang; R. Vyas, S. Bhattacharya, and M. M. Tentzeris, "Design and integration of inkjet-printed paper-based UHF components for RFID and ubiquitous sensing applications" *IEEE Microwave European Conference*, pp:724-727, Oct 2007
- [8] Vyas, R.; Rida, A.; Li Yang; Tentzeris, M. M., "Design and Development of a Novel Paper-based Inkjet-Printed RFID-Enabled UHF (433.9 MHz) Sensor Node", *Microwave Conference, 2007. APMC 2007. Asia-Pacific*, vol., no., pp.1-4, 11-14 Dec. 2007
- [9] R. Vyas, A. Rida, L. Yang, M. M. Tentzeris, "Design, Integration and Characterization of a Novel Paper Based Wireless Sensor Module", *IEEE International Microwave Symposium*, accepted June 2008
- [10] S. Basat, S. Bhattacharya, A. Rida, S. Johnston, L. Yang, M. M. Tentzeris, and J. Laskar, "Fabrication and Assembly of a Novel High-Efficiency UHF RFID Tag on Flexible LCP Substrate", *Proc. of the 56th IEEE-ECTC Symposium*, pp.1352-1355, May 2006

- [11] K. V. S. Rao, Pavel V. Nikitin, Sander F. Lam, "Impedance Matching Concepts in RFID Transponder Design", autoid, pp.39-42, *Fourth IEEE Workshop on Automatic Identification Advanced Technologies (AutoID'05)*, 2005
- [12] P.V. Nikitin, K.V.S. Rao, S.F. Lam, V Pillai, R. Martinez, and H. Heinrich, "Power Reflection Coefficient Analysis for Complex Impedances in RFID Tag Design", *IEEE Transactions on Microwave Theory and Techniques*, 2005, vol. 53, issue 9, pp. 2721-2725
- [13] P. V. Nikitin and K. V. S. Rao, "Response to Comments on 'Antenna design for UHF RFID tags: a review and a practical application'", *IEEE Transactions on Antennas and Propagation*, pp. 1906-1907, vol. 54, no. 6, June 2006
- [14] Nikitin, P.V.; Lam, S.; Rao, K.V.S., "Low cost silver ink RFID tag antennas", *Antennas and Propagation Society International Symposium, 2005 IEEE* , vol.2B, pp. 353-356 vol. 2B, 3-8 July 2005
- [15] K. Kurokawa, "Power waves and the scattering matrix," *Microwave Theory and Techniques, IEEE Transactions on.*, vol. MTT-13, no. 3, pp. 194–202, Mar. 1965
- [16] David M. Pozar, "Microwave Engineering Third Edition," *John Wiley and Sons Inc.*, 2005
- [17] Χ. Καψάλης, Π. Κωπτής, "Κεραίες, Ασύρματες Ζεύξεις", Εκδόσεις Τζιόλα, 2005
- [18] Νικόλαος Κ. Ουζούνoglου, "Εισαγωγή στα Μικροκύματα", Β΄ Έκδοση, Εκδόσεις Παπασωτηρίου, Αθήνα 1994
- [19] Joshua D. Griffin, "A Radio Assay for the Study of Radio Frequency Tag Antenna Performance", M. Sc. thesis, Georgia Institute of Technology, Atlanta, Georgia, USA, May 2005
- [20] Toccafondi, A.; Cueing, A.; Mariottmi, F.; Braconi, P., "Broadband Uniplanar UHF Meander Line Antenna for Multistandard RFID Transponders", *Electromagnetics in Advanced Applications, 2007. ICEAA 2007. International Conference on* , vol., no., pp.101-104, 17-21 Sept. 2007
- [21] Ray, K.P.; Ranga, Y., "CPW-fed modified rectangular printed monopole antenna with slot", *Microwave and Optoelectronics Conference, 2007. IMOC 2007. SBMO/IEEE MTT-S International* , pp.79-81, Oct. 29 2007-Nov. 1 2007
- [22] Ray, K.P.; Ranga, Y., "Printed rectangular monopole antennas", *Antennas and Propagation Society International Symposium 2006, IEEE* , pp. 1693-1696, 9-14 July 2006

- [23] Wen-Shan Chen; Yu-Chen Chang; Hong-Twu Chen; Fa-Shian Chang; Hsin-Cheng Su, “Novel design of printed monopole antenna for WLAN/WiMAX applications”, *Antennas and Propagation Society International Symposium, 2007 IEEE* , pp.3281-3284, 9-15 June 2007
- [24] Zhang, M.-T.; Jiao, Y.-C.; Zhang, F.-S., “Dual-band CPW-fed folded-slot monopole antenna for RFID application”, *Electronics Letters* , vol.42, no.21, pp.1193-1194, 12 Oct. 2006
- [25] Ansoft HFSS Version 10.0 - User’s Guide. Ansoft Corporation, 2005
- [26] Motorola AN-400 RFID Antenna Data Sheet. Available:
http://www.motorola.com/Business/US-EN/Business+Product+and+Services/RFID/RFID+Reader+Antennas/AN400_US-EN
- [27] DMP-2831 Datasheet. Available: <http://www.dimatix.com/files/DMP-2831-Datasheet.pdf>
- [28] <http://en.wikipedia.org/wiki/RFID>
- [29] <http://www.dimatix.com>
- [30] <http://www.intermec.com>